PROBING THE STRUCTURE OF DEXTRAN SYSTEMS AND THEIR ORGANIZATION

by

YUNHONG RONG

A thesis submitted to the

Graduate School-New Brunswick

Rutgers, The State University of New Jersey

in partial fulfillment of the requirements

for the degree of

Master of Science

Graduate Program in Food Science

written under the direction of

Professor Jozef L. Kokini

and approved by

_____

_____

_____

_____

New Brunswick, New Jersey

May, 2008

ABSTRACT OF THE THESIS

Probing the Structure of Dextran Systems and Their Organization

by YUNHONG RONG

Thesis Director:

Professor Jozef L. Kokini

Dextran with molecular weight 9,700 (T10) was dissolved directly in water (66%) at room temperature to form a concentration of three times its overlap concentration. Wide angle x-ray scattering (WAXS) and differential scanning calorimetry were used to monitor the change in the crystallinity of concentrated dextran solutions with time. Dextran solutions (66%) were also probed with steady and dynamic rheological measurements to understand the changes in structure as the concentrated dispersion aged, Finally FTIR was used to understand the molecular origins of the crystalline changes of the concentrated dextran solution.

Concentrated dextran solutions showed a phase transition from clear solution to opaque semi-solid without water losses a result of aging time. Both WAXS and DSC measurements indicated that the sample crystallinity increased with time, and reached a plateau after 4 hours and remained relatively stable after that. FTIR spectra showed an increase of the concentration of hydrogen bonds with time. Rheological measurements indicated that both the storage and loss moduli (G' and G") increased gradually with time and showed a sudden increase at 3-4 hours. These findings provided fundamental understanding of a unique crystalline phase in the liquid state for the behavior of dextran molecules and serve as a model possibly for other carbohydrates in solution and their

aggregation, which in turn helps improve the quality of carbohydrates containing concentrated semi-solid foods.

DEDICATION

This dissertation is dedicated to my husband, Zhenyu, for his love, support and understanding while doing research and writing this thesis, and to my families in China for their emotional and financial support which gave me the opportunity to pursue my professional development.

ACKNOWLEDGEMENTS

This thesis is the culmination of research conducted under my mentor, Dr. Jozef L. Kokini. Without his guidance, expertise, patience and kindness, this thesis would not have come to fruition. Thank you for the opportunities to be a part of those endeavors, all the support, advisement and reassurance throughout this journey.

I own special thanks to Dr. Thomas Emge for his help and use of the X-ray diffraction in the chemistry department at Rutgers. Dr. Jaap Schut for use of the micro differential scanning calorimetry in his lab in chemistry department at Rutgers. Dr. Qinrong Huang and his postdoctoral research assistant Dr. Qiang Wang for the help of using the Fourier Transform Infrared in the food science department at Rutgers. Dr. Hulya Dogan, for sharing her valuable idea and friendship with me. Dr. Curt Wissbrun for helping me to understand phase transitions in concentrated liquid systems.

I also would like to thank Miriam Gonzalez for scheduling appointments; Jackie Revolinsky for her help in all the student issues throughout the years; Paulette Arico for her kind and warm words which made me feel at home. And to the rest of the students in Dr. Kokini's lab for their support and encouraging words.

Last but not the least I would like to acknowledge the financial support CAFT (center for advanced food technology) without which I could not completely devote myself to the research.

TABLE OF CONTENTS

LIST OF TABLES

LIST OF FIGURES

I. Introduction

Polysaccharide polymers are widely used in the food and pharmaceutical industry to provide useful functions like texture, stability, delivery, and palatability. The properties of final products are influenced by the interactions between polysaccharide molecules and solvent. Retrogradation, an intermolecular association driven by associative hydrogen bonding occurs when carbohydrate molecules comprising of gelatinized starch begin to reassociate in an ordered structure and ultimately, under favorable conditions, a crystalline order appears. (Atwell et al., 1988). Pectin gels due to the formation of junction zones by hydrophobic interactions and hydrogen bondings (Iijima et al., 2002).

Dextran is a water-soluble polysaccharide which consists mainly of α-1,6 linked D-glucopyranose residues with a low percentage of α-1,2, α-1,3 and α-1,4 linked side chains (Stenekes et al., 2001). The well defined molecular weights of dextran make it a perfect candidate to understand the molecular interactions between molecules having similar chemical structure and composition, as a model for structurally compatible systems.

The purposes of this study were:

1) to characterize the conformation of dextran in solution based on the rheological properties of the dilute solutions of the polymer

2) to understand the molecular interactions between dextran molecules and their solvents through rheological, thermal and spectroscopic methods.

The primary objectives of this study were to understand the formation of dextran crystallites through dextran/dextran and dextran/water molecular interactions at high concentrations of low molecular weight dextran in water. This is very peculiar behavior which is not observed at high molecular weight because the high molecular weight dextarn molecules are not able to effectively associate due to steric hindrance.

Through understanding of the mechanism of dextran hydrogen bonding driven self association resulting in crystallization and how the molecular interactions affect rheological properties such as viscosity and elasticity of solutions. It is possible to predict and improve the polysaccharides containing system based on this understanding. These results can be used as a tool to design food of desired or improved properties and stability during shelf life.

II. Background

Dextrans have been extensively studied under dilute aqueous solutions (Jeanes et. al., 1948; Gekko, 1981; Wu, 1992; Ioan et. al., 2000). Less is known about their behavior at high concentrations. Sperling (1992) stated that amorphous materials exist in a thermodynamic metastable, non-equilibrium state below the equilibrium melting temperature. There is always a driving force towards the equilibrium, crystalline state, which is defined as one that diffracts X-rays and exhibits the first-order melting transition. Stenekes et al. (2001) showed that crystalline polymer could be developed from polymer melts, supersaturated polymer solution and by forming association of the chains through hydrogen bonding. Dextrans are excellent model systems for food carbohydrate polymers since their molecular structures are similar and dextrans are readily available in a wide range of molecular weights.

A. Dextran

1. Chemical Structure

Dextrans are varying molecular weight polymers of glucose obtained by the fermentation of sucrose with *Leuconostoc mesenteroides* NRRL B-512(F). Dextran molecules consist of α (1→6)-linked glucan with side chains attached to the 3-positions of the backbone glucose units. Figure II-1 shows the structure of dextran molecule. From periodate analysis (Rankin and Jeanes, 1954; Dimler et al., 1955; Vianna-Soares et al., 2002) and methylation analysis (Van Cleve et al, 1956; Larm et al, 1971; Jeanes and Seymour, 1979; Laumonier et al., 2004), the degree of branching is usually estimated as

5%. The degree of branching is found to decrease on partial acid hydrolysis, although the effect is not dramatic (Lindberg and Svensson, 1968; Naessens et al., 2005). The dextran branches are not clustered but are distributed in a relatively regular manner (Covacevich and Richards, 1977). Sequential degradation has been employed to investigate the length of the side chains. Larm and colleagues (Larm et al, 1971) concluded that 40% of the side chains are one glucose unit long, 45% are two units long and the remaining 15% longer than two.

Figure II-1: Structure of dextran molecule.

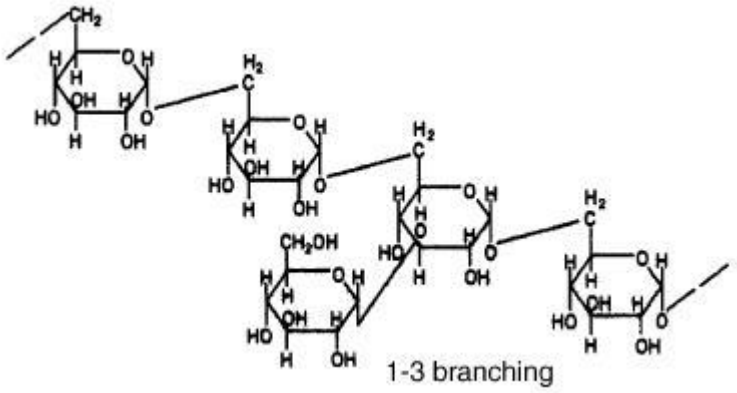

Table II-1: Dependence of degree of branching on molecular weight. (Lindberg and Svensson, 1968).

Dextran	Branching (%)
Native dextran	4.6
Dextran 80	3.8
Dextran 10	3.0

2. Manufacturing

Dextran for clinical and technical products is produced throughout the world. Most producers use the *Leuconostoc mesenteroides* NRRL B-512(F) or b-512 strain for the fermentation. The major process of dextran is based on the batchwise culture of *Leuconostoc* in the presence of sucrose. The viscous culture fluid is then precipitated in ethanol or methanol. Native dextran obtained this way is hydrolyzed in dilute acid and the desired dextran is isolated by fractionation. Dextran can also be produced in laboratory scale (Tsuchiya et al, 1964; Nadel et al, 1953; Lawford et al, 1979).

3. Applications

Dextran was studied since the early 1940's (Stacey and Swift, 1948). The main application of dextran at that time was using a 6% solution of dextran fraction as a plasma substitute. The generally marketed dextran was dextran 70, with an approximate molecular weight of 70,000 as a 6% solution in normal saline and as the plasma volume expander of choice. It is recommended for the treatment of shock or impending shock

due to hemorrhage, burns, surgery or trauma (Shoemaker, 1976; Zhang et al., 2003). With the increased use of clinical dextrans, more research and development followed on dextran. Dextran 40, with a molecular weight of 40,000 is used during the first 24 hours in patients undergoing high risk surgery or suffering from high risk trauma (Koekkenberg, 1962). Dextran 1, with a molecular weight of 1000, is used prior to the dextran 40 or 70 infusion could considerably reduce the incidence of severe dextran-induced anaphylactoid reactions (DIARs) (Richter and Hedin, 1982).

Dextran has also gained wide application in the food industry. Innumerable applications of dextrans in food applications were patented in the 50's and 60's (Glicksman, 1982; de Belder, 2003). Dextrans are considered as safe as components of food packaging materials. Dextran can be also used as a non-active ingredient in pharmaceutical formulations. Dextran is an unusually flexible polysaccharide that promotes high solubility and low solution viscosities, its behavior would not be expected to conform to traditional food uses (Whistler, 1973). Dextran could be suitable for certain food use application not associated with thickening or gelling functionalities. Examples include use as a source of dietary fiber, as a cryostabilizer and fat substitute in frozen food systems, as a flavor carrier in fluid foods or as a low calorie bulking agent for sweeteners (McCurdy et. al., 1994).

4. Physical-chemical properties

The α(1→6) linked polysaccharides represent a class of very flexible and extended polymers. Dextrans behave as flexible, slightly branched random coils in dilute solutions (Nordmeier, 1993). This results in highly soluble polymers in water even at the

highest molecular weights. The molecular dimensions are dependent on the solvent, and the M_w and concentration of the polysaccharide (Table II-2).

Table II-2: Molecular dimensions of dextran as radius of gyration of Stokes' radius.(Granath, 1958)

M_w x10^{-3}	Radius of gyration (Å)	Stokes' radius (Å)
2000	380	270
1000	275	199
500	200	147
200	130	95
100	95	69
70	80	58
50	68	49.5
40	62	44.5
10	_	23.6

Dextran is freely soluble in water, methyl sulphoxide, formamide, ethylene glycol, glycerol, 4-methylmorpholine-4-oxide, and hexamethyl phosphoramide. Dextran coils are rather compact in poor solvents, but they expand considerably in a good solvent such as methyl sulphoxide or formamide (Basedow and Ebert, 1979; Snabre et al., 1985). Above M_w 2000, dextran behaves as an expandable coil in solution (Granath, 1958). The solution properties indicated that dextran molecules with $M_w > 10^5$ behave as if they were highly branched.

As the M_w increases further, the molecules attain even greater symmetry (Granath, 1958; Wales et al., 1953). The molecular dimensions of dextran decrease with increasing

concentration. From the single crystal electron diffraction data of dextran fraction with M_w=199 000, the dextran crystal adopts a ribbon-like conformation with consecutive glucose units in a near twofold screw relationship, the unit cell containing two antiparallel chains of two glucose units (Chanzy et al., 1980; Guizard et al., 1984).

The relationship between dextran M_w and intrinsic viscosity [η] in water has been investigated over a wide range of M_w. The deviation from linearity at higher M_w is ascribed to the increase in branching and the polymolecularity of the fractions used. Granath (1958) obtained the relationship of intrinsic viscosity and molecular weight for dextran in the clinical range.

$$[\eta] = 2.23\times10^{-3}\,\overline{M}_w^{\,0.43} \quad (\text{for } M_w < 5\times10^5) \text{ (Equation II-1)}$$

The value of the exponent decreases with the increasing of M_w suggesting that the radius of gyration decreases as molecular weight and chain branching increases. In high molecular weight dextran fractions a lower value has been derived. Recently an exponent value of 0.22 was derived for dextran with molecular weights of $>10^6$ (Senti et al., 1955). The Newtonian behavior of dextran solutions is the result of excellent dissolution of dextran in water and the lack of aggregation.

From the measurements of osmotic pressure of dextran 40 and 70 (Figure II-2), the increasing divergence of the osmotic pressures of dextran from those of albumin at higher concentrations reflects the greater interaction between dextran and water, which is a good solvent for dextran, and the properties conferred by the random coil structure (de Belder, 2003).

Dextran molecules dissolved in water and in physiological saline liquid are nearly ideal coils and no association occurs (Basedow and Ebert, 1979). In a poor solvent such as glycerol, dextran coils are rather compact, whereas they are more expanded in a good solent such as formamide. In dilute saline solutions, dextran coils are slightly more expanded than in water (Basedow and Ebert, 1979).

Dextran molecules once dissolved showed no or only very little change in coil dimensions during dilution and that association-dissociation phenomena did not occur with partially hydrolyzed dextrans in dilute solutions. Fedin et. al. (1975) found that in concentrated solutions dextans produced by various bacterial strains are strongly associated and these aggregates are highly stable with dilution at low temperature, but disintegrate rapidly at a temperature around 100ºC. Dextran aggregation is explicitly observed only for sample at the low end of molecular weights (less than 10,000). Concentrated solutions of dextrans of low molecular weight grow perceptibly turbid over time. This is a sign of an order disorder transition which will be the core of this investigation in this thesis. Visual effects do not accompany aggregation of dextrans with a higher molecular weight in solution (Hirata et. al., 2003).

Figure II-2: Divergence of the osmotic pressures of dextrans from albumin with concentration.

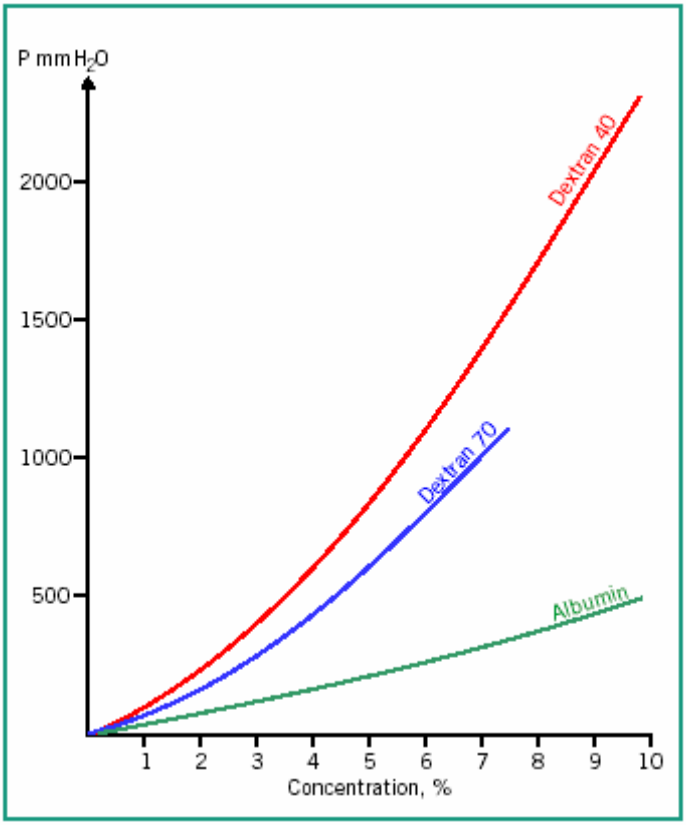

(de Belder, 2003)

B. Encapsulations in food or pharmaceutical system

Encapsulation is widely used in food industry to improve or enhance nutrition or flavor. In pharmaceutical industry encapsulation of drug ingredients allows the controlled release of the active components. In encapsulation, the active material is buried to various depths inside of the wall material. Encapsulation methods of choice are generally spray drying, melt extrusion, melt injection, complex coacervation, microemulsion and liposomal carrier systems. In a number of these methods the generation of a glassy state carrier needs to be considered. Crystallization of carbohydrate syrups has been widely used in the encapsulation of flavor oils (Beristain et. al., 1996; Quellet et. al., 2001; Madene et. al., 2006). In the pharmaceutical industry, controlled release systems based on crystalline and semicrystalline polymer phases have been developed (Mallapragada and Peppas, 1997; DesNoyer and McHugh, 2001; Laarhoven et. al., 2002).

C. Dilute solution molecular theory

Linear and substantially linear polymers behave in a qualitatively predictable way with respect to the relationship of their viscosity to their structure and conformation. Molecular conformation of polymers in solution can be characterized through the study and application of dilute solution theories. In the study of dilute solutions it is assumed that each molecule is isolated from all other molecules in the system. In reality, this ideal condition is only an approximation since the interaction between molecules can not be completely eliminated. Therefore, all data must be extrapolated to infinite dilution. In dilute solutions the relationship between their viscosity and their structure and conformation depends effectively on the hydrodynamic volume, the volume "swept out"

by the molecules as they tumble in solution. At these low concentrations, where there is effectively no interaction between molecules and they are at their most extended conformation, the viscosity may be very close to that of the solvent.

Dilute solution theories have idealized the flexible random coil polymers through the use of the bead and spring model. This representation is shown in Figure II-3. Each polymer molecule is divided into segments, represented as springs, which are connected at junctions and shown as beads. These junctions allow free rotation and thus impart an overall flexibility. Steric hinderance may reduce or hinder rotation at the junctions and result in a more rigid conformation.

The relationship between viscosity and concentration is generally linear up to a critical concentration where entanglements and interactions begin. This dependency means that more extended molecules increase the viscosity to greater extents at low concentrations than more compact molecules of similar molecular weight. Generally less-flexible links between sequential monomers in the polymeric chains give rise to more extended structures but the linkage spacing, direction and charge density are all important factors. The molecules most capable of an extended structure due to the maximal linkage spacing and direction are -(1$\longrightarrow$4)-diequatiorially linked between pyranose residues whereas those least capable.

Figure II-3: Representation of a flexible random coil macromolecule by the bead-spring model. The random coil conformation is a result of flexibility between numerous stiff sections of the polymer molecule.

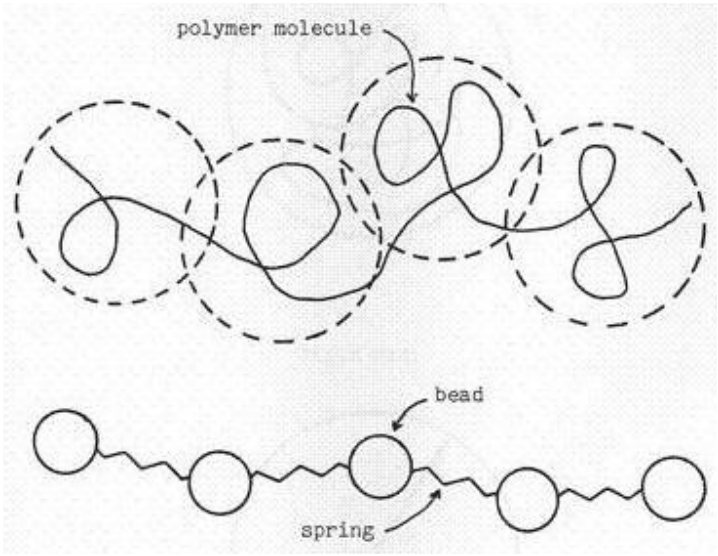

(Ferry, 1980)

contain -(1⟶3)-diaxially linked pyranose residues. Where residues are negatively charged, the repulsion between similar charges increases molecular extension but this can be reduced at higher ionic strength by interrupting the like charge ionic network or below the pKa's of the anionic groups and this reduction is particularly noticeable for polymers with high molecular weight. The lack of much change in viscosity of such molecules with ionic strength is indicative of an inflexible rod-type conformation (Chaplin, 2006).

Rigid rod and random coil conformations are the two extreme types of molecular arrangement of biopolymers in solutions. Figure II-3 shows the effect of chain rigidity on solution viscosity. In the figure the rigid rod and random coil molecules each occupy the same hydrodynamic volume in solution therefore each imparts the same viscosity. The

rigid molecule contributes more viscosity per unit mass while the flexible coil imparts a greater elasticity at the same viscosity. Thus, conformation plays an important role in determining rheological properties.

Figure II-4: Effect of chain rigidity on hydrodynamic volume and rheological properties of polymers. Rigid macromolecules occupy a greater hydrodynamic volume per unit mass than flexible coil molecules.

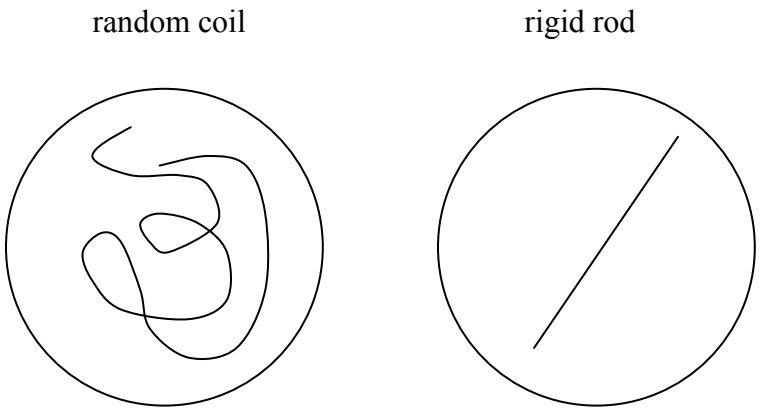

The relative viscosity, specific viscosity and the intrinsic viscosity are important rheological properties used to characterize the contribution of the polymer and its conformation to solution viscosity. The relative viscosity (η_r) is defined as a ratio of the solution viscosity to the solvent viscosity:

$$\eta_r = \frac{\eta}{\eta_s} \quad \text{(Equation II-2)}$$

where η is the viscosity of the polymer solution and η_s is the solvent viscosity.

The specific viscosity (η_{sp}) is a measure of the viscosity contributed by the polymer and is defined as:

$$\eta_{sp} = \frac{\eta - \eta_s}{\eta_s} \quad \text{(Equation II-3)}$$

The specific viscosity, divided by concentration and extrapolated to zero concentration, yields the intrinsic viscosity ([η]). The intrinsic viscosity is a measure of the radius of gyration and hydrodynamic volume of the molecule:

$$[\eta] = \lim_{c \to 0} \frac{\eta_{sp}}{c} = \lim_{c \to 0} \frac{\eta - \eta_s}{c \eta_s} \quad \text{(Equation II-4)}$$

For dilute solutions, where the specific viscosity is just over unity, when dividing ln η_r by c and extrapolating to zero concentration also yields the intrinsic viscosity:

$$[\eta] = \lim_{c \to 0} \frac{\ln(\eta_r)}{c} \quad \text{(Equation II-5)}$$

Intrinsic viscosity may be determined experimentally from plotting η_{sp}/c vs. c and extrapolating to zero concentration (Huggins plot) or to plot (ln η_r)/c vs. c and extrapolating to zero concentration (Kraemers' rule) (Morris and Ross-Murphy, 1980). Both lines must extrapolate to the same intercept at zero concentration (Sperling, 1992). Figure II-5 shows the schematic to determine [η].

The relationship between the intrinsic viscosity and the weight average molecular weight results in the Mark-Houwink relationship. The relationship can be used to characterize the conformation of the polymer. In studies of carbohydrate polymer conformation, intrinsic viscosity and the Mark-Houwink exponent α are the most often used parameters to characterize their conformation. (Kenley et al., 1987; Tsaih and Chen, 1997, 1998; Brugnerotto et al., 2001).

Mark-Houwink equation is an empirical relationship between the molecular weight and the intrinsic viscosity.

$$[\eta] = KM_V^{\alpha} \quad \text{(Equation II-6)}$$

where K and α are constants for a particular polymer-solvent pair at a particular temperature. It must be pointed out that since viscosity-average molecular weights are difficult to obtain directly, the weight-average molecular weights of sharp fractions or narrow molecular weight distributions are usually substituted to determine K and α (Sperling, 1992). The exponent in the Mark-Houwink equation is an indication of the conformation and stiffness of the molecule and tells the conformation of a polymer.

Conformation of a polymer is a function of its chain flexibility, solvent properties, and concentration of solute. Parameters usually used to characterize the conformation of a polymer in solution include Mark-Houwink type exponents such as: α, b, ε, ν. These parameters are obtained from the plots of log intrinsic viscosity, sedimentation coefficient, diffusion coefficient, and radius of gyration, respectively, vs. log molecular weight of the polymer. The slopes of the plots are the corresponding parameters. Table II-3 shows the

numeric value of the exponents and the conformation of polymer corresponding to (Chen and Tsaih, 1999). Table II-4 shows the Mark-Houwink relationships for different carbohydrate polymers.

Table II-3: The relationships of polymer conformations and the exponents of Mark-Houwink type equations (Chen and Tsaih, 1999).

Mark-Houwink type equations	Conformation		
	Sphere	Random coil	Rod
$[\eta] = kM^{\alpha}$	0	0.5 ~ 0.8	1.8
$s = k'M^{b}$	0.7	0.4 ~ 0.5	0.2
$D = k''M^{-\varepsilon}$	0.3	0.5 ~ 0.6	1.0
$R_g = k'''M^{v}$	0.3	0.5 ~ 0.6	1.0

Table II-4: The Mark-Houwink relationships of different carbohydrate polymers (Castro et al., 2005; Wolff et al., 2000; Picout et al., 2002; Avaltroni et al., 2004).

Carbohydrate Polymer	Mark-Houwink exponents
Locust Bean Gum	$\alpha = 0.77 \pm 0.09$
Tara Gum	$\alpha = 0.79 \pm 0.12$
Guar Gum	$\alpha = 0.70 \sim 1.05$
Pullulan	$\alpha = 0.733$
Inulin	$\alpha = 0.67$ ($M_w < 10^5$), $\alpha = 0.05$ ($M_w > 10^5$)
Maltodextrin	$\alpha = 0.337$ (DE= 2 ~ 18)
Linear Starch	$\alpha = 0.486$

Figure II-5: Schematic of a plot of η_{sp}/c and ln η_{rel}/c vs. c and extrapolation to zero concentration to determine [η].

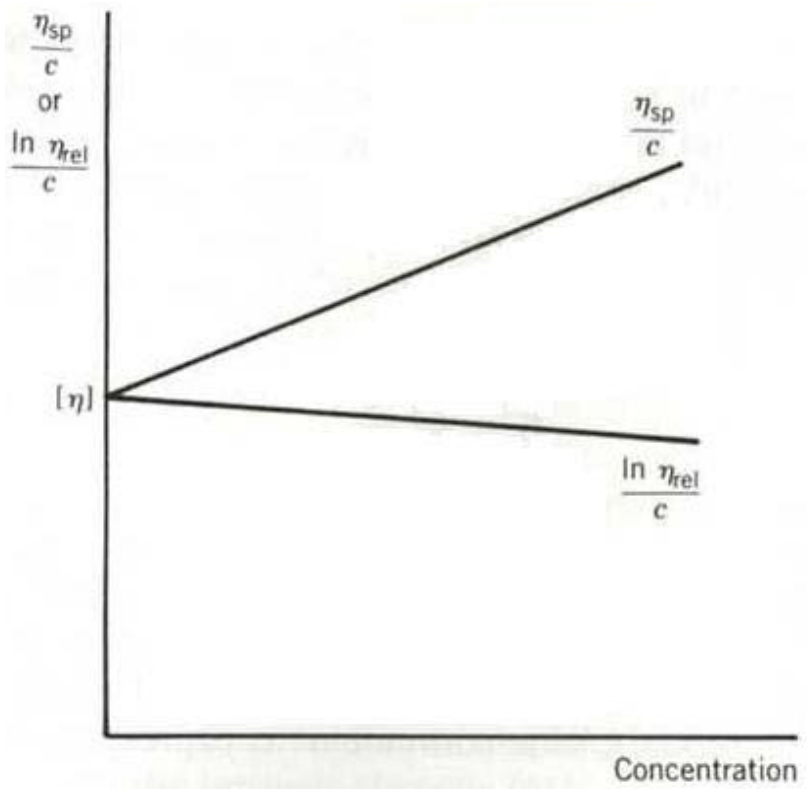

One can describe the stiff coil as a random coil with no intramolecular hydrodynamic interactions. This type of coil allows a more extended conformation than that of a random coil which has intramolecular hydrodynamic interactions (Rouse, 1953). The second type of random coil is less extended due to dominant hydrodynamic interactions within the molecule which cause it to fold in on itself. Wang et. al. (1991) determined the Mark-Houwink equation for chitosans with different degrees of deacetylation. Due to a reduction of rigidity of the molecular chain and an increase of the electrostatic repulsion force of the ionic groups along the polyelectrolyte chain in chitosan solution, the values of alpha decreased from 1.12 to 0.81. This has shown that chitosan conformation changes from a stiff coil to a random coil with changing degrees of deacetylation. It should be noted that although attaching short sugar units as branch-points to linear polysaccharides does increase their rigidity, this is at the cost of greatly increased molecular weight.

The extended nature of the molecules has a strong effect on the molecular weight dependency of the viscosity as the hydrodynamic volumes (and hence viscosities) of compact (highly flexible but poorly hydrated) molecules increase approximately as the cube root of their molecular weight. Those of more-extended well hydrated molecules (such as alginate and xanthan gum) increase approximately linearly with molecular weight. In the absence of any organizing factor (e.g., the hydrophobic, hydrophilic or ionic interactions) a polymer will take on an extended random coil configuration in solution.

Any molecular property that favors polymer-polymer repulsion or favors polymer-solvent interactions will favor a more expanded coil. Any property that favors

polymer-polymer interactions will tend to collapse the coil to a smaller hydrodynamic radius. In very dilute polymer solution, each coil behaves as an isolated sphere and will add to the viscosity of a solution. As the concentration is increased the polymer coils will quickly start to overlap and interact. The interactions between polymer chains, resulting in aggregation and effectively an increase in molecular size lead to a very rapid increase in viscosity. The interactions between molecules, which extend over the entire system and form an infinite molecular sized network, allow it to instantaneously transmit mechanical forces and behave as a solid.

The Mark-Houwink exponent does not change in a relatively small molecular weight range of about two orders of magnitude. However the molecular stiffness changes with the polymer chain arrangements. Brugneroto et al. (2001) showed that chitosan with the same molecular weight (the same degree of acetylation), a non-homogeneously N-reacetylated chitosan is stiffer. Different solvent systems also change molecule stiffness. Poly(lactide-co-glycolide) polymer has Mark-Houwink exponent α of 0.761 in THF while α is 0.794 in hexafluoro-2-propanol (HFIP) (Kenley et al., 1984). Molecular weight induced conformational transition has been reported for amylase (Nakanishi et al., 1993) and pullulan (Pavlov et al., 1994). The conformation of these polysaccharides becomes more extended as the molecular weights increase. Excluded volume effects have been shown to have a prevailing influence on the chain length of these polysaccharides (Pavlov et al., 1994). Moreover, molecular weight induced conformational changes of schizophyllan (Yanaki et al., 1980), and pectin (Hourdet and Muller, 1991) which result in the collapse of the hydrodynamic volume results in contraction as molecular weight increases. The contraction of polymers has been attributed to intermolecular aggregation

and precipitation of the polymer, different composition of the polymer, and alteration in the intra- and inter-molecular attraction (Tsaih and Chen, 1997). Nagy (1996) showed that the α value of PEF decreased with increasing molecular weight of PEF. This suggested a more compact or tightly coiled structure at higher molecular weight due to branching and aggregation.

Most recent studies have shown that dextran is a random coil polymer in aqueous solvent system. α=0.60 was obtained for the hypothetical linear dextran with $1.1\times10^4 < M_n < 3.7\times10^5$ (Gekko, 1981). Scott et al. (1956) reported the equation $[\eta] = 1.09\times10^{-3} M_n^{0.50}$ for hydrolyzed dextran with $1.5\times10^4 < M_n < 1\times10^5$ in water at 25ºC. For M_w<500,000, $[\eta] = 2.23\times10^{-3} M_w^{0.43}$ (dextran handbook Amersham Sciences). For 40,000<Mw<2,000,000 a α-value =0.33 was obtained by Tirtaatmadja and colleagues (2001). Granath (1958) suggested that the α-value for dextran should increase for lower molecular weights because it had been found that brancing in dextran diminishes rapidly when the molecular weight decreases to 10^4. Dextran is also more extended at low molecular weights.

Although dextran can not be considered as a real fractal, there is evidence for the presence of randomly distributed branches in the molecule (Smit et al., 1992). Wittgren and Wahlund (1997) showed a slope of 0.36 for dextran T500. However the slope for dextran T500 showed a tendency to decrease with increasing molecular molecular weight. The decreasing slope indicates that the high molecular end of the distribution consists of more branched, compact macromolecules. The plot of dextran T2000 if using only the high molecular weight fractions, showed a α value of 0.27, which suggests a highly branched structure. Nagy (1996) measured commercial dextran and obtained the α value

about 0.38 which is typical for random coil polymers. He concluded that the commercial dextran is highly branched. Literature reported values for dextran range between 0.40 – 0.60 and such variation maybe possible because of the variation in the origin and molecular mass range of the dextran studied (Roessner and Kulicke, 1994). Amylose, carboxymethylcellulose, arabinoxylans and guar all have exponents α of about 0.7 (Chaplin, 2006).

D. Overlap concentration

The viscosity of polymer molecules increases with concentration until the shape of the volume occupied by the molecules becomes elongated under shear causing some overlap between molecules and a consequent reduction in the overall molecular volume. This reduces the amount that viscosity increases with concentration (in shear). At higher concentrations, usually above a critical overlap concentration C*, all the polymer molecules in the solution effectively interpenetrate and become entangled. The total hydrodynamic volume of the polymer molecules appear larger than the solution volume, even without being stressed, so changing the solution behavior from mainly viscous to mainly elastic with the viscosity (η_0 at zero stress) is mainly governed by the mobility of the polymer molecules. At high shear rate, C* will depend on the shear rate as the molecules take up a less volume. At higher concentrations the viscosity increases up to about the fifth power of the concentration and this can cause apparently synergistic behavior of hydrocolloid mixtures, particularly if they cause phase separation.(Chaplin, 2006).

Figure II-6: overlap concentration of maltodextrin determined by the change of zero shear specific viscosity with concentration.

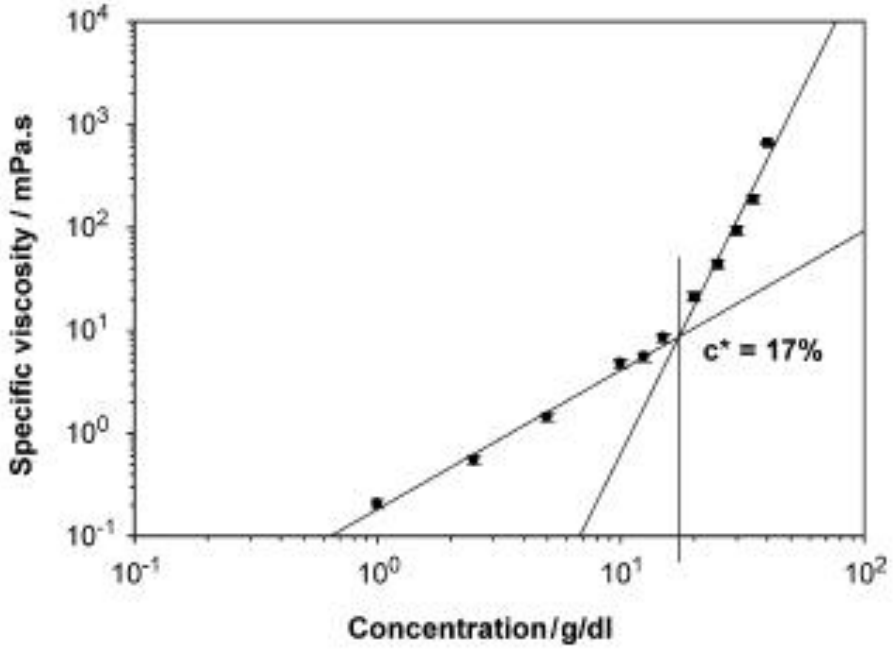

(Loret et. al., 2004)

E. Phase transitions in food system

Phase transitions are important in determining the physical state during processing, storage and consumption of foods. For most food products phase transitions are observed in the main ingredients such as carbohydrates, lipids, proteins and water. Food products demonstrate both equilibrium and nonequilibrium similar to that of polymers. In their chemically pure state and in the absence of water, most food ingredients might exist in completely crystalline, semicrystalline or amorphous states. Equilibrium thermodynamics approximate phase behavior in foods as a function of temperature, volume and pressure. (Roos, 1992).

1. First order transitions

First order transition is a thermal transition that involves both a latent heat and a change in the heat capacity of the material. First order transitions take place during physical state changes, such solid, liquid and gas phase changes, which occur isothermally (as in the case of melting and crystallization). A characteristic amount of heat is either released or required as the latent heat of the transition (ΔH_f), and an entropy change accompanies the heat of transition. DSC has been used to quantitatively characterize first order transitions of food ingredients by integration of the first order transition peak, which results in the heat (ΔH) of the transition (Roos, 1992).

Melting constitutes a first order phase transition. If a sample does not contain colorants, it is usually hazy in the crystalline state because of the difference in refractive index between the amorphous and crystalline portions. On melting, the sample becomes more transparent (Sperling, 1002). When heating temperature reaches the polymer's

melting temperature, or T_m, polymer crystals begin to undergo an order disorder transition, they melt. The chains come out of their ordered arrangements, and begin to move around freely.

2. Second order transitions

Second order transitions are also called the continuous phase transitions. These transitions have no associated latent heat but result in a change in heat capacity. In second order transitions, the Gibbs energy (G) and its first derivatives are continuous functions of temperature and pressure. At least one of the second derivatives of G has a discontinuity at the transition temperature. The glass transition is a second order transition.

F. Molecular weight, molecular conformation, and crystalline structure

When molecular weight decreases, molecules assume a more extended conformation in dilute solution. The extended molecules are favored to align each other and form inter- and/or intra-molecular hydrogen bonds which result in crystalline structure. Chitosan with different molecular weights demonstrate different molecular conformations. Chitosan with molecular weight ranging from 401 kDa, to 220, 112 and 105 kDa shows a decrease in radius of gyration from an initial value of 58 nm, to 38, 27, and 26 nm. The $\log(R_g)$ verses $\log(M_w)$ plot slopes decreased from initial 0.48 to 0.41, 0.36, and 0.32 indicating transition in spherical molecular and random coil conformation with reduction in molecular weight (Wu et. al, 2005). Guar, a random coil polysaccharide, can form both inter- and intra-molecular hydrogen bonds. Its crystalline structure in the

relative humidity range of 40 – 80% is determined to be an extensive network of both direct sugar – sugar and water – mediated hydrogen bonds. (Cheng and Prud'homme, 2002).

G. Crystalline properties of food materials

1. Crystallization kinetics

Amorphous materials organize themselves in the form of crystals as a function of time. Kinetics of crystallization can be studied by measuring volume changes on melting (dilatometrically) with time. The plot of cyrstallinity vs. time has a sigmoid shape (Figure II-7), since the crystallization rate occurs slowly at the beginning, then increases, and decreases again at the end of the process (Roos, 1995).

Crystallization kinetics of amorphous polymers with low degrees of crystllinity are modeled using the Avrami equation, which results from a probability density equation derived by Poisson (Sperling, 1992):

$$P_x = \frac{e^{-E} E^x}{x!} \quad \text{(Equation II-7)}$$

where P_x is the probability that a point P is crossed by x fronts of growing spherulites and E represents the average number of fronts of all such points in the system. Jouppila et al. (1998) took the Avrami equation and rewrote it in order to fit X-ray diffraction peak areas and DSC melting enthalpies vs. time of crystallization of amorphous corn starch

Figure II-7: Sigmoid shaped plot of crystallinity vs. time.

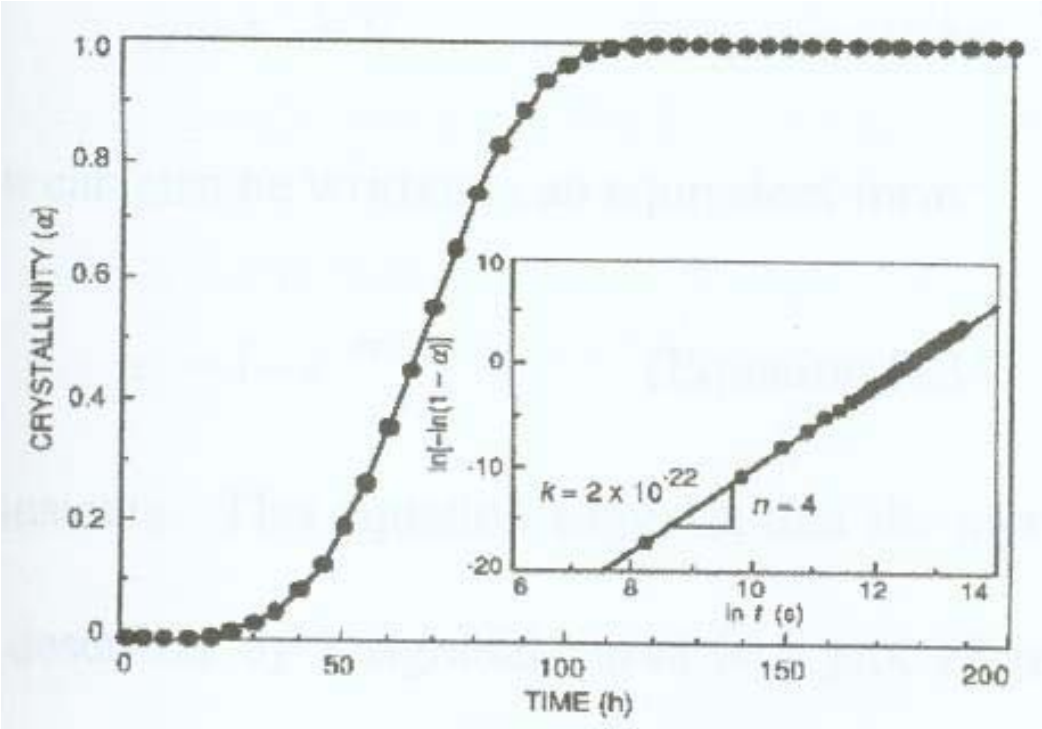

(Roos, 1995)

samples at 60%, 70% and 80% solids stored at various temperatures. The rewritten Avrami equation is as follows:

$$1-\alpha=\frac{A_f-A_t}{A_f-A_0}=e^{-kt^n} \quad \text{(Equation II-8)}$$

where A_f corresponds to the leveling-off value of peak area (counts) or leveling-off value of melting enthalpy where crystallization stops; A_t corresponds to the peak area or melting enthalpy at time t, and A_0 represents the peak area of 0 counts or melting enthalpy of 0 J/g for a noncrystalline amorphous material. Figure II-8 shows the peak area in X-ray diffraction pattern of cornstarch as a function of time, solid content and storage temperature. Equation II-7 was fitted to the data as represented by the lines in Figure II-8.

In a similar manner, crystallization kinetics of cornstarch determined by DSC at various temperatures and water contents (60%, 70% and 80% solids) followed the Avrami equation, represented as solid lines in Figure II-9.

Figure II-8: Peak area in X-ray diffraction pattern for cornstarch as a function of time and solid contents.

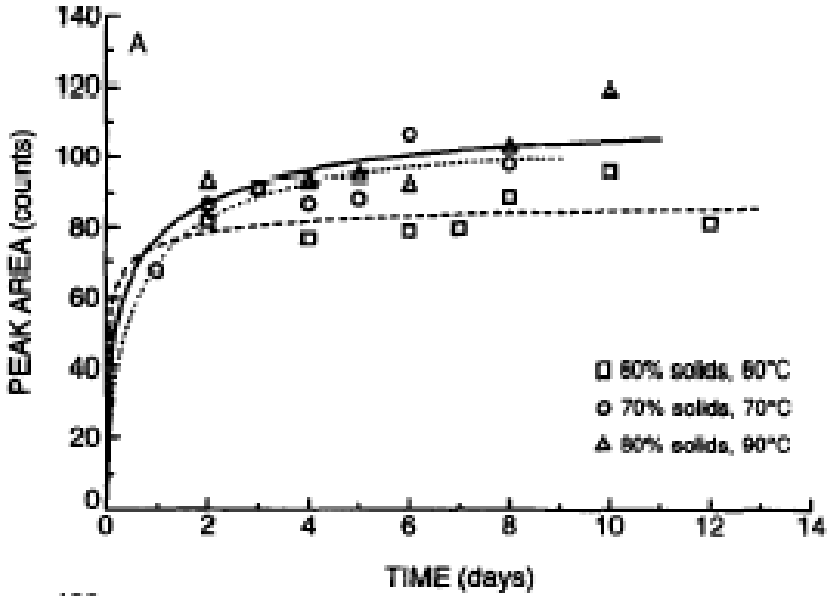

(Jouppila et al., 1998)

Figure II-9: Melting enthalpies indicating extent of crystallization as a function of storage time and temperature for cornstarch at 80% solids.

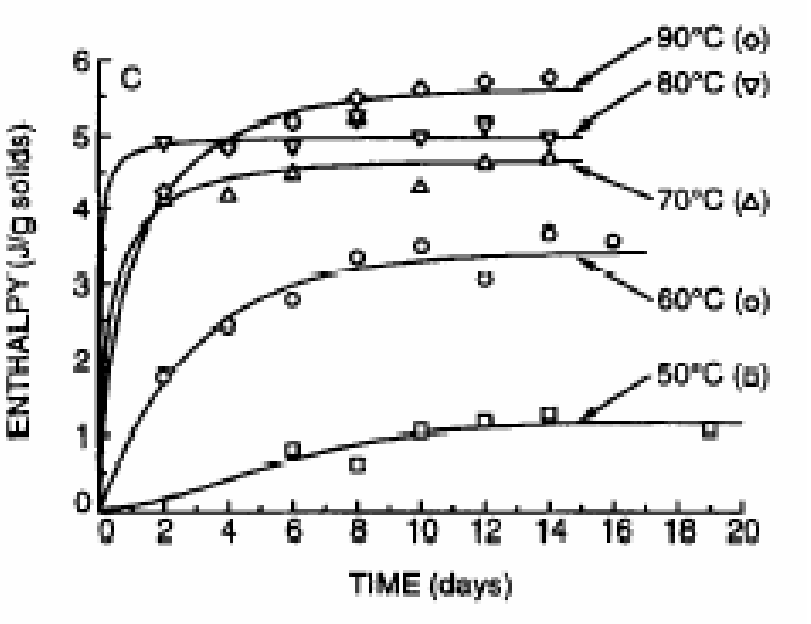

(Jouppila et al., 1998)

2. Crystallization: Definition

Amorphous materials exist in a thermodynamic metastable, nonequilibrium state below their equilibrium melting temperature. There is always a driving force towards the equilibrium, crystalline state, which is defined as one that diffracts X-rays and exhibits the first-order transition known as melting (Sperling, 1992). When a polymer has a large degree of order it is called a crystalline polymer. The range of order may be as small as about 2 nm in one or more crystallographic directions and is usually below 50 nm in at least one direction. A crystalline domain in the crystalline polymer is called a polymer crystal and usually limited by well-defined boundaries. Crystallinity may be detected by diffraction techniques, heat of fusion measurements, etc. (Allegra et. al, 1989). A crystal is also defined as the regular polyhedral form, bounded by smooth surfaces, which is assumed by a chemical compound under the action of its interatomic forces, when passing from the state of a liquid or gas to that of a solid under suitable conditions (Klug and Alexander, 1974).

Crystals may form from a supersaturated solution. The driving forces for crystallization are the rates of nucleation and crystal growth. Fudge is classified as a crystalline candy. It is one of the rare exceptions to the rule that sugar crystals are not desirable in candy. The fudge crystal grows from a supersaturated solution. The crystals formed are very fine so that the fudge is soft but firm with a smooth texture. Low molecular weight amorphous food components may crystallize at a temperature higher than their glass transition temperature (T_g) and lower than their melting temperature (T_m), crystallizing to the thermodynamically favorable form (Roos, 1995). The occurrence of complete crystallization of polymers is unlikely due to their long-chain nature and

entanglements; the crystallites are usually embedded in a residual amorphous matrix (Sperling, 1992; Roos, 1995).

3. Crystallization process

Crystallization involves three consequent steps: 1) nucleation, 2) growth of crystal and 3) crystal perfection.

Nucleation is the first step in crystallization. A large supersaturation driving force is necessary to initiate primary nucleation. Nucleation may be either homogeneous or heterogenous, however the latter is more likely to occur in foods due to the presence of impurities (Roos, 1995). Heterogeneous nucleation involves the presence of foreign bodies or impurities that may act as the nucleating sites. The foreign bodies form favorable sites which reduce the energy needed for the formation of the critical nuclei, facilitating crystallization. Homogeneous nucleation occurs spontaneously. Molecules organize to form the nuclei. The extent of supersaturation in heterogeneous nucleation is lower than that in homogeneous nucleation (Roos, 1995).

Crystal growth needs diffusion of molecules to the surface of the growing nuclei. The rate of the process is very sensitive to the extent of supersaturation or impurities. The following parameters that required for the growth of existing nuclei: 1) diffusion of the compound from bulk to the solid surface; 2) removal of solvent; 3) diffusion of solvent away from the crystal surface; 4) proper orientation of the molecules; 5) surface diffusion of the molecules to appropriate sites; 6) incorporation of the growth unit into the crystal lattice, and 7) removal of latent heat.

4. Morphology of polymer crystals

Polymer crystallization is a first order phase transition that is complicated by severe kinetic limitations due to the size of the polymer, a metastable endpoint, and inclusion of single molecules in multiple crystallites. The conditions under which a polymer crystallizes affect the resulting morphology (Olsen et. al, 2005). The bulk of polymer crystals is characterized by the regular repetition of the unit cell. However, most polymer crystals are microscopic. Therefore, the interface between the crystal and the amorphous regions must be considered. The simplest morphological building block of macroscopic crystalline structure is the lamellae. The shape of the lamellae generally mirrors the shape of the unit cell.

It was observed that when polymers crystallize from dilute solutions, they form lamellar-shaped single crystals. When they crystallize from somewhat more concentrated solutions, various multilayered dentritic structures are observed (Sperling, 1997). On cooling from the melt, the first structure that forms is the single crystal. When polymers crystallize from a polymer melt, rather than from solution, lamellae begin to interconnect and stack into sheath-like structures. Amorphous, non-crystallizable material becomes trapped in the spaces between the lamellae. The lamellae of the spherulite are interconnected by polymer chains that started growing on one crystal face and subsequently continued on another. The lamellae in the spherulite are held together by covalent bonds. Eventually, crystal growth is terminated as spherulites start to grow into each other (Toda et al., 2001).

When crystal is formed from supersaturated solutions, a crystalline driving force is needed. Cooling a heated solution would lead to supersaturation and thus crystallization. The crystal structure is determined by the cooling process, not the heating process. For example properly made fudge is a soft solid, consisting of sugar in a microcrystalline condition, bonded by a matrix of highly viscous syrup. This is a unique crystalline structure where a crystal co-exists with a liquid phase in a metastable equilibrium. Tiny microcrystals in fudge are small. Fudge is made from cooling boiled viscous syrup. When cooling, the syrup becomes a supersaturated solution. If this solution is stirred while it is hot enough to have relatively little viscosity but is already supersaturated, crystallization will commence and proceed readily and large crystals will grow. The final product will be coarse-grained.

Figure II-10: Structure of fudge crystals.

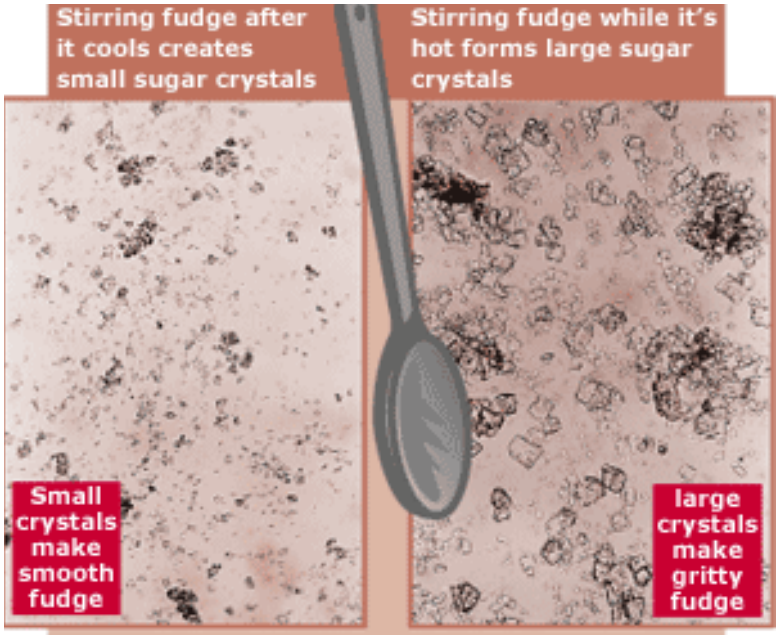

(Harold McGee microscopy images, Exploratorium)

Carbohydrate polymers due to their chain lengths and branches have different solubility in water. The long chain carbohydrate polymers in water inhibit solubility and some promote gelation. Maltodextrins are a hydrolysis product of starches and are complex mixtures of high and low molecular weight materials. Loret et al. (2004) observed a turbidity increase in 25% maltodextrin solution within 7 minutes and before gelation and explained it as the nucleation of the sample crystallites. The rheology of the maltodextrin samples remained largely unchanged during the crystallization period. The gel network formed implied that the crystallites formed are the building blocks from which the gel arises. This is a very different gelation mechanism compared to classical gels which are the result of entanglements or crosslinks. The crystallization and gelation period is probably governed by a further crystallization or rearrangement, but diffusion of macromolecules is slow due to the high viscosity of the medium. A sol-gel transition of low molecular weight dextran (M_w=6000 g/mol) from concentrated solutions was reported by Stenekes et al. (2001). The precipitation was time dependent and was demonstrated to be crystalline by IR spectroscopy and DSC. Stenekes et al. (2001) hypothesize that the crystallinzation is due to association of the chains through hydrogen bonding, induced by the large polymer/water ratio in concentrated dextran solutions.

5. Methods of analysis

There are different methods for the analysis of polymer crystallinity and for the degree of the crystallinity of a substance. X-ray diffraction and DSC methodologies are widely used now for qualitative and quantitative analysis of crystalline compounds. X-ray diffraction constitutes the fundamental basis for crystal cell size and form (Sperling, 1992) and DSC can determine the heat of melting and melting temperature.

a) X-ray diffraction (WAXS)

One of the useful X-ray diffraction studies is wide-angle X-ray scattering (WAXS). Under various conditions, crystalline materials diffract x-rays to give spots or rings. WAXS data gives information on 1) conformational orientation in the axial direction, which is a measure of how ordered or straight a given chain might be, and 2) organization in the radial direction, which is a direct measure of intermolecular order (Sperling, 1992).

When a material is irradiated with a parallel beam of monochromatic X-rays, the atomic lattice of the sample acts as a three dimensional diffraction grating causing the X-ray beam to be diffracted to specific angles. Bragg's law is widely applicable in the x-ray methods, which explains the distance *d* between successive crystalline identical planes:

$$d = \frac{n\lambda}{2\sin\theta} \quad \text{(Equation II-9)}$$

where λ is the x-ray wavelength, θ is the angle between the x-ray beam and the atomic planes, and n represents any whole number. Both the x-ray wavelength and the distance between crystal planes are of the order of 1 Å.

The diffraction from a single crystal produces a series of spots. However not every crystalline substance can be obtained in the form of macroscopic crystals. When the crystals are oriented at random the spots become cones of diffracted beams that can be recorded as circles on a flat photographic plate. Amorphous materials, including

ordinary liquids, also diffract x-rays, but the diffraction is much more diffusing, sometimes called halos.

Each reflection corresponds to a specific *d*-spacing that is a function of the substance's molecular conformation and crystalline order. Basically, the intensity of the diffraction depends on the scattering power of the individual atoms, which in turn depends on the number of electrons in the atom (Sperling, 1002).

Several types of crystal structures were observed in biopolymers. For example, in starch products, there are crystal structures known as V, A, B or C type. These types of crystals differ in the packing density of the single or double helices and in water content (Soest and Vliegenthart, 1997).

Cereal starches give an A type crystalline pattern and possess densely packed crystallites. Potato starch and certain other tropical tuber starches have a B type crystalline patter. They contain much more water than type A starchs (Jacobs and Delcour, 1998). The C type is the same as A except for the addition of the medium to strong peak at about 18 degree. Appearance of the inner 18 degree peak depended on the presence of moisture, and was sometimes missing on dry or partially dry specimens (Zobel, 1988).

Figure II-11: X-ray diffractograms of maize, patato and pea starch, and crystallized amylase. The peak positions are characteristic of A, B, C, and V_H type crystallinity, respectively.

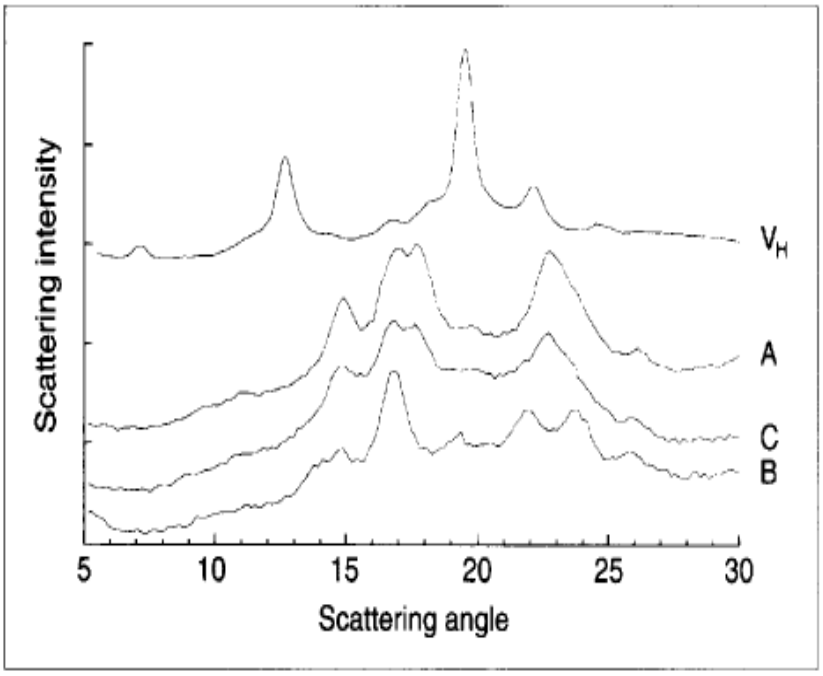

(Soest and Vliegenthart, 1997)

b) Differential scanning calorimetry (DSC)

Differential scanning calorimetry (DSC) is a technique to study a polymer's thermal behavior. As illustrated in figure II-12, the principle of the DSC method consists of supplying energy at a varying rate to the sample and the reference, so that the temperatures of the two stay the same. DSC yields peaks related to endothermic and exothermic transitions and shows changes in heat capacity (Murphy, 1978). DSC output plots energy supplied against average temperature. The area under the peaks can be directly related to the enthalpic changes quantitatively. At a first order transition temperature, such as melting temperature, the enthalpy change occurs isothermally and is equal to the latent heat, ΔH_f, of the transition. A typical DSC plot is shown in Figure II-13.

This DSC plot shows characteristic transitions. The crystallization dip and the melting peak will only show up for polymers that can form crystals. Completely amorphous polymers won't show any crystallization, or any melting either. But polymers with both crystalline and amorphous domains will show all the features in the above plot. The phase transition of first-order shows a sharp DSC peak and thermal hysteresis.

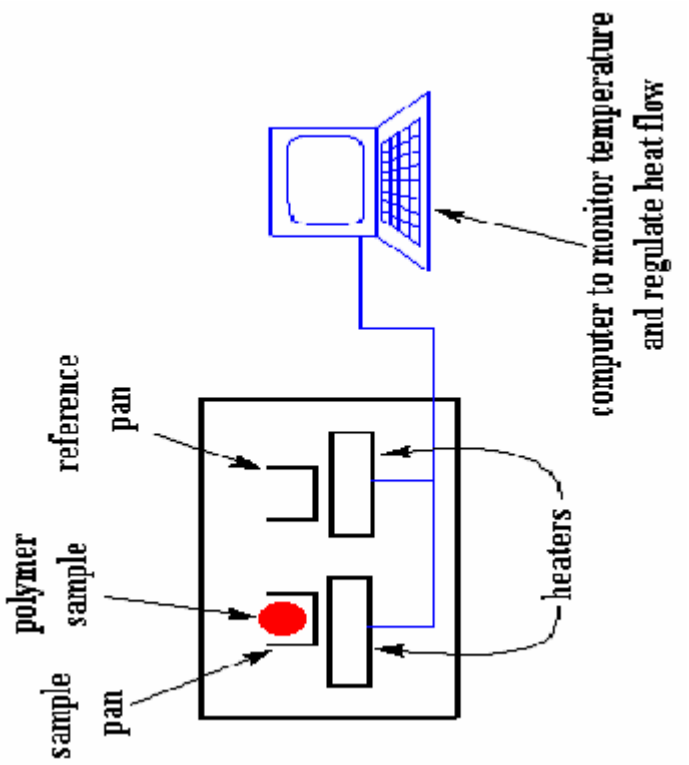

Figure II-12: Differential scanning calorimetry working principle (Polymer learning center, 2005).

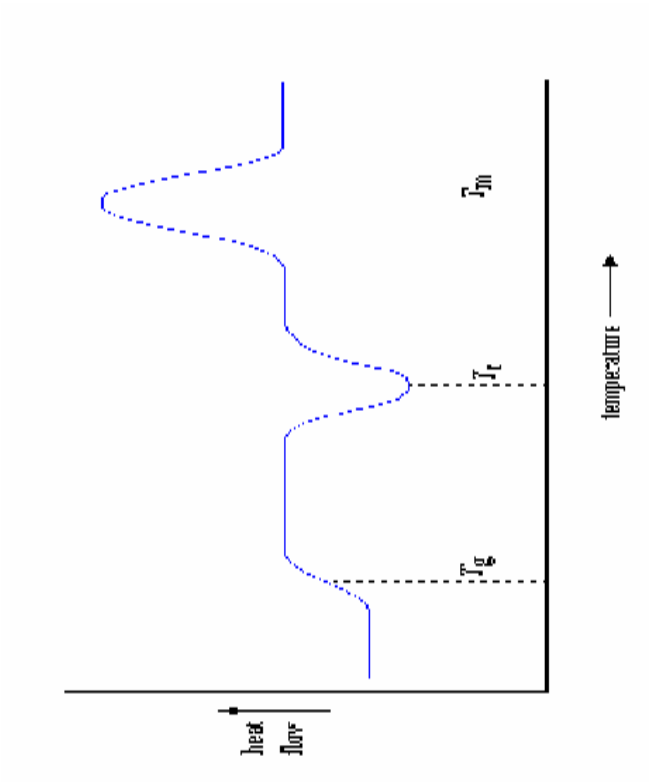

Figure II-13: Typical DSC plot.

Illustrated in Figure II-14, first order phase transitions produce peaks on DSC thermograms. The heat of fusion of the crystalline portion is given by the area under the peak, permitting an estimate of the percent crystallinity (Sperling, 1992).

Figure II-14: (a) The heat of fusion of poly(ethylene oxide) by DSC. The heat of fusion of the crystalline portion can be determined by melting depression experiments, permitting an estimate of the percent crystallinity (Sperling, 1992). (b) DSC curve of $(C_5H_5NH)_2ZnCl_4$ (Horiuchi, 2004).

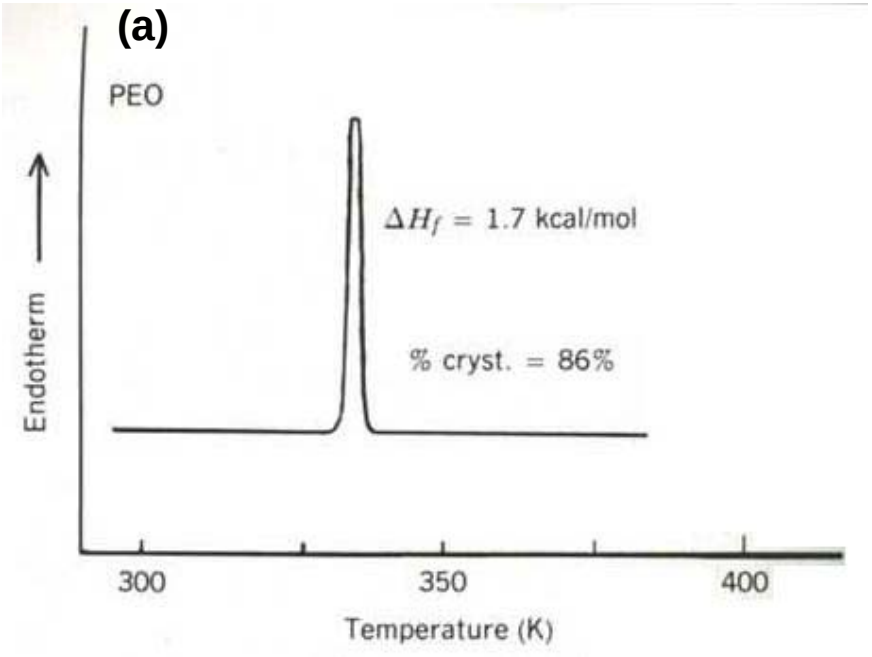

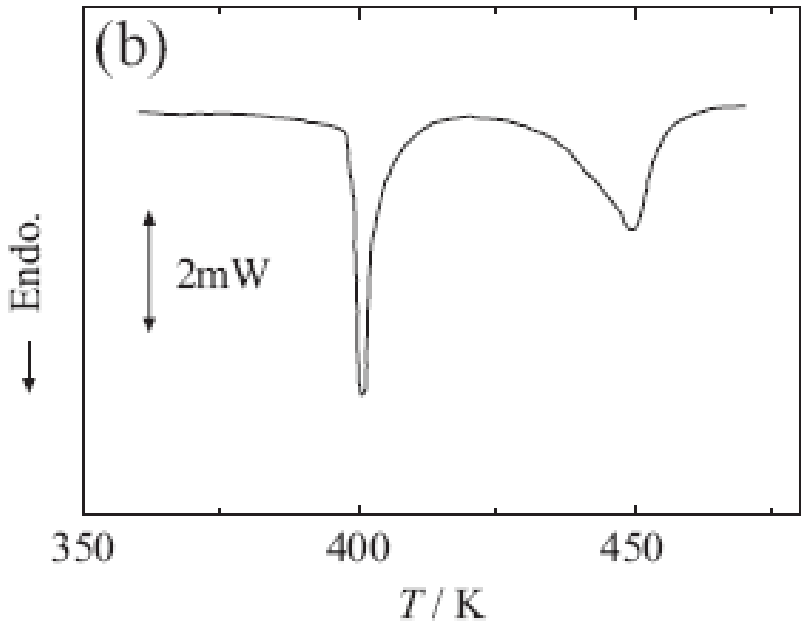

Biliaderis et. al. reported that native starch melted with a lower enthalpy than did its waxy counterpart, because waxy rice starch is more crystalline than native starch. Chung et. al. (2004) studied different starch samples and reached the conclusion that the enthalpy increase proceeded rapidly at the beginning of aging, and reached a plateau as aging continued. Starch crystallizes during aging. The enthalpy plateau is caused by a decrease in free volume and increasing crystallization causes a decrease in mobility.

Figure II-15: Enthalpy vs. aging time for different starches (Chung et. al., 2004).

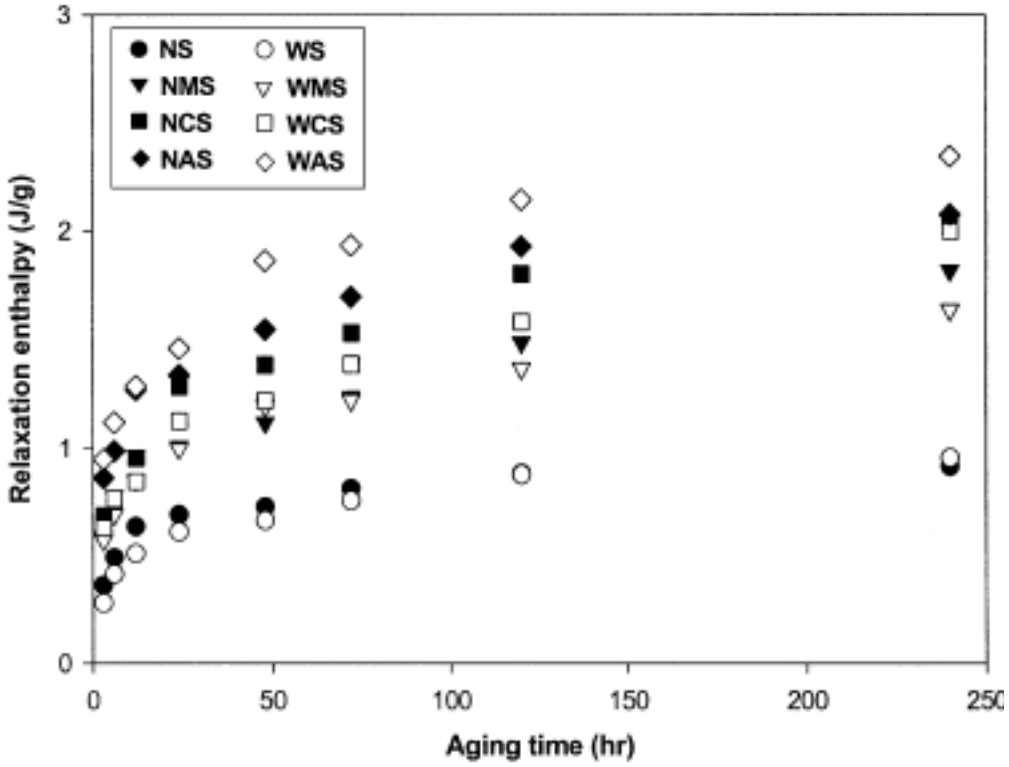

c) Fourier Transform Infrared Spectroscopy (FTIR)

It is well known that carbohydrates owe some of their functionality to glycosidic bonds and hydrogen bonding. In an aqueous environment hydrogen bonding and possible folding around the glycosidic linkages play an important role in the solution and phase behavior of carbohydrates (Kačuráková and Mathlouthi, 1995). Vibrational spectroscopy proves to be an effective tool for studying changes in molecular organization and interactions of carbohydrates. Tadokoro (1979) summarized that infrared spectra of semicrystalline polymers show "crystallization sensitive bands". The intensities of these bands vary with the degree of crystallinity and have been used as a measure of crystallinity (Sperling, 1992).

FTIR spectroscopy is used primarily for qualitative and quantitative analysis of molecular interactions in organic compounds, and also for determining the chemical structure of many inorganic compounds. Because chemical bonds absorb infrared energy at specific wavelengths or frequencies, the basic structure of compounds can be determined by the spectral locations of their IR absorptions. The plot of a compound's IR absorption vs. wavelengths is its finger print, which when compared to reference spectra identifies the material. The infrared spectra with wavelengths from 400 to 4000 cm^{-1} produces information on molecular vibration and rotation. The principle of the FTIR analysis is shown in Figure II-16. OH stretching band arising from sugar OH groups locates between 3600 and 3000 cm^{-1}. The bands in the 1500 ~ 1200 cm^{-1} region arise mostly from C-H deformation vibrations, and the bands between 1200 and 900 cm^{-1} arise predominantly from a combination of C-O stretching and OH bending vibrations. The

1500 ~ 900 cm^{-1} region of FTIR spectra of sugar solutions is not perturbed by water and one of the richest in structural information (Kačuráková and Mathlouthi, 1995).

Figure II-16: The principle of the FTIR analysis.

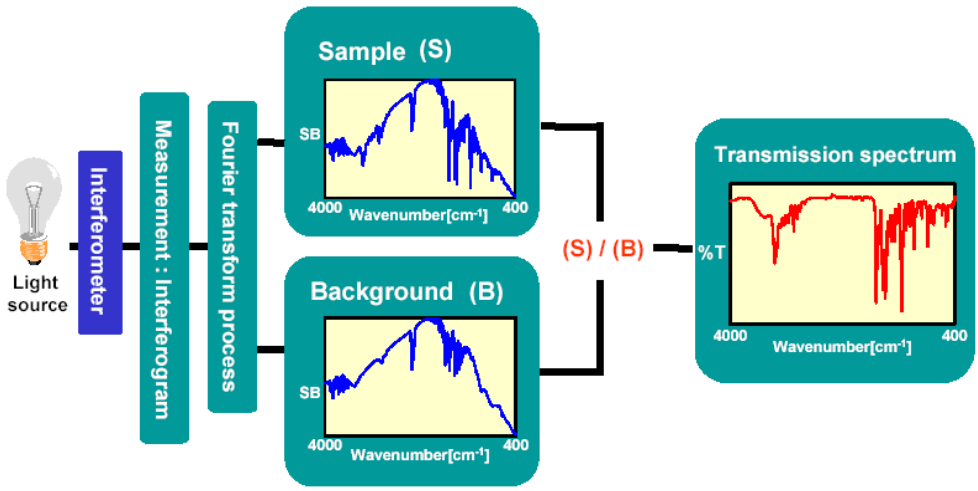

(Jasco, FTIR seminar)

Figure II-17: FTIR absorption positions

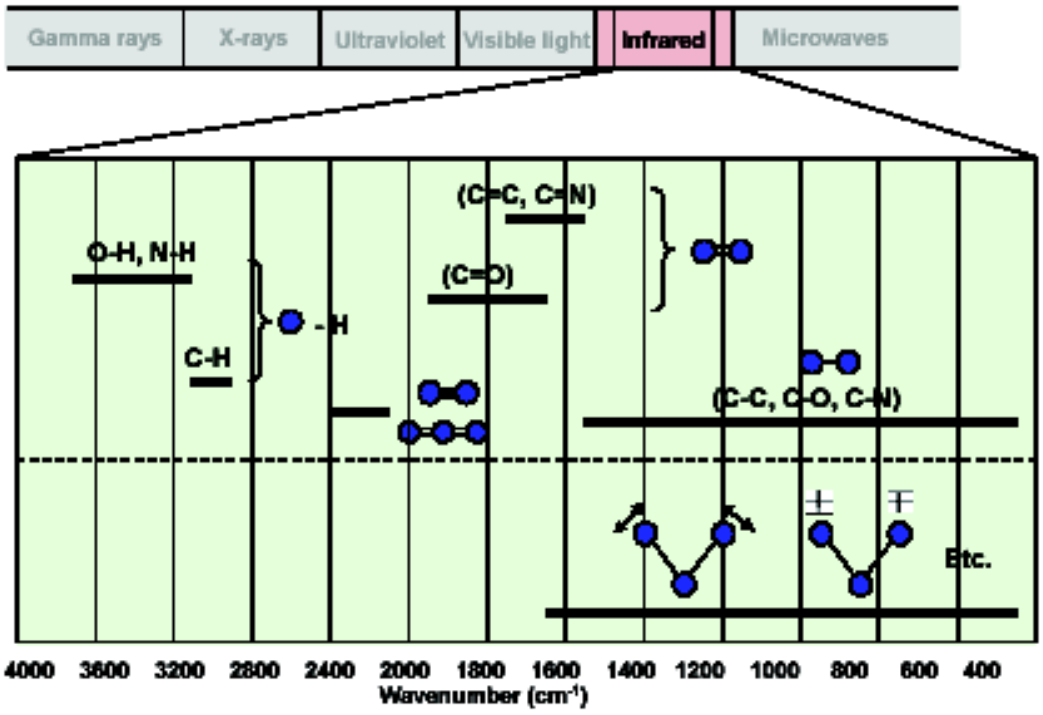

(Jasco, FTIR seminar)

Infrared spectra are obtained by passing infrared radiation through the sample of interest and observing the wavelength of absorption peaks. The absorption of light at different wave lengths is an expression of the molecular structure of the compound to be analyzed. For data processing, Fourier Transform mathematics is used to turn the measured absorption values into molecular vibration and rotation information for the analyzed samples. Figure II-17 shows the absorption positions of different chemical bonds (FTIR seminar, Jasco, France). The qualitative analysis can be done through the analysis of functional group and patterns to determine the existence of functional groups by the presence of specific functional group peaks while pattern analysis is to estimate compound materials by comparing standard spectra.

Quantitative analysis is possible since the strength (absorbance) of the absorption band is proportional to the number of molecular interactions. Transmission and reflection are two techniques to measure molecular interactions further via FTIR. Both techniques support liquid samples. Attenuated Total Reflectance (ATR) FTIR has been widely used to analyze aqueous solutions (Sperline et al., 1992; Dunn et al., 2002; Kolhed et al., 2003). ATR-FTIR provides a unique configuration in which the infrared spectrum of a liquid phase can be obtained in a slurry in-situ without phase separation. Figure II-18 illustrates the principle of ATR-FTIR. The IR penetrates a fraction of a wavelength beyond the reflecting surface into the rarer medium of refractive index n_2 and there is a certain displacement D upon reflection (Harrick, 1967). Using ATR techniques, surface layer information can be measured in a nondestructive manner and there is no need for sample preparation, and state analysis is possible (Jasco, FTIR seminar).

Figure II-18: Principle of ATR-FTIR.

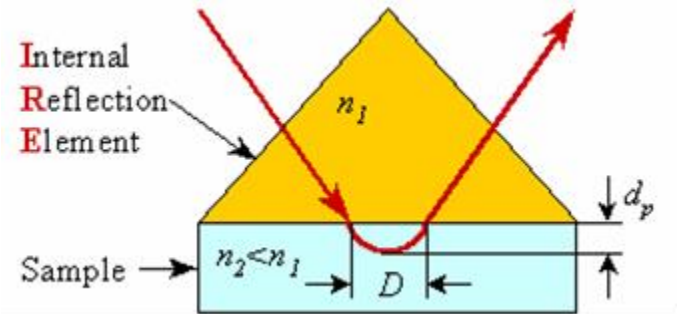

Wolkers et al. (2004) studied different sugar glasses and showed the OH stretching of dextran was around 3400 cm^{-1} wavenumber (Figure II-19).

Figure II-19: IR region of the OH stretching region of different sugars at 24ºC.

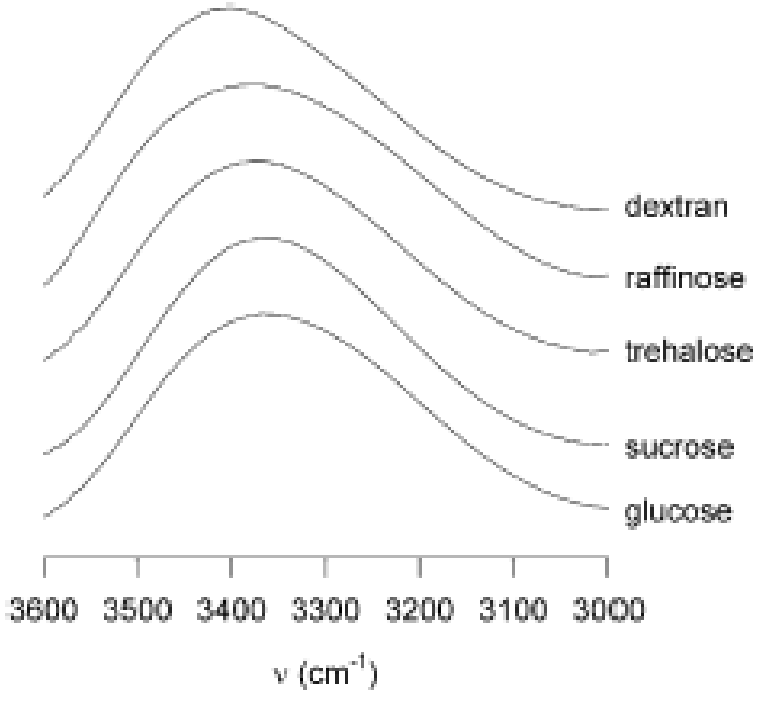

(Wolker et al., 2004)

H. Rheological properties of polymer solution

Rheological properties such as viscosity and viscoelasticity offer useful information to understand structural changes in materials an in particular to evaluate order disorder and conformational transitions.

1. Viscosity

Viscosity is a property of fluids that indicates resistance to flow. The viscosity (η) is the tendency of the fluid to resist flow and is defined by:

$$\eta = \frac{shearstress}{shearrate}\left(Pa \cdot s\right)$$

Increasing the concentration of a dissolved or dispersed substance generally gives rise to viscosity (i.e. thickening), as does increasing the molecular weight of a solute. With Newtonian fluids, typically water and solutions containing only low molecular weight solutes, the viscosity is independent of shear strain rate and a plot of shear strain rate against shear stress is linear and passes through the origin (figure II-20). At moderate concentrations above a critical value, C*, polymer solutions exhibit non-Newtonian behavior where their viscosity depends on the shear strain rate.

Figure II-20: Polymer viscosity behavior.

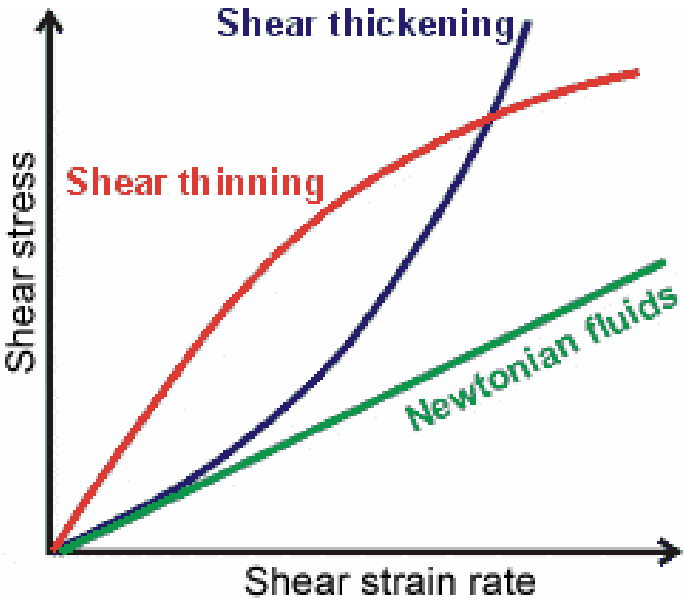

Polymers can be modified to achieve different applications. Ionic amphiphilic dextran derivatives were synthesized by the attachment of hydrophobic groups on the native polysaccharide. Amphiphilic dextrans have been used to modify the surface of nanospheres and microparticules used as drug delivery systems (Rouzes et. al, 2000; Fournier et. al., 1998). Vieira et. al. (2003) stated that the presence of hydrophobic groups bound to the polysaccharide chain can lead to the formation of large aggregates, which can change solution properties such as viscosity, surface tension and solubility.

When polymers experience phase transitions like gelation, crystallization, and retrogradation, the viscosity response would change. Knowledge of a constitutive relation between the viscosity and the relative degree of transition is extremely important in modeling, predicting, and interpreting the transformation process of polymers. Acierno

and Grizzuti (2002) found that before reaching a “solidified” state, the crystallizing polymer showed a yield stress of the order of 100 Pa. An order of magnitude increase can be appreciated at the lower shear rates compared to amorphous polymers. As long as dilute liquid-like behavior is observed, all viscosity curves seem to converge over the corresponding complex viscosity curves especially at higher frequencies. Figure II-21 shows the shear viscosity at different crystallization stages. Goossens and Lemstra (2006) stated that the degree of the polymer orientation depends on the strength of the flow, the molar mass distribution and the temperature. When a crystallized polymer is subjected to shear stress, the orientation might change affecting viscosity. As shown in Figure II-22, a large decrease in viscosity with silica concentration (increase orientation) can be observed.

Figure II-21: Isotactic polypropylene steady state shear viscosity as a function of the shear rate and at different crystallization stages.

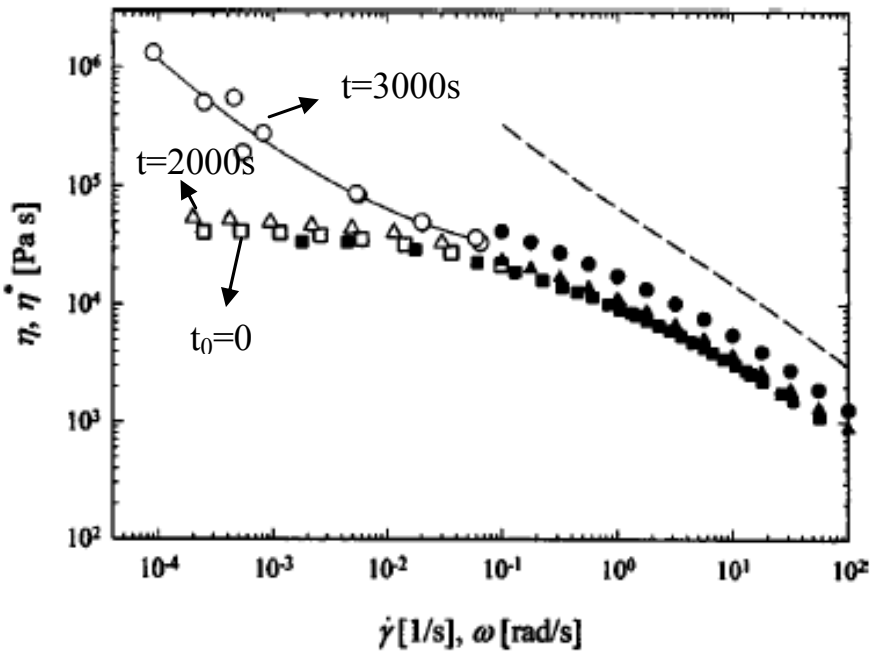

(Acierno and Grizzuti, 2002)

Figure II-22: The dynamic viscosity of silica-filled PP versus frequency at a 1% strain and 180ºC.

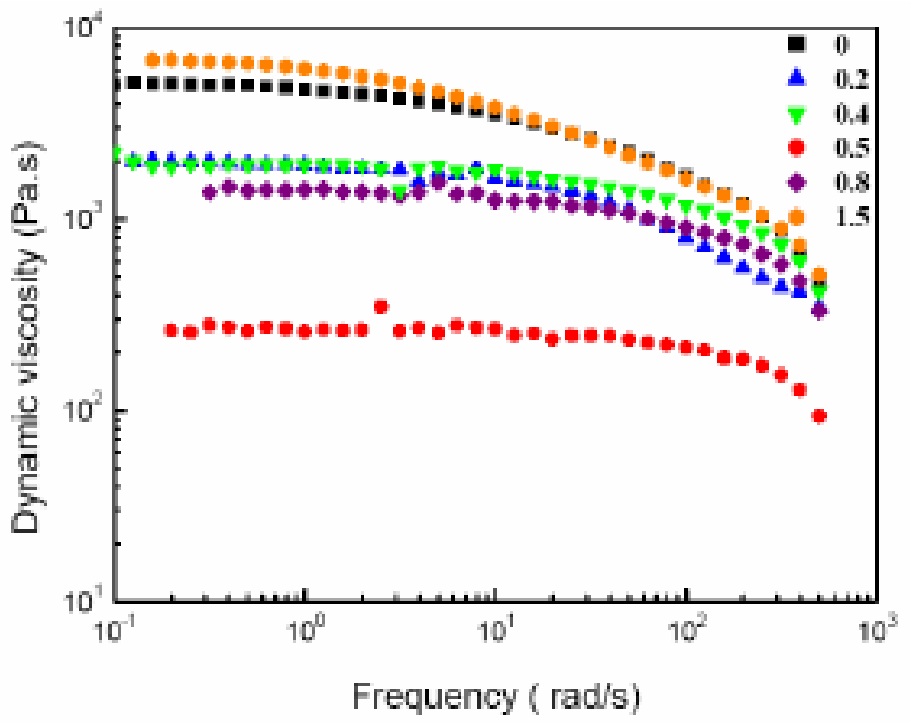

(Goossens and Lemstra, 2006)

2. **Viscoelasticity**

Most biopolymers of large molecular weight are viscoelastic, i.e. they exhibit solid (elastic) and liquid (viscous) like behavior. An elastic material will deform when subjected to an applied force and return to its original shape when that force is removed. In an ideally elastic system the amount of deformation characterized by strain is directly proportional to the force per unit area (stress). Because rheological properties of viscoelastic materials are both dependent on the magnitude of strain and strain rate hey demonstrate time dependence. They are often tested using dynamic methods in which the strain is oscillated at various frequencies and the resulting oscillatory stress is measured (Padmanabhan et. al., 2003).

Shear stress, shear strain and the ratio of stress to strain which is defined as a modulus are important terms used in polymer rheology. The shear stress and shear strain are defined as in figure II-23.

The complex modulus (G*) is the ratio of the shear stress to the shear strain as follows: $G^* = G' + iG''$. G' is called the storage modulus and G'' is called the loss modulus: $G^{**} = \sqrt{G'^2 + G''^2}''$.

At high strain rate and sufficient concentration polymeric molecules entangle and cannot de-entangle because the experiment time is lower than the longest relaxation time. This results in increasing values of the storage modulus and the system may become more ordered and elastic. Shear flow causes molecules to become more stretched and aligned with flow resulting in isotropic solutions becoming anisotropic. After cessation of flow molecules relax back with time if the time allowed is larger than the longest relaxation time. At low concentrations below the critical value (C*), the shear modulus of polymer

solutions is mainly determined by the loss modulus at low frequencies. G' becomes more important at higher frequencies. At higher concentrations in viscous solutions G' is generally greater than G" throughout a wide frequency range. This difference is very large for strong gels when the frequency has almost negligible effect (i.e. G' is much larger than G" for gels and in particular strong gels which makes them highly elastic materials). Gels form as a result of crosslinks or long range entanglements essentially creating infinite molecular materials. This typically happens above a critical concentration specific to the hydrocolloid, where junction zones occur as a result of intermolecular associations.

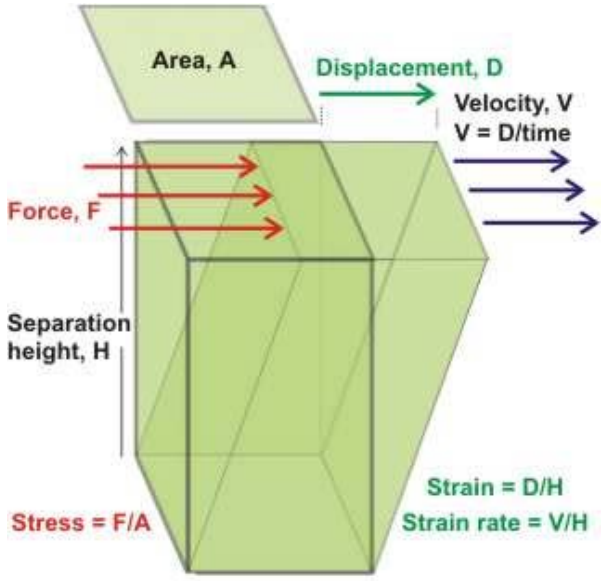

Figure II-23: Definition of shear stress and shear strain.

Van Soest (1996) studied the tensile properties of waxy maize starch with different water content and crystallinity (Figure II-24). When water content was low, samples were glassy. When water content was high, samples were in the rubbery state. Amorphous waxy maize in the rubbery state is a soft gel, having low tensile strength and

modulus. A semi-crystalline thermoplastic starch has higher values of tensile strength and tensile modulus.

Loret et. al. (2004) studied a gel developed in concentrated maltodextrin solution due to crystallization. A typical example of the variation of the storage modulus, G', and the loss modulus, G", during maltodextrin gelation is shown in Figure II-25. During a first induction period, the sample remains clear and the rheological response is fluid-like (G'<G"). When crystallization occurs, gelation takes place and particles are formed and the optical density increases. During this period the rheology remains largely unchanged. Crystallites provide the building blocks from which the gel forms, a network is formed, as indicated by an increase in G', this is governed by further crystallization and rearrangement. Diffusion of macromolecules slows due to high viscosity of the sample.

Figure II-24: a) Influence crystallinity on the strain behavior of waxy maize starch. b) Influence degree of crystallization on the stress-strain properties of the waxy maize starch.

a)

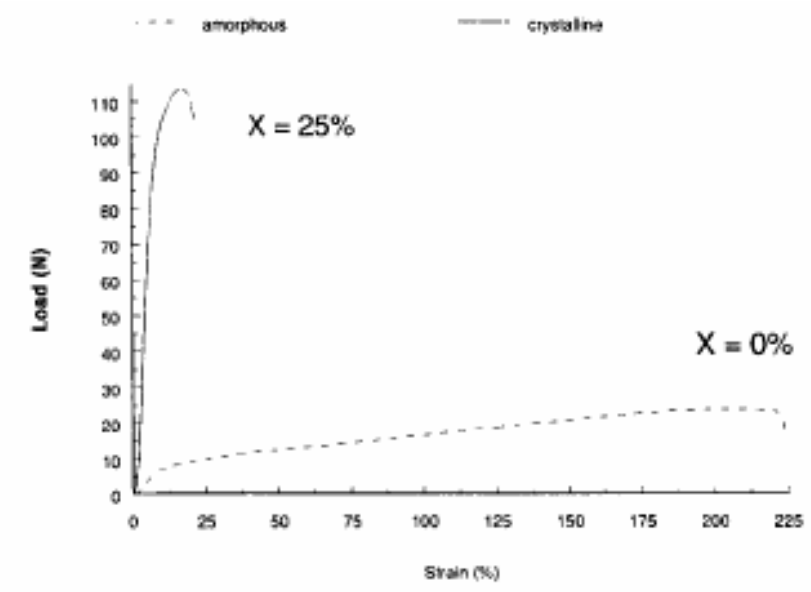

b)

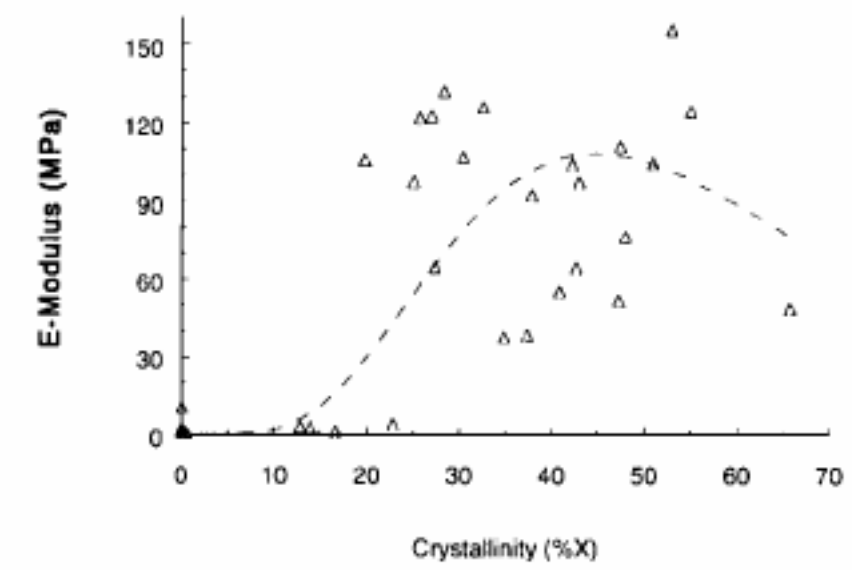

Figure II-25: Variation of G' and G" and evolution of optical density as a function of time for 25% maltodextrin sample.

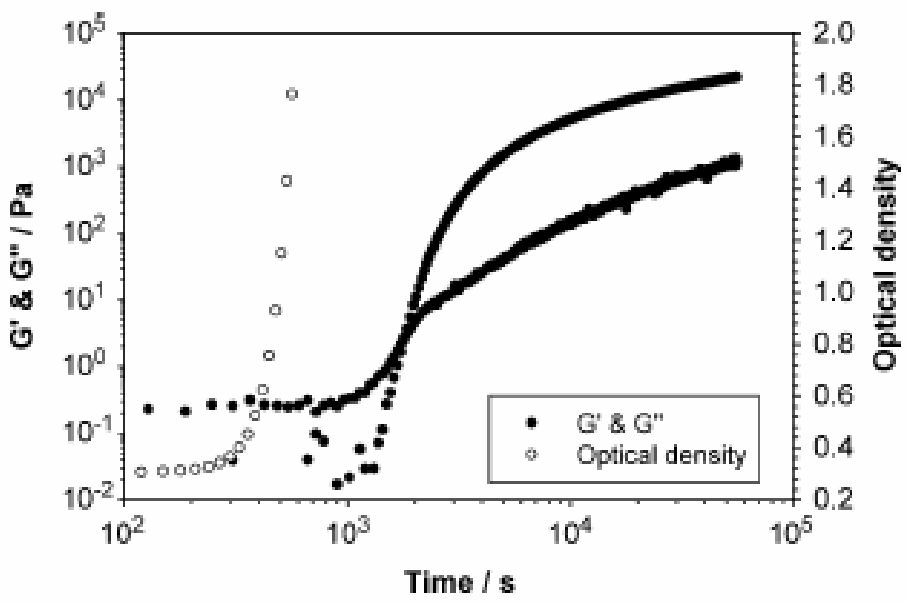

(Loret et. al., 2004)

III. Materials and Methods

A. Materials

Dextrans with molecular weight 960 ~ 2,000,000 were purchased from GE Healthcare (formerly Amershame Biosciences, New Jersey) and Pharmacosmos (Denmark). When Amersham Biosciences, now GE Healthcare, terminated production of Dextran, Pharmacosmos entered a worldwide agreement with Amersham to overtake its supplies of its high quality pharmacopeial Dextran products. Pharmacosmos is manufacturing Dextran with the same quality as Amersham Biosciences/GE Healthcare and with same degree of branching and dextran fractions are characterized by their average molecular weights and molecular weight distributions. The dextrans used in this study are technical grade dextran which are high purity Dextran fractions with selected average molecular weights and molecular weight distributions.

In this study, all dextran samples are prepared in aqueous solutions with concentration up to 75%.

B. Methods

1. Strategy of research

The experimental work can be divided into 2 regimes: a) dilute solutions and moderate concentration solutions ($<2C^*$) and b) concentrated solutions ($\geq 3C^*$) where C^* is the concentration where the solution transitions from dilute to concentrated. In the first

part of this study, under dilute concentration environment, dextrans molecule conformation were determined; in dilute solution, the zero shear viscosity of dextran at different concentrations was obtained and the overlap concentration of dextran at different molecular weight was determined.

The second part of this study was to understand the molecular interaction between dextran molecules and its solvent. Phase behavior of dextran in concentrated apparent solution was studied by Wide Angle X-ray scattering (WAXS), Differential Scanning Calorimeter (DSC), Rheology and Fourier Transform Infrared Spectroscopy (FTIR). All qualitative measurements except WAXS were at least duplicated and numerical average data are reported. Sample preparation

Dextran under low and moderate concentration environment was prepared by sprinkling the dry dextran powder into the vortex of the de-ionized water and blending for 30 seconds. The diluted samples for molecular conformation study had concentrations from 0.025 to 0.25 g/dl and were prepared in 50ml volumetric flasks. Samples subjected for viscosity measurements had concentrations from 1% to 45%. The resulting dispersion was then mixed by hand to help dissolving the powder lumps and the vortex was used again until complete dissolution of the particles. All sample preparations were conducted at room temperature (~23ºC). Molecular conformation measurement is sensitive to temperature so a water bath set at 25ºC±1ºC was used. Concentrated dextran (3C*) were prepared by suspending the corresponding amount of dry dextran powder into 10 gram de-ionized water and the suspension was mixed by hand for 10 minutes to completely hydrate the particles when sample formed a transparent solution. The air bubbles in the liquid were removed by Fisher Scientific centrifuge at 11×10^3 RPM for 2 minutes.

Sample preparations were done at room temperature (~23ºC). All the resulting samples were used for measurements right after preparation or sealed in glass vials and centrifuge tips to prevent water loss till the desired aging time.

2. Capillary viscometry measurements

The intrinsic viscosity of each sample at a certain concentration was determined from data obtained using a size 50 Cannon Fenske capillary viscometer shown in Figure III-1. Measurements were made in a constant temperature both at 25±1ºC. Dextran solutions of 0.025, 0.04, 0.075, 0.1, 0.15 and 0.25 g/dl were prepared and viscosities measured. Seven milliliters of dextran sample were pipeted into the viscometer. The liquid level was raised using rubber bulb. When the suction was released, the liquid level dropped due to the gravity. A stop-watch was used to record the time for the liquid level to drop between the etched lines. The time t was recorded and used to determine the kinematic viscosity, v, according to the following equation:

$$v = tc \quad \text{(Equation III-1)}$$

where t represents time in seconds for the liquid to drop and c is the viscometer constant for a given viscometer. The constant for the size 50 Cannon Fenske viscometer used for this research was 0.004038 centistoke/second. Kinematic viscosity ν must be converted from Centistokes to centapoise through the following equation:

$$\eta = v\rho \quad \text{(Equation III-2)}$$

where ρ is the density of the solution. Density is determined using a Gay Lussac pycnometer (Figure III-2) and the following equation:

$$\rho = \Delta W / V \quad \text{(Equation III-3)}$$

where ΔW is the difference in weight before and after filling the pycnometer with sample solution and V is the volume of sample that is held. Measurements were at least duplicated and average data are reported.

Figure III-1: Cannon-Fenske Viscometer.

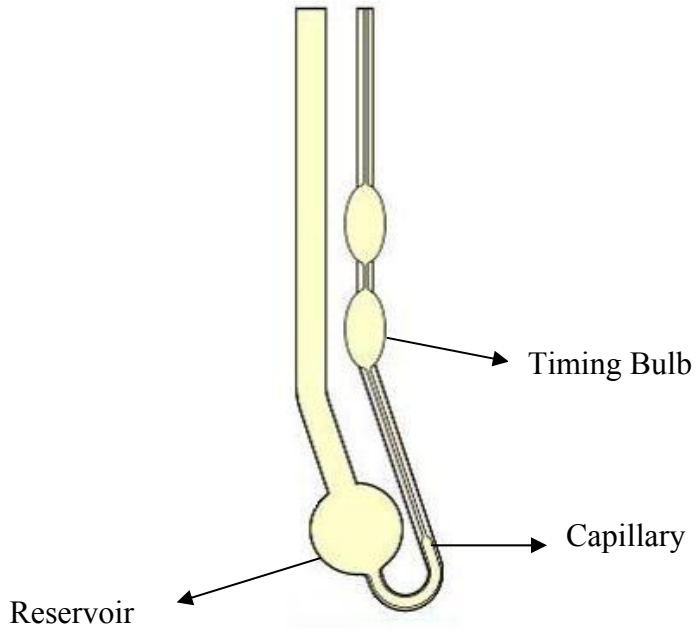

Figure III-2: Gay Lussac pycnometer.

3. Visual analysis

Visual observation of the physical behavior of the concentrated dextran samples were recorded as digital pictures at different aging times by Sony CyberShot DSC-W5 digital camera (5-megapixel, 3× optical zoom). Fluorescent light was the illuminated light source. Visual inspection was conducted on all prepared samples. All the concentrated samples were sealed in either hermetically sealed glass vial or parafilm wrapped centrifuge tips. The whole sample holder and sample were weighted within the observation time to make sure there is no water loss.

4. Wide angle X-ray scattering

As an X-ray beam travels through a substance, electrons surrounding the nuclei in atoms scatter X-rays in specific directions which are dependent on the conformation of the substance. Wide angle X-ray scattering (WAXS) is an X-ray diffraction technique that is often used to determine the crystalline structure of polymers. This technique specifically refers to the analysis of Bragg Peaks scattered to wide angles, which implies

that they are caused by small structures. These X-ray diffraction patterns are governed by Bragg's law:

$$n\lambda = 2d\sin(\theta) \quad \text{(Equation III-4)}$$

where n is an integer, λ is the wavelength of x-rays, d is the spacing between the planes in the atomic lattice and 2θ is the angle between the incident and diffracted rays.

Each reflection corresponds to a specific *d*-spacing which is a function of the molecular conformation and the reflections are captured on a refraction image. This is the crystalline signature of a crystal. A high density of reflection is collected as a ring on the image and the intensity of the reflection is related to the concentration of spatial arrangement of the individual atoms.

When the reflection intensity is plotted against 2θ a diffraction pattern is obtained. Individual peaks on a diffraction pattern correspond to individual rings on the diffraction image. The intensities of the peaks on a diffraction image serve as an indication of both the molecular shape and the packing arrangement within and between unit cells in the substance (Sperling, 1992).

Samples for analysis included dextran T10 66%, T70 42% and T500 21% solutions at different aging time from 0 hour up to 4 hours. T10 66% samples were also scanned after 1 day and 4 days. All the reported X-ray diffractograms are marked from a to z according to their aging time. Freshly prepared concentrated dextran sample was loaded in a capillary glass tube. The capillary tube was sealed with wax at both ends to prevent water loss from the sample. Samples were analyzed using an X-ray

diffractometer (Crystallographic Laboratory Chemistry Department, Rutgers University, New Jersey) consisting of HiStar multiwire area detector (Bruker AXS, Wisconsin, USA) a 3-kW FR571 rotating-anode X-ray generator (Nonius, 40 kV and 50 mA) with graphite monochromatized fine-focus Cu Kα radiation (λ=0.1514 nm). The capillary tube with concentrated dextran sample was then scanned every 5 minutes up to 6 hours. The same capillary sample tube was kept in a petridish at room condition for longer aging time. After 3 days and 4 days the samples were also scanned with the same experiment set up. An empty glass capillary tube was scanned with the same set up before the real measurement to make sure no reflections from the tube itself was counted as from the sample.

Crystallinity was defined by Chinachoti and Steinberg (1986) as the ratio of peak area (crystalline material) to the total area (crystalline and amorphous material). The ratio value represents percent crystallinity on a total material basis. The area of the peak and in the amorphous region was calculated by automated image analysis software SigmaScan Pro Version 3.00. Figure III-3 shows an example of this method in determining the crystallinity on the diffraction pattern of concentrated dextran with 1 day aging time. % crystallinity equals 100×blue area/ (blue area + red area). In this case, the sample crystallinity is 11.703%. There was no duplication of the X-ray diffraction measurement due to the limited availability of the equipment.

Figure III-3: Example of calculation of relative crystallinity: X-ray diffraction pattern of dextran T10 66% with 250 min aging time.

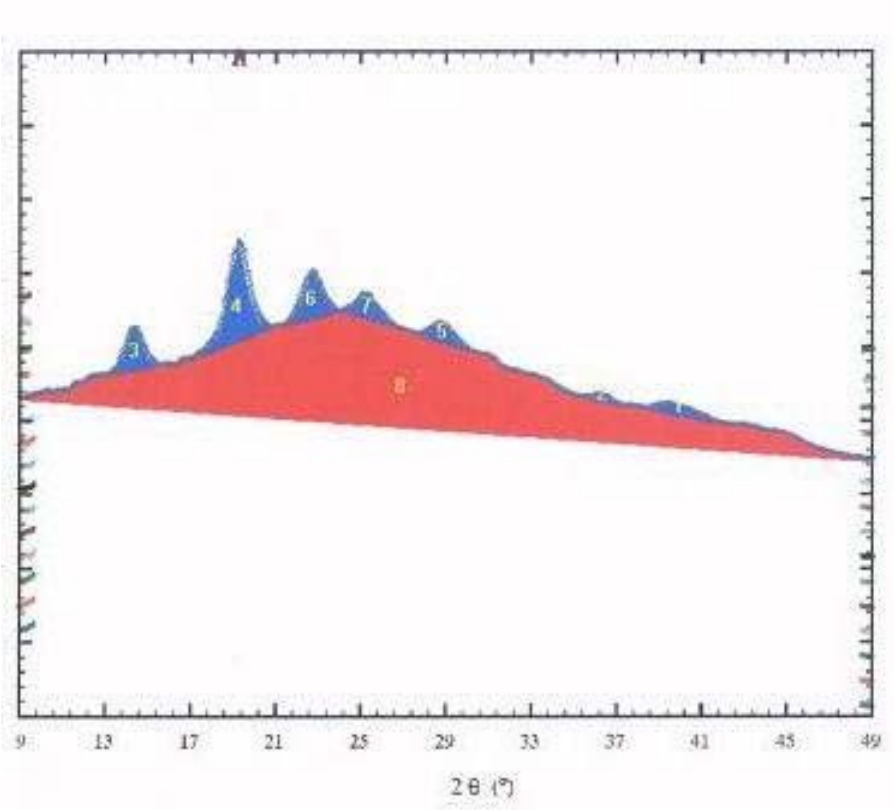

5. Differential scanning calorimetry

Concentrated dextran samples with different aging times were analyzed using DSC 2920 (TA instruments, NJ) to characterize the melting properties of the crystalline material that developed with time. Perkin-Elmer large volume stainless steel pans and lids with O-rings which would hold high temperature and high pressure were used. The Viton™ O-Ring allows formation of a seal which suppresses the vaporization of a solvent or contains a volatile reaction product, thereby eliminating the interfering effects of the heat of vaporization. Capsules can withstand an internal pressure of 24 atmospheres which equivalent to the water vapor at 220°C. Large sample capacity yields higher sensitivity. The fresh dextran solutions were weighted into DSC stainless steel pans and hermetically sealed right away with a rubber O-ring and stainless steel lid to prevent water loss. Dextran samples were aged in the sealed DSC pans till the desired time. The DSC pans with dextran samples were weighted several times before DSC analysis to ensure there was no moisture loss. Each dextran sample was heated from 0°C to 200°C at a heating rate of 10°C/min. Melting of crystal constitutes a first-order phase change. On the DSC scan it is characterized by an endothermic peak. In the melting endotherm of the dextran, the midpoint in the melting temperature range was at about 170°C. Figure III-4 shows a melting endotherm for 66% dextran T10 with 1 day aging time. The integration of the peak leads to the melting enthalpy which corresponds to the sample crystalline content (Chung et. al., 2004).

Figure III-4: DSC melting endotherm of 66% dextran T10 with 1 day aging time.

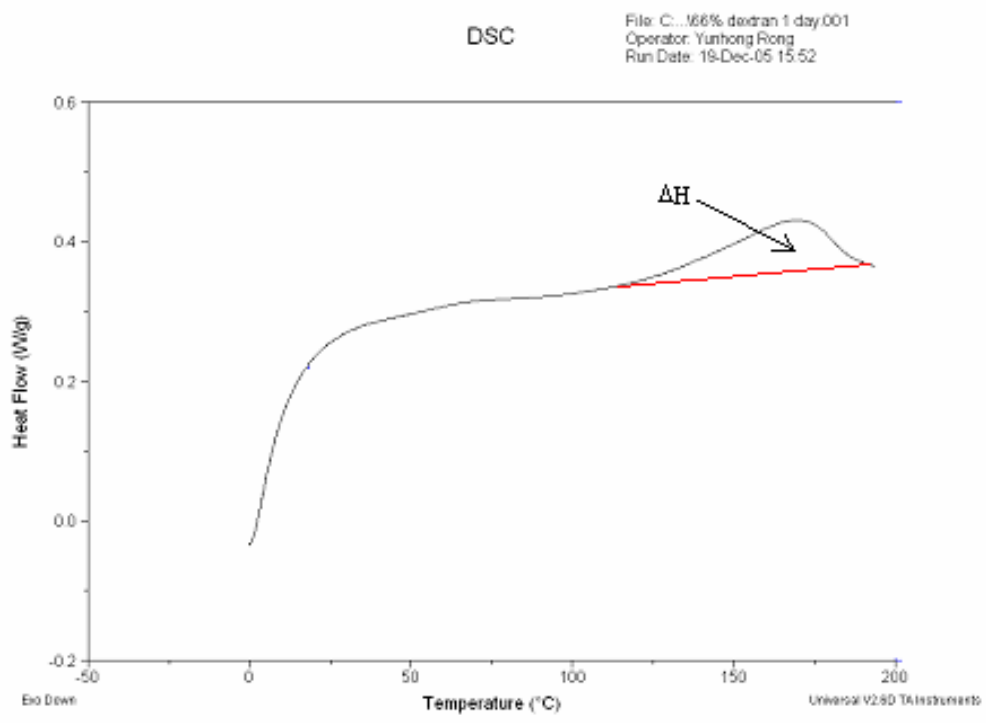

6. Rheological measurements

Rheological measurements were conducted using a strain-controlled rheometer, the Advanced Rheometric Expansion System (ARES) (TA Instruments, NJ). Parallel plate (25 mm and 50 mm diameter and 25 mm diameter serated) and cone and plate (25 mm, 0.1 radians cone angle and 50 mm diameter, 0.04 radians cone angle) geometries were used, depending on the sample viscosity. The gap for parallel plate was 1000 microns and for cone and plate was 50 microns. A new sample was used in every measurement to avoid structure change by rheological measurement. Measurements on samples with the same concentration were at least duplicated. The parallel plate and cone and plate geometries are illustrated in Figure III-5a and b.

Figure III-5: ARES geometries a) parallel plates; b) cone and plate.

a)

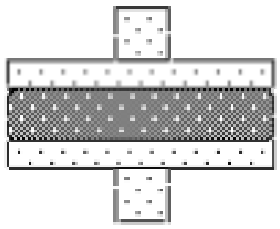

b)

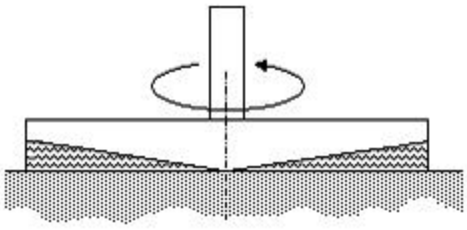

a) Steady shear

Steady shear measurements in which the apparent viscosity (η) was plotted against shear rate ($\dot{\gamma}$) were conducted at an increasing shear rate from 0.5 to 100 s^{-1} with 15 data points per decade. In order to avoid the underestimation of the viscosity due to slip (sample lost contact with the plates at high shear rate), serrated plates were used for the measurements of aged concentrated dextran samples which have the consistency of a concentrated suspension. The experiments were conducted at ambient temperature around 23ºC. For dextran at low and moderate concentration environments steady shear technique was used to obtain the zero shear viscosity. Zero shear viscosity is the viscosity at vanishing shear rates. Zero shear viscosity provides a consistent, uniform comparison with different systems. For dextran at concentrated environment apparent viscosity of the samples were measured.

b) Strain sweep

Strain sweep is utilized to determine the linear viscoelastic region of a material during a small amplitude oscillatory test. The maximum strain up to which G' remains constant is called the critical strain. The critical strain, which indicates the minimum energy needed to disrupt the structure, is material dependent. Therefore, if the difference in the critical strain of two samples is known, the different extent of dispersion of particles or ingredients can be measured. The higher the critical strain, the more stable the structure is under shear.

c) Small Amplitude Oscillatory Measurements

In dynamic analysis the lower plate of the geometry is oscillated at a constant frequency with selected amplitude of oscillation. Strain sweep measurements at a constant frequency are conducted to find out the region of linearity, where the rheological properties are independent of the imposed strain. Strain sweeps were conducted at strain values ranging from 0.1 to 100%. Frequency sweeps were run at the appropriate strain within the linear region for each particular sample. All dynamic analyses were carried out at room temperature around 23ºC. The data of interest are the complex viscosity and both components of the complex moduli. The storage and loss moduli, G' and G" as a function of frequency, were recorded at several concentrations with different aging times.

d) Cox-Merz rule

The empirical Cox-Merz rule relates complex viscosity η* (from oscillatory rheometry) to shear viscosity η (from steady shear flow) as follows:

$$\eta\left(\dot{\gamma}\right) = \left|\eta^{*}(\omega)\right| \text{ at } \dot{\gamma} = \omega \quad \text{(Equation III-4)}$$

This rule has been found to be non-applicable to biopolymer dispersions with high-density entanglements or aggregates (Bistany and Kokini, 1983). Padmanabhan et al. (2003) showed that the functional dependence of η and η* of a water-insoluble dextran were different and they did not show any tendency to converge (Figure III-6). The difference may be from the certain dextran structured systems.

Figure III-6: Steady shear viscosity and complex viscosity plotted against shear rate and frequency for water-insoluble dextran sample (250mg/ml).

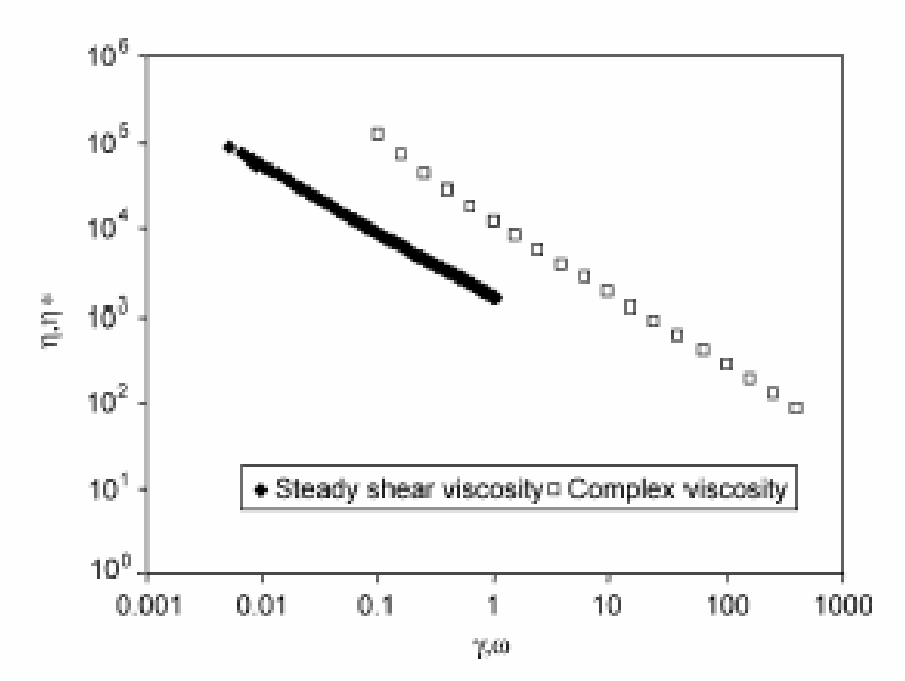

(Padmanabhan et al., 2003)

7. Fourier Transform Infrared Spectroscopy

Dextran samples with different concentrations and different aging times were analyzed by a thermal Nicolet Nexus 670 FT-IR with Mid-IR, Near IR, Liquid N_2 MCT detectors, Attenuated Total Reflectance (ATR) and Smart SAGA Grazing Angle reflectance accessories. The FTIR absorbance spectra as averages of 100 scans at a resolution of 4 cm^{-1} were recorded. The samples with the same concentration were scanned at lease in duplicate. A new sample was prepared for the duplication.

The air absorbance background was subtracted from the sample scans to prevent peak overlays. All the FTIR analyses were conducted at room temperature around 23ºC.

IV. Results and discussion

A. Rheological measurements of dextran in dilute and moderate concentration environment

Several rheological analysis techniques were used to generalize the solution behavior of dextrans in solution and predict their conformation and overlap concentration and measure intrinsic viscosities and zero shear viscosity.

1. Intrinsic viscosity

The intrinsic viscosities of dextrans T1 to T2000 with molecular weight from 970 to 2,000,000 g/mol are shown in Table IV-1. In all cases, intrinsic viscosity increases as molecular weight increases.

The Mark-Houwink relationship between intrinsic viscosities and molecular weights was obtained by plotting intrinsic viscosities and molecular weights in a logarithmic plot. The relationship is shown in Figure IV-1.

From the relationship clear deviations from the linear range were observed for dextran with molecular weight lower than 5000 g/mol and higher than 70,000 g/mol. For dextran with molecular weight between 5000 and 70,000 a Mark-Houwink equation can be derived as $[\eta] = 1.05 \times 10^{-3} M_w^{0.51}$ (Equation IV-1). With α-value=0.51, dextran with molecular weight 5000 to 70,000 assumes a random coil conformation. When molecular weight is lower than 5 000 and higher than 70 000 the Mark-Houwin exponent α is small

Table IV-1: Intrinsic viscosities of different molecular weight dextrans.

Sample ID	intrinsic viscosity (dl/g)	M_w (g/mol)
T1	0.07	1047
T5	0.08	5200
T10	0.13	10800
T20	0.16	21400
T40	0.25	43000
T70	0.30	67200
T500	0.48	482000
T2000	0.52	2000000

Figure IV-1: Mark-Houwink relationship of dextrans.

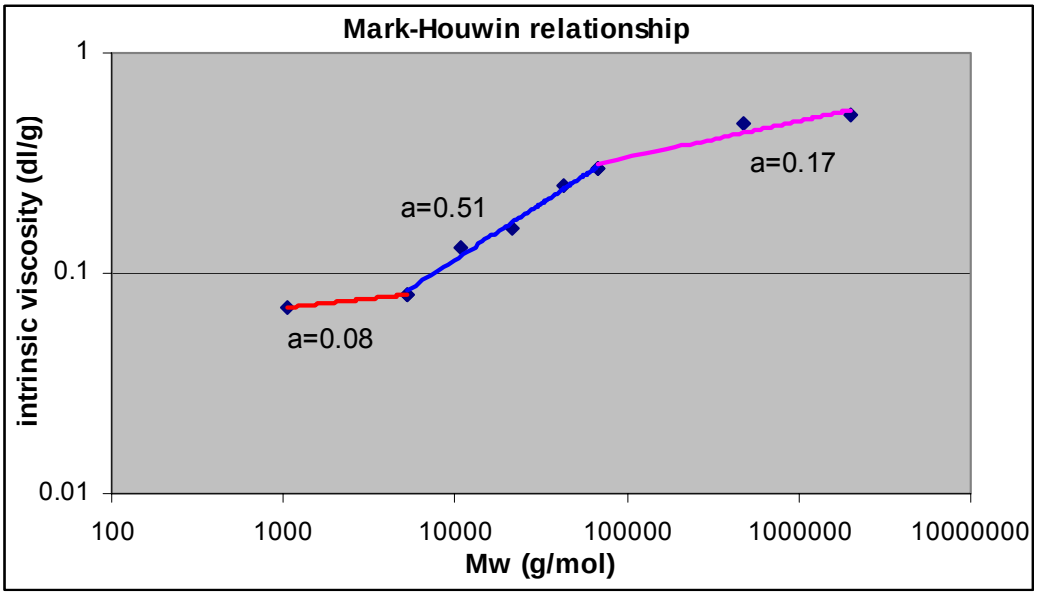

which indicates a more extended molecular conformation. For M_w higher than 10^6 α =0.17 which is comparable to the literature value of 0.22 (Senti et al., 1955). The upward curvature at lower molecular weight indicates that small molecular weigh dextran has a more expended conformation. The downward curvature at higher molecular weight means the higher molecular weight dextran has long chain branches.

2. Steady shear measurements

Dextrans with a random coil conformation in between 5000 and 70,000 g/mol molecular weight were subjected to steady shear measurements. A higher molecular weight sample which has long chain branches was also measured. Samples with concentration 1%, 5%, 10%, 15%, 20%, 25%, 30%, 35%, 40% and 45% (wt/v) were selected for dextran T10, T40, T70 and T500. The steady shear viscosity vs. shear rate results for different molecular weights are shown in Figure IV-2 a, b, c and d. From the steady shear flow behavior of dextran T10, T40, T70 and T500, all the samples at low and moderate concentrations were Newtonian fluids. The viscosity increased with increase in concentration.

When shear rate was extrapolated to zero, a zero shear viscosity at each concentration can be obtained for dextrans T10, T40, T70 and T500. The zero shear viscosity vs. concentration plot for each dextran molecular weight are shown in Figure IV-3 a, b, c and d.

Figure IV-2: Flows behavior of different molecular weight dextrans at different concentrations, a) dextran T10, b) dextran T40, c) dextran T70, d) dextran T500.

a)

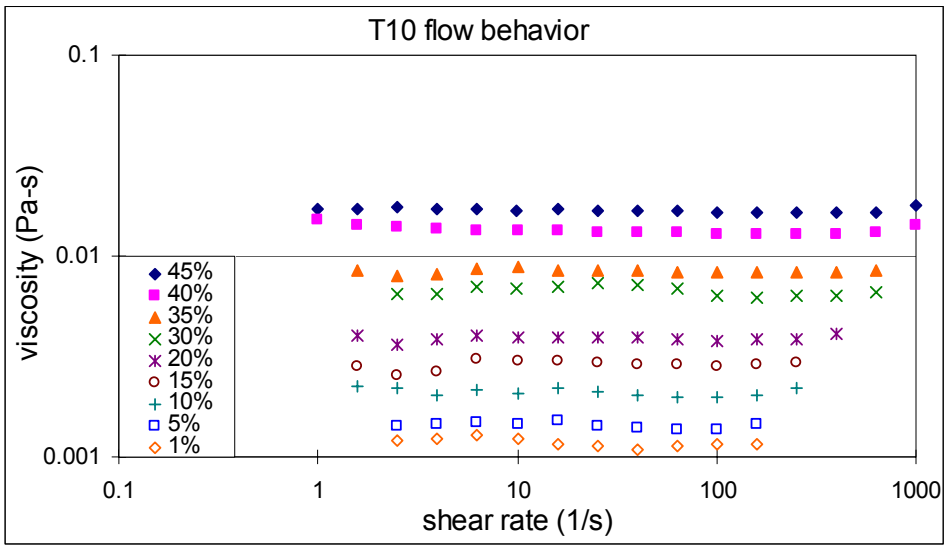

b)

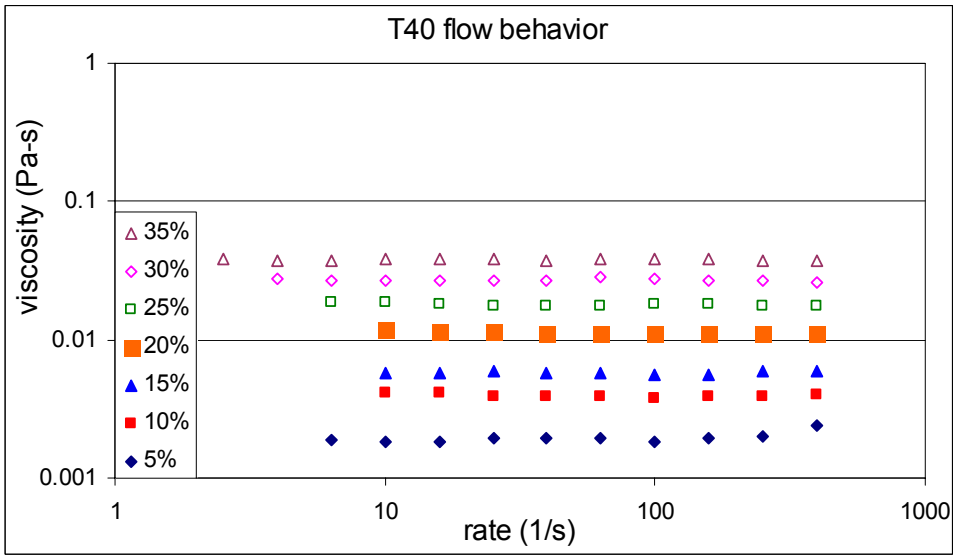

c)

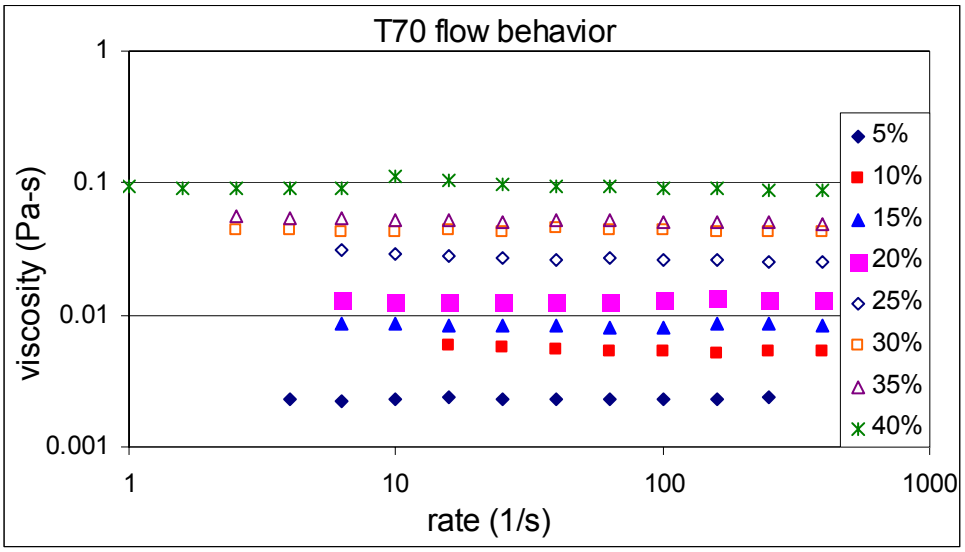
T70 flow behavior
viscosity (Pa-s)
1
0.1
0.01
0.001
1
10
100
1000
rate (1/s)
5%
10%
15%
20%
25%
30%
35%
40%

d)

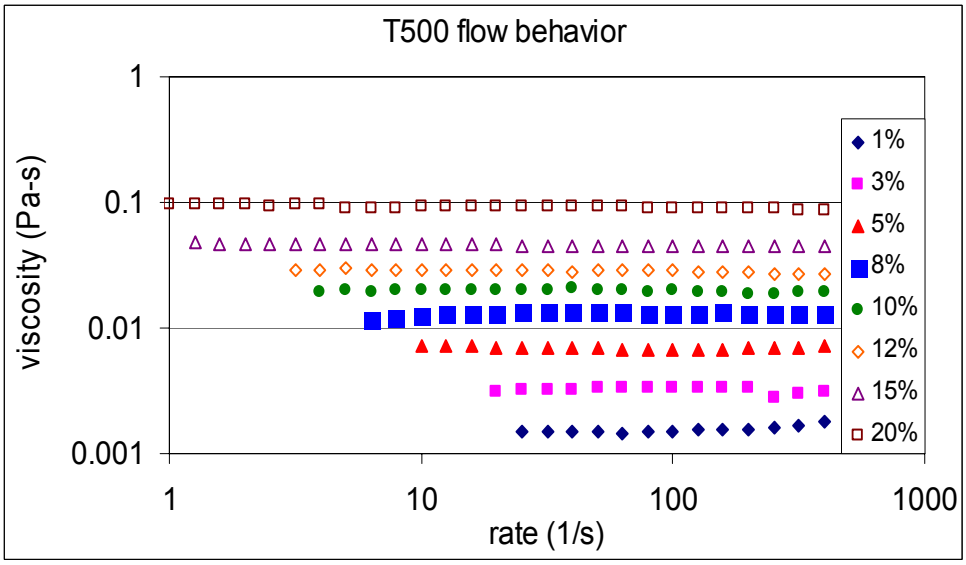
T500 flow behavior
viscosity (Pa-s)
1
0.1
0.01
0.001
1
10
100
1000
rate (1/s)
1%
3%
5%
8%
10%
12%
15%
20%

Figure IV-3: zero shear viscosity vs. concentration for different molecular weight dextrans a) dextran T10, b) dextran T40, c) dextran T70, d) dextran T5000.

a)

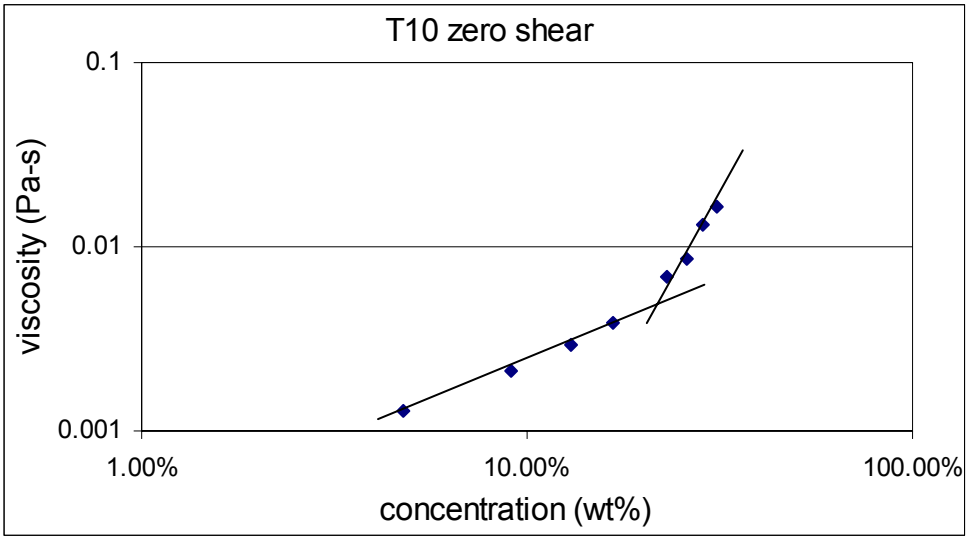

b)

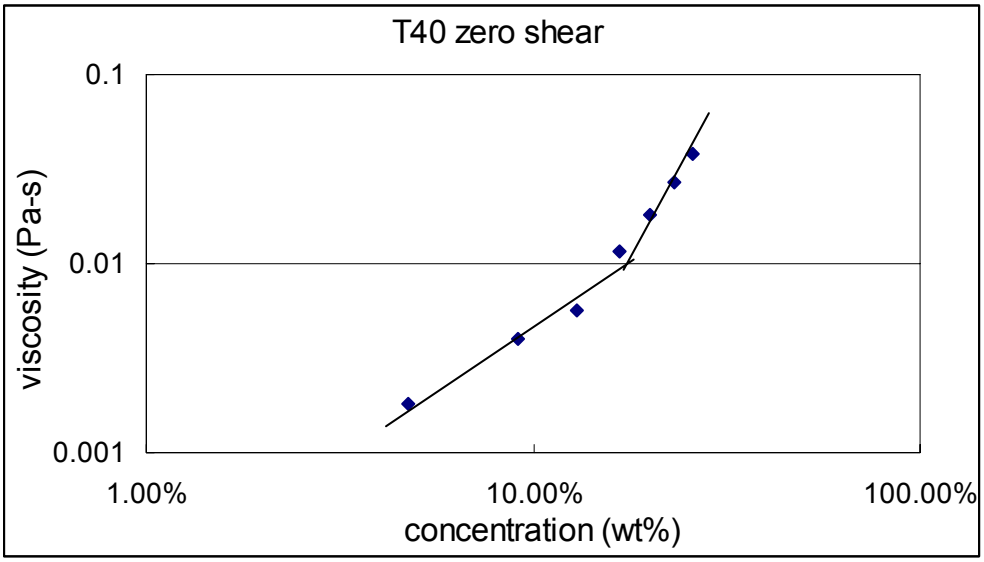

c)

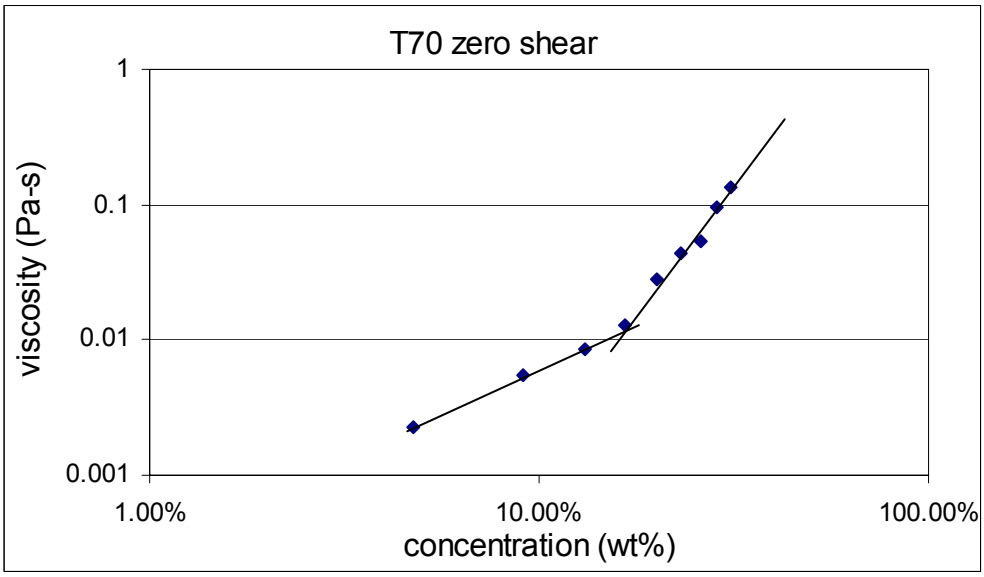
T70 zero shear
1
0.1
0.01
0.001
viscosity (Pa-s)
1.00%
10.00%
100.00%
concentration (wt%)

d)

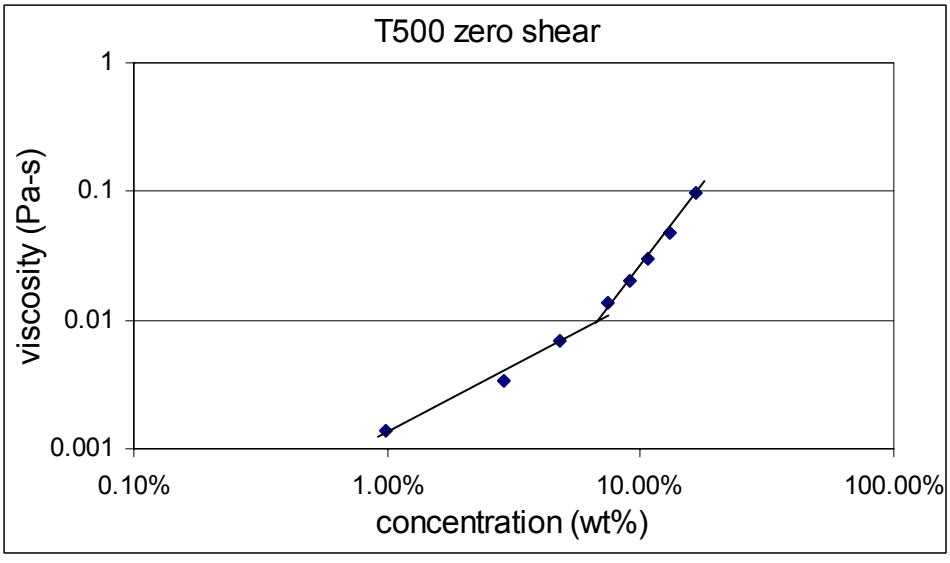
T500 zero shear
1
0.1
0.01
0.001
viscosity (Pa-s)
0.10%
1.00%
10.00%
100.00%
concentration (wt%)

From the change in slope of the zero shear viscosity vs. concentration plot, the overlap concentration for each molecular weight dextran can be determined and is shown in Table IV-2.

The overlap concentration decreases when molecular weight increases which is expected. When molecular weight increases, dextran long chain branches increases. The high molecular weight dextran with long chain branches occupies a greater hydrodynamic volume per unit mass than the lower molecular weight dextran. Thus a lower overlap concentration is expected for higher molecular weight dextran.

Table IV-2: Overlap concentration for different molecular weight dextrans.

Sample ID	Molecular weight	Overlap concentration (wt%)
T10	10 800	22%
T40	43 000	17%
T70	67 200	14%
T500	482 000	7%

B. Phase transition of dextran above the overlap concentration, in high concentration

1. Macroscopic behavior

Dextran T10 above the overlap concentration, at 3 times its overlap concentration (66%) showed a clear phase behavior change when observed even after 30 minutes of storage at room temperature. Dextran T70 and T500 with concentration of 3 times of their overlap concentration, 42% and 21% respectively, appeared homogeneous with no macroscopic signs of phase transition when observed even after 1 week of storage at room temperature.

The phase transition observed in dextran T10 concentrated samples with time was found throughout the span of the sample without phase separation. The aged sample was white in color, opaque and more rigid (after visual examination), while fresh sample was transparent and more deformable.

Figures IV-5, IV-6 and IV-7 show pictures for dextran samples T10, T70 and T500 at 3 times of their overlap concentrations, 66%, 42% and 21% respectively, at different aging time. Macroscopic phase transition occurred only for the dextran T10 66% sample.

Figure IV-5: Photographs of dextran T10 samples at 66% concentration with different aging time of: a) 0 hr; b) 1 hr; c) 2 hr; d) 3 hr and e) 4 hr at room temperature.

a) b)

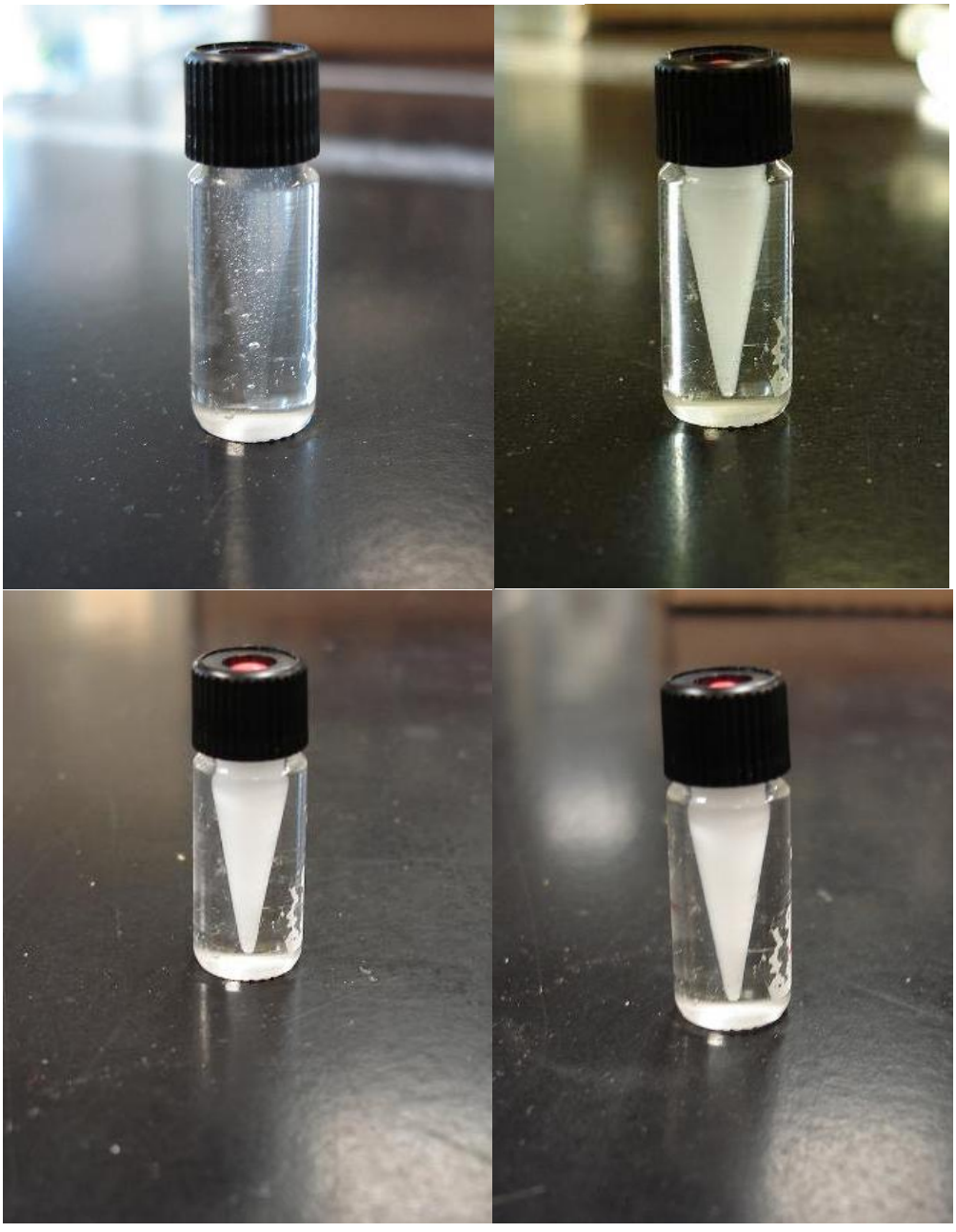

c) d)

e)

Figure IV-6: Pictures of dextran T70 samples at 42% concentration with different aging time of: a) 0 hr; b) 4 hr and c) 1 week at room temperature.

a)

b)

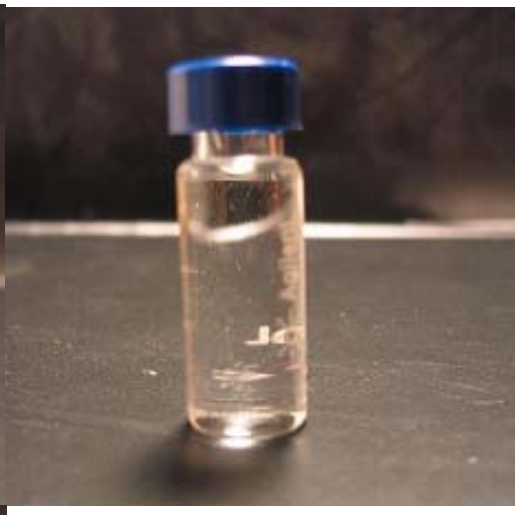

c)

Figure IV-7: Pictures of dextran T500 samples at 21% concentration with different aging time of: a) 0 hr; b) 4 hr and c) 1 week at room temperature.

a)

b)

c)

2. X-ray diffraction

Diffractograms showing the degree of crystallinity for dextran T10 66%, T70 42% and T500 21% systems are shown in Figure IV-8, IV-9 and IV-10. The diffractograms of dextran T10 samples were shifted by 20 units to have a better comparison.

Figure IV-8: X-ray diffractograms for dextran T10 66% at different aging times: a) 0 min; b) 25 min; c) 50 min; d) 75 min; e) 100 min; f) 125 min; g) 150 min; h) 175 min; i) 200 min; j) 225 min; k) 250 min; l) 275 min; m) 300 min; n) 1 day and o) 4 days.

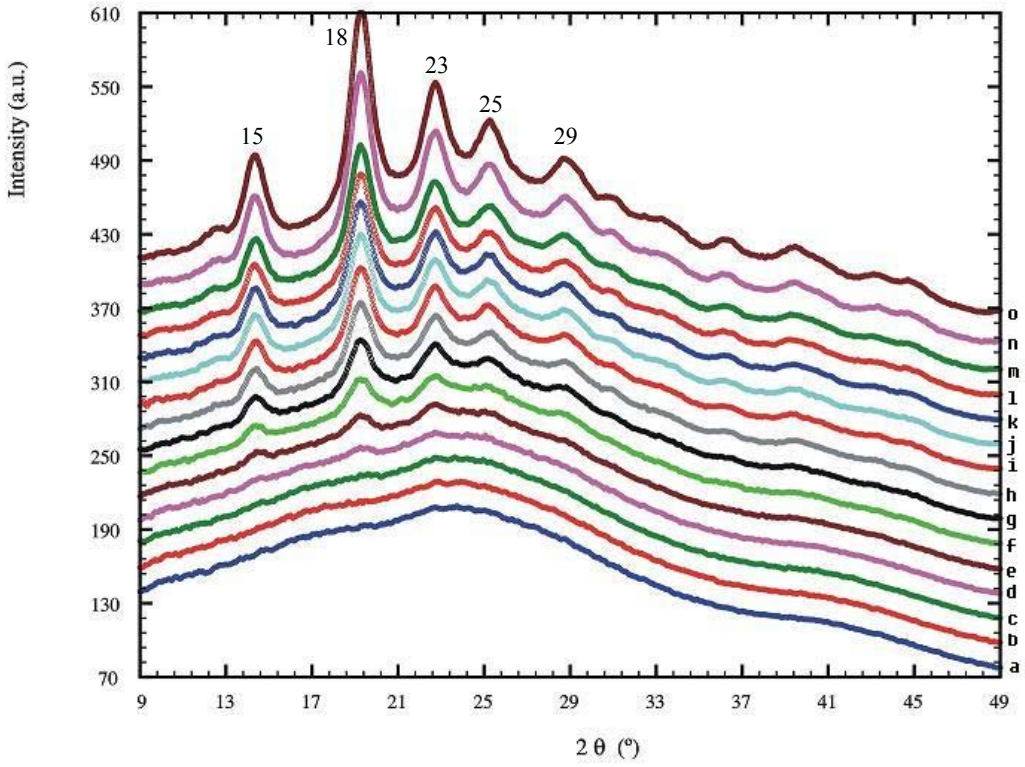

Figure IV-9: X-ray diffractograms for dextran T70 42% at different aging times: a) 0 hr; b) 1 hr; c) 2 hr; d) 3 hr; e) 4 hr.

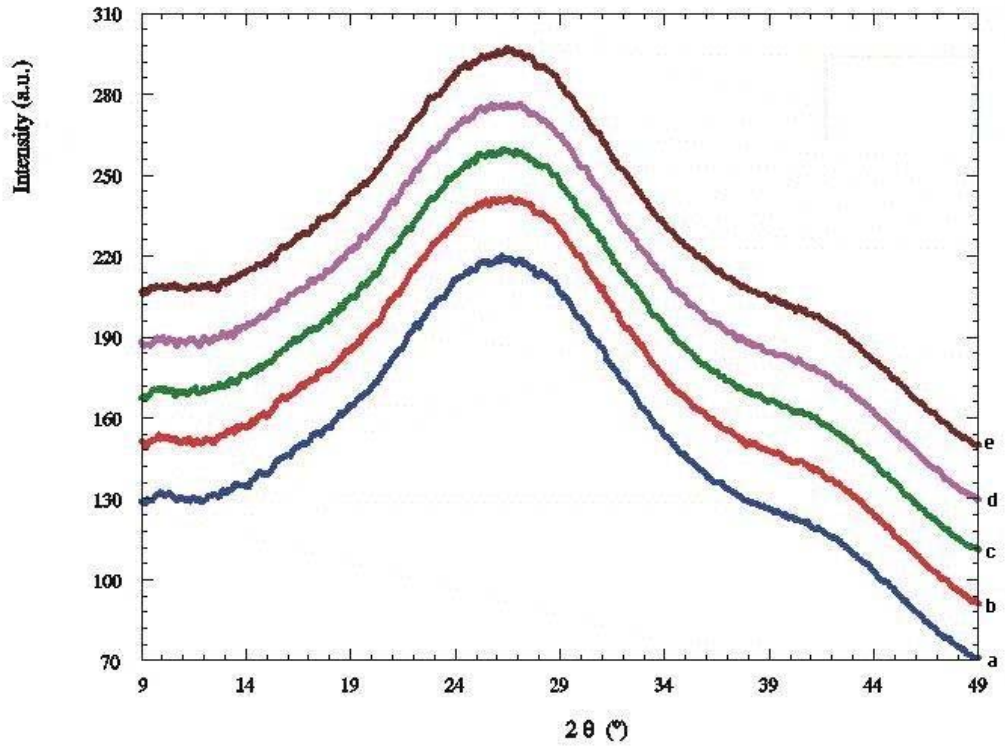

Figure IV-10: X-ray diffractograms for dextran T500 21% at different aging times: a) 0 min; b) 1 hr; c) 2 hr; d) 3 hr; e) 4 hr.

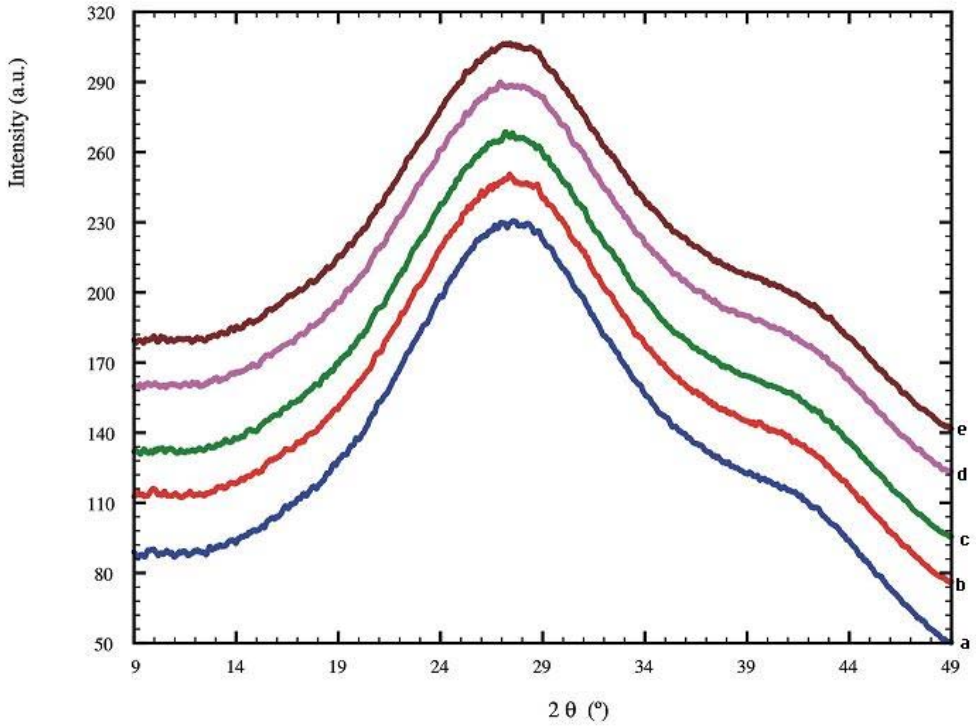

The X-ray diffraction analysis of dextran T10 66% samples revealed a change in the structure of the solution system in relation to the time. The diffractograms of the dextran T10 presented 5 distinct peaks for the Bragg angles of 15, 18, 23, 25 and 29 degrees. The diffraction at 15, 18 and 23 degrees is characteristic of C type starch/carbohydrate crystals. A strong peak at 18 degree is due to the presence of water in the sample. Higher crystalline regions were formed with increased aging, indicated by higher X-ray diffraction peak areas. The crystalline regions detected at 18 degree dominated the overall crystallinity. One of the possible explanation is the crystal was formed due to the hydrogen bonds that developed between dextran and water molecules with the presence of water.

The overall relative crystallinity in dextran T10 66% samples with different aging times increased from ~0.35% at 1 hour to ~17% after 4 days at room temperature, indicating that crystallization had occurred. The relative crystallinities of dextran T10 66% samples with different aging times are shown in Table IV-3. Figure IV-11 shows the relative crystallinity of sample increased with time.

Table IV-3: Relative crystallinity of dextran T10 66% at different aging times.

ID #	time (min)	% crystallinity
c	50	0.353
d	75	0.817
e	100	2.243
f	125	4.508
g	150	7.056
h	175	8.296
I	200	9.335
j	225	11.005
k	250	11.703
l	275	12.499
m	300	12.759
n	1440	16.159
o	5760	17.16

Figure IV-11: Relative crystallinity of dextran T10 66% increased with time.

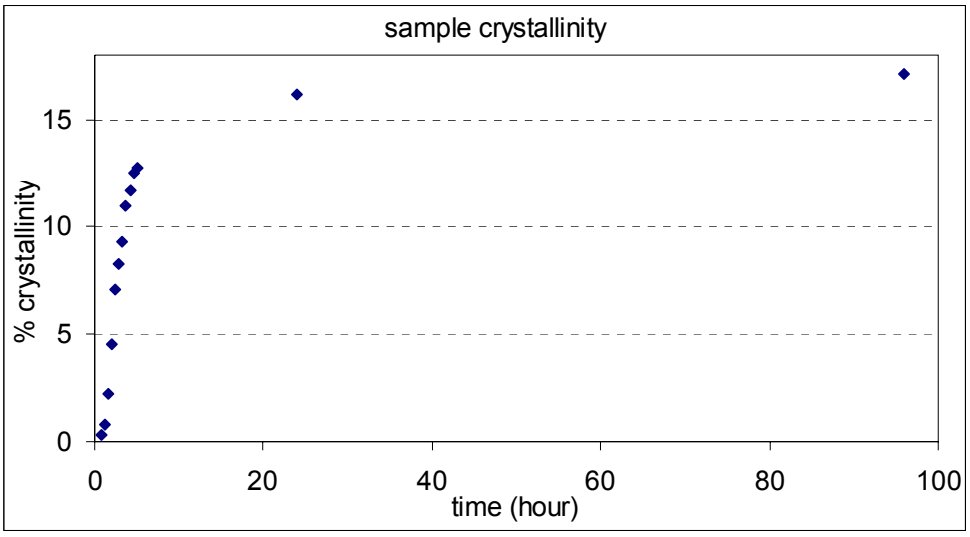

The crystallinity of dextran T10 66% increased very fast during the first several hours and gradually slowed down at increasing aging times. Sample crystallinity reached a steady state after 1 day. CurveExpert 1.3 was used to derive the correlation between the percent crystallinity and time. Figure IV-12 shows the correlation by CurveExpert 1.3. The correlation equation was determined to be:

$$y = 18.91 \times e^{-\frac{2.47}{x}}$$ (Equation IV-2)

Figure IV-12: Correlation of percent crystallinity vs. time for dextran T10 3c* by CurveExpert 1.3.

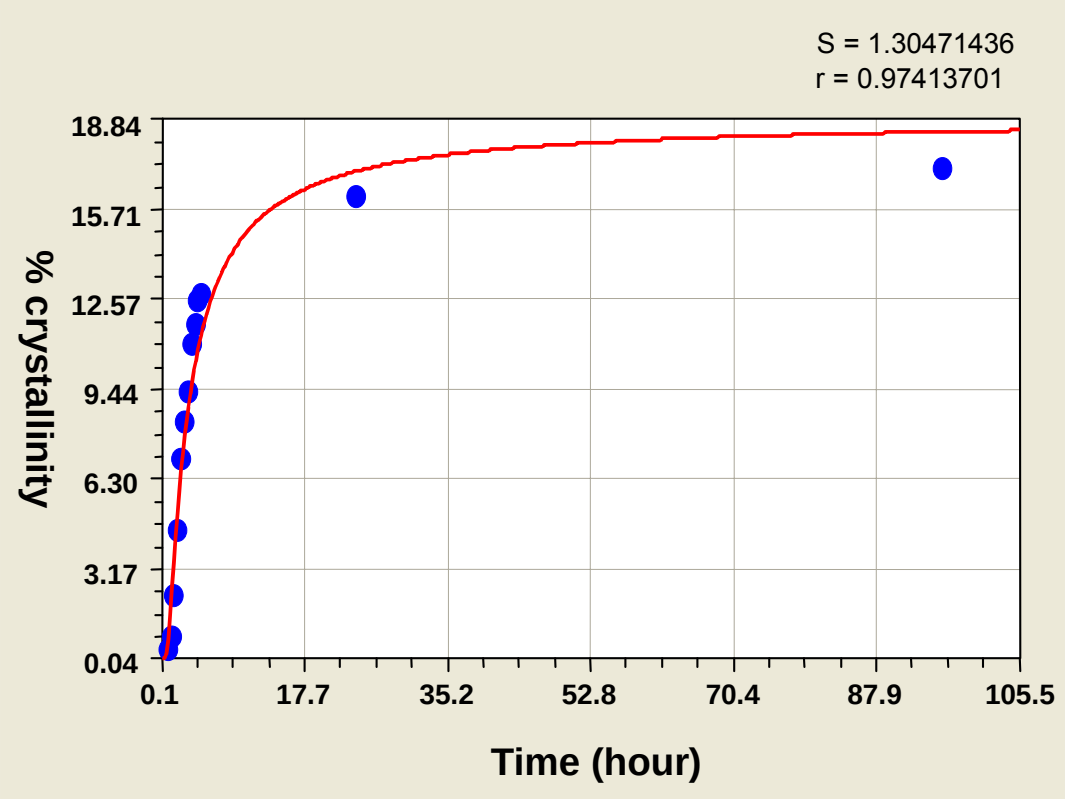

The curve showed that the extent and rate of crystal phase formation decreased with increasing crystallinity because the crystalline phase acted as physical cross-links that retard amorphous relaxation (Chung et. al., 2004). In the equation the sample percent crystallinity is a modified exponential function of aging time. That means the longer the sample aged the higher the percent crystallinity. Crystallinity appears to converge to an asymptotic value of 18.91%. Dextran T70 42% and T500 21% did not show any diffraction peak indicating that the samples were amorphous without becoming crystalline during aging at concentrations as high as 3 times that of the overlap concentration.

When dextran T70 and T500 concentration were increased to much higher than 3 times of their overlap concentrations, like T70 to 66% (~4c*) and T500 to 50% (~7c*), no diffraction peak on the diffratograms were observed indicating that the samples were amorphous and did not have crystalline material develop with time even though the concentrations were much higher than the overlap concentration. The possible reason for these high molecular weight dextrans not forming a crystal at high concentration is that the polymer chains interact with each other to form a network instead of packing in an orderly manner to form a crystal structure.

Figure IV-13: X-ray diffractograms for dextran T70 66% at different aging times: a) 0 min; b) 1 hr; c) 2 hr; d) 3 hr; e) 4 hr.

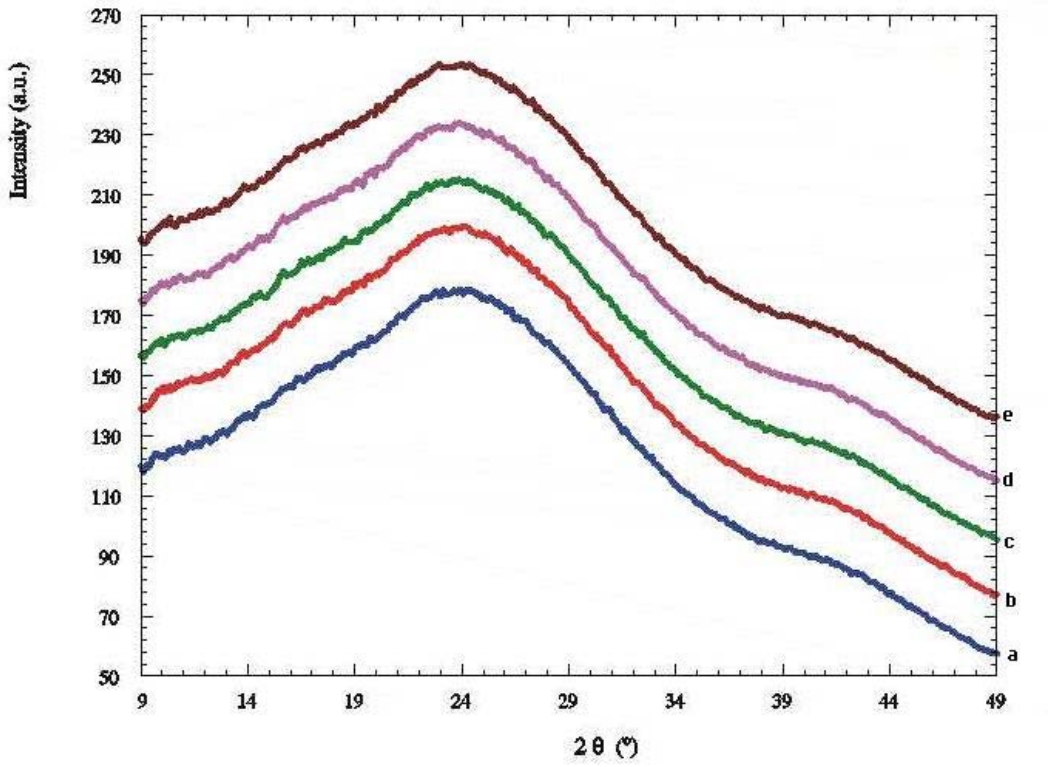

Figure IV-14: X-ray diffractograms for dextran T500 50% at different aging times: a) 0 min; b) 1 hr; c) 2 hr; d) 3 hr; e) 4 hr.

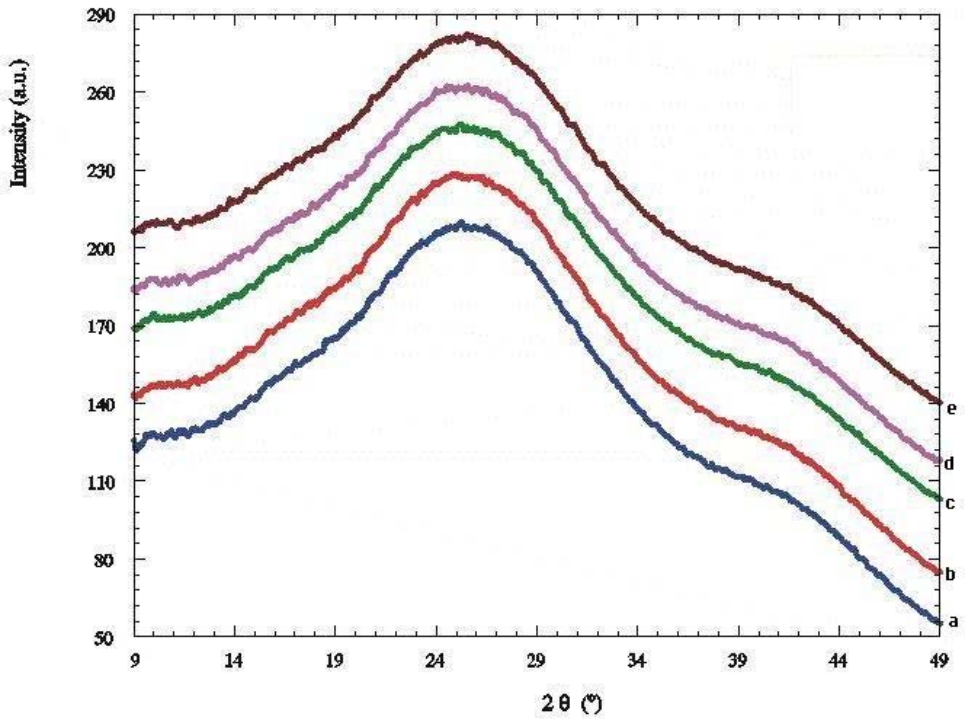

3. Differential scanning calorimetry

Changes in crystallinity with different aging times were also investigated through Differential Scanning Calorimetry. Figures IV-15, IV-16 and IV-17 show DSC thermograms for dextran T10 66%, T70 42% and T500 21% at a) 0 hr, b) 1 hr, c) 2 hr, d) 3 hr and e) 4 hr.

Figure IV-15: DSC thermograms of dextran T10 3c* (66%) at different aging times a) 0 to24 hr, b) 1 hr, c) 2 hr, d)3 hr, e) 4 hr, f) 24 hr and g) 72 hr.

a)

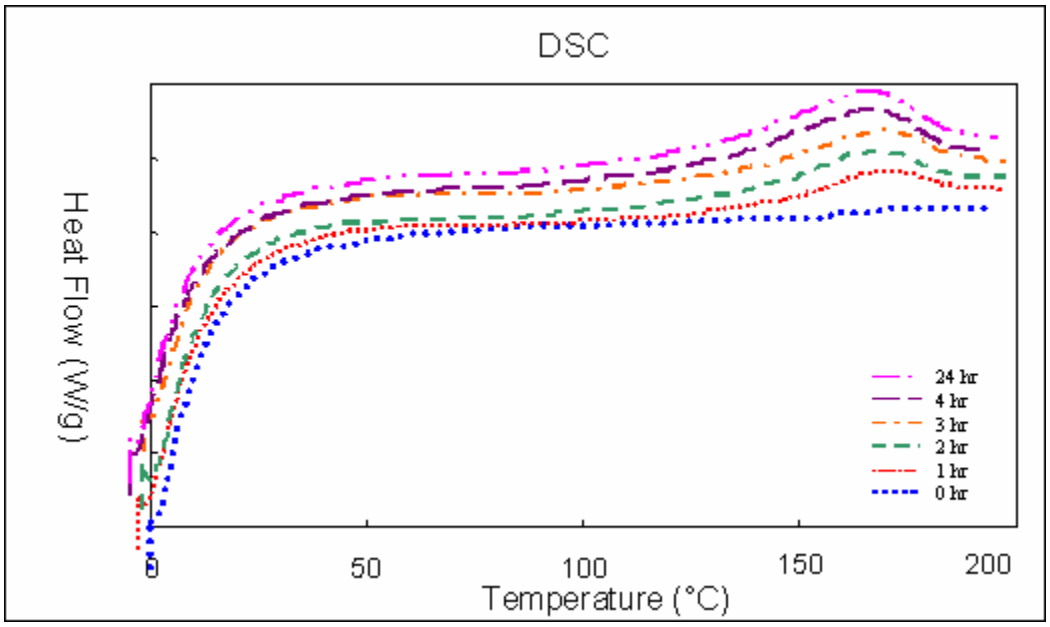

b)

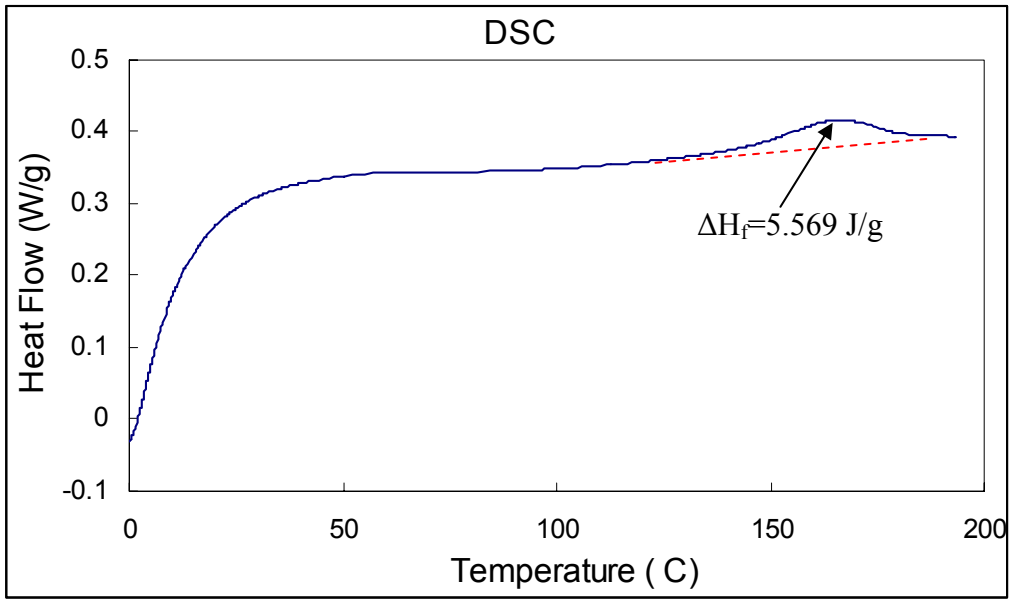
DSC
Heat Flow (W/g)
0.5
0.4
0.3
0.2
0.1
0
-0.1
0
50
100
150
200
Temperature (C)
ΔHf=5.569 J/g

c)

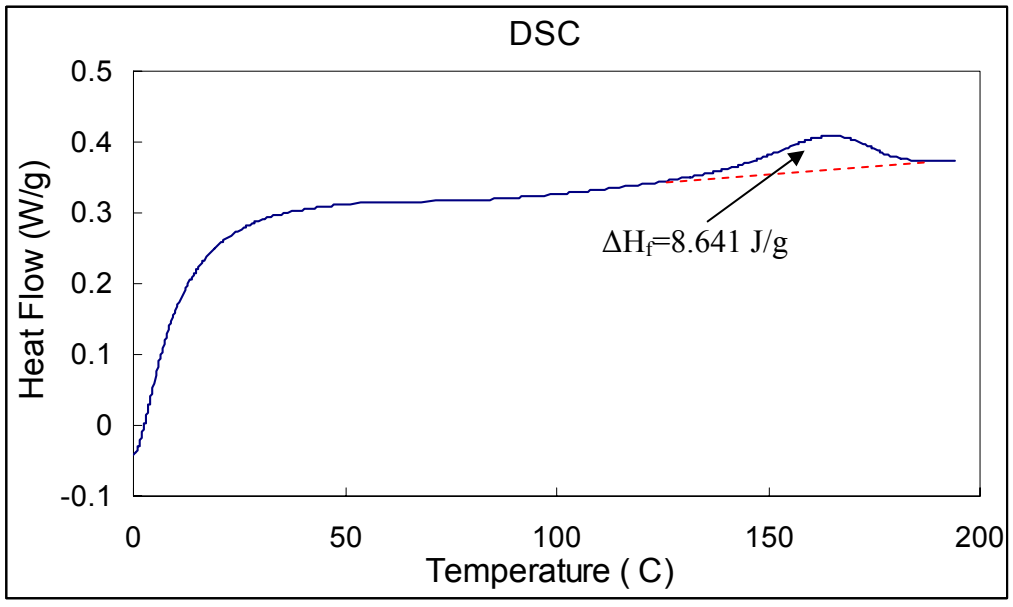
DSC
Heat Flow (W/g)
0.5
0.4
0.3
0.2
0.1
0
-0.1
0
50
100
150
200
Temperature (C)
ΔHf=8.641 J/g

d)

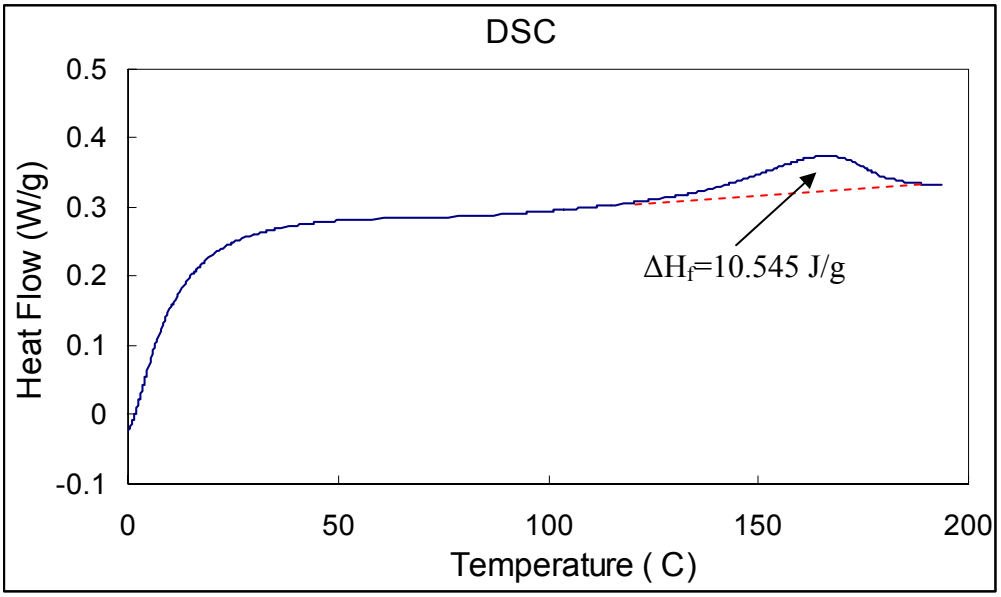
DSC
Heat Flow (W/g)
0.5
0.4
0.3
0.2
0.1
0
-0.1
0
50
100
150
200
Temperature (C)
ΔHf=10.545 J/g

e)

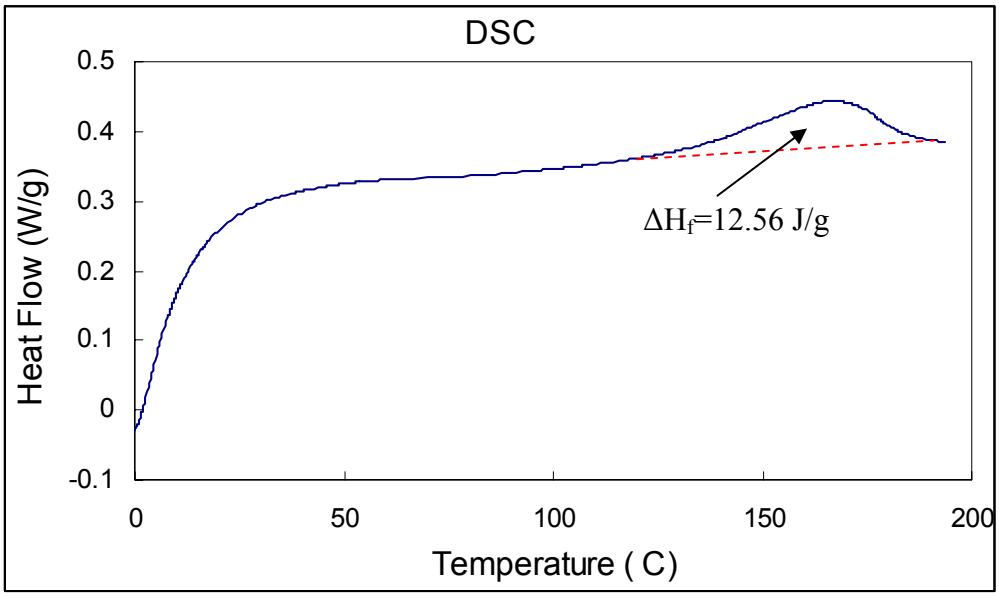
DSC
Heat Flow (W/g)
0.5
0.4
0.3
0.2
0.1
0
-0.1
0
50
100
150
200
Temperature (C)
ΔHf=12.56 J/g

f)

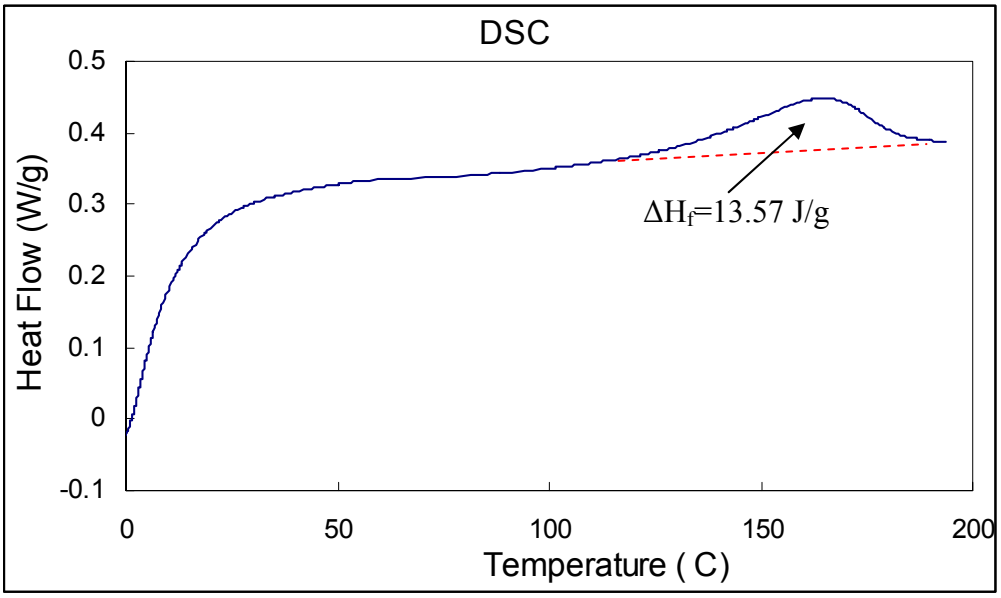

g)

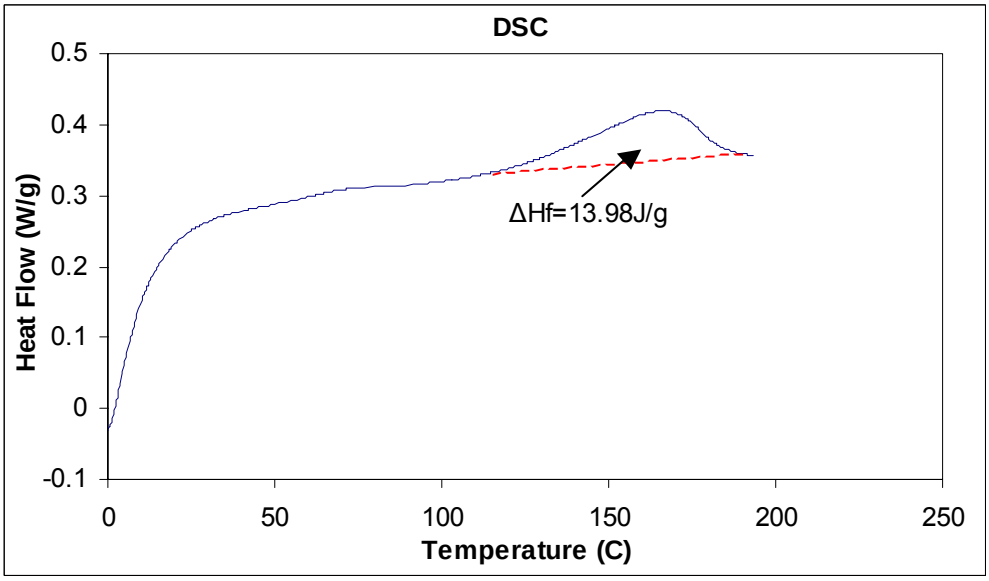

Figure IV-15a shows a DSC thermogram without any transition for dextran T10 66% for a fresh sample at zero time, indicating no crystallinity, which is in agreement with the X-ray diffraction result (Figure IV-8a). Figure IV-15b shows the start of the

development of an endotherm at around 140ºC, corresponding to the development of crystalline material with time confirmed by large enthotherms (melting of crystals).

By integrating the endotherm peak area the heat of fusion of the crystalline portion of dextran samples can be determined. The heat of fusion of the crystalline portion of dextran samples with different aging times is shown in Table IV-4.

Table IV-4: Heat of fusion for the crystalline portion of dextran T10 3c* with different aging times.

time (hour)	Heat of fusion (J/g)
1	5.569
2	8.641
3	10.545
4	12.56
24	13.57
72	13.98

The heat of fusion increased with time indicating that sample crystallinity increased as time increased. Thus more heat of fusion was needed to melt the crystal that developed in the sample with time. The plot of heat of fusion vs. time illustrates crystallinity change with time (Figure IV-16).

Figure IV-16: Heat of fusion versus time for dextran T10 3c*.

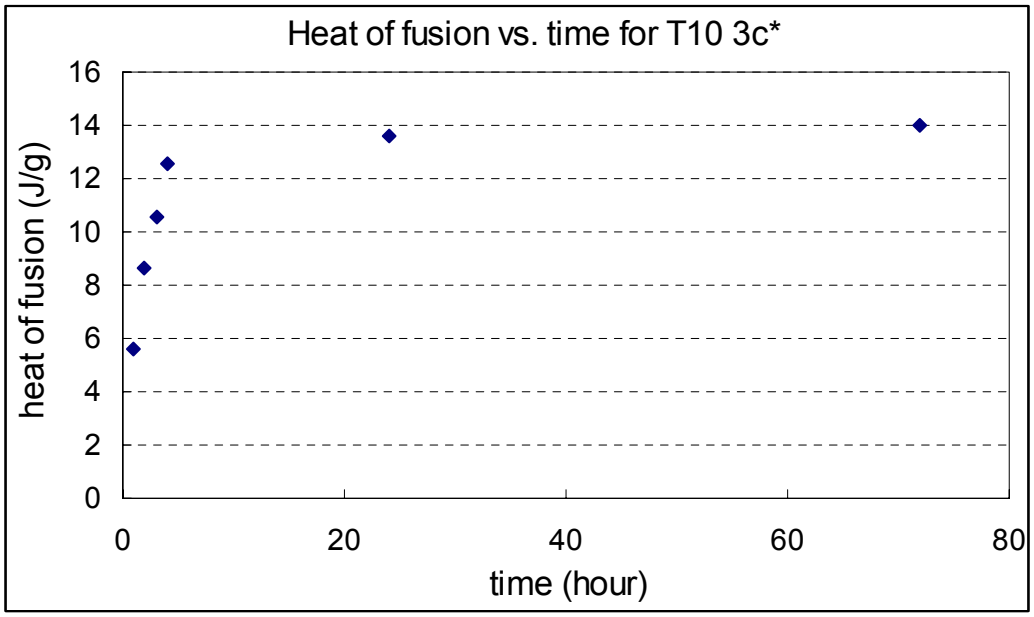

The DSC results for dextran T10 3c* with different aging times meet the results from X-ray diffraction. Both showed the sample crystallinity increased fast within the first several hours and reached the steady state after 1 day. CurveExpert 1.3 was used to find out the relation of heat of fusion and time. Figure IV-17 shows the relation. The correlation equation was determined to be

$$y = 14.41 \times e^{-\frac{0.92}{x}} \quad \text{(Equation IV-3)}$$

which is comparable to the equation (Equation IV-2) that obtained from X-ray diffraction.

Figure IV-17: Correlation of heat of fusion and time by CurveExpert 1.3.

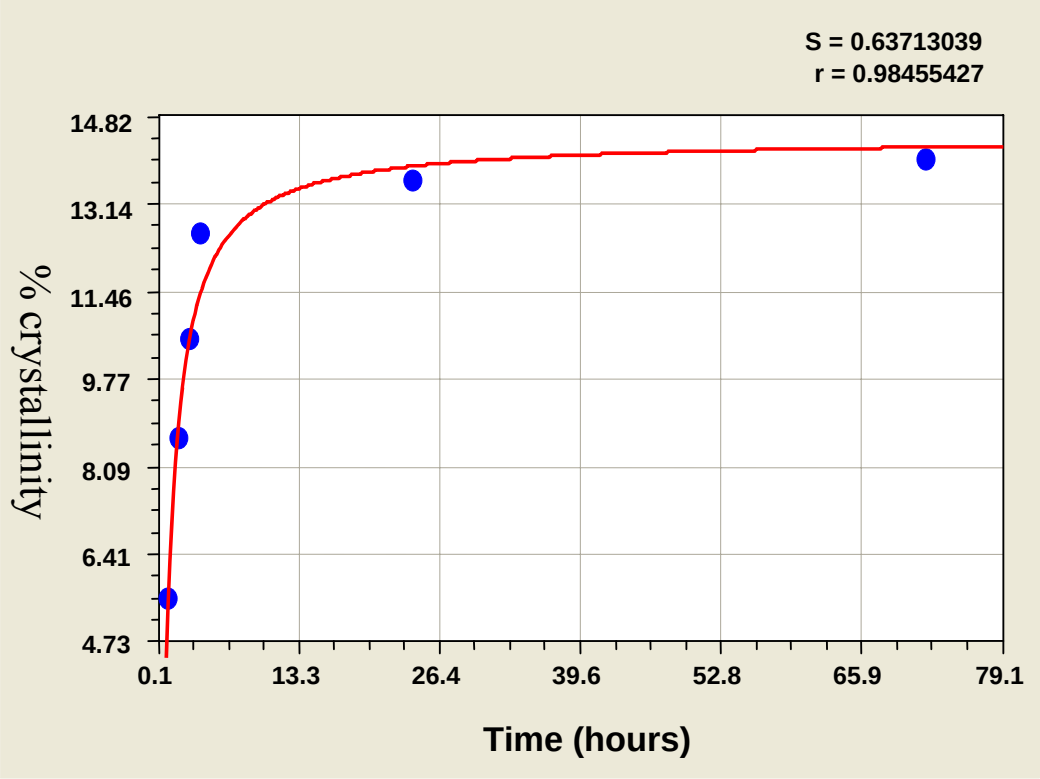

Figure IV-18: DSC thermograms of dextran T70 3c* (42%) at a) 0 hr and b) 4 hr.

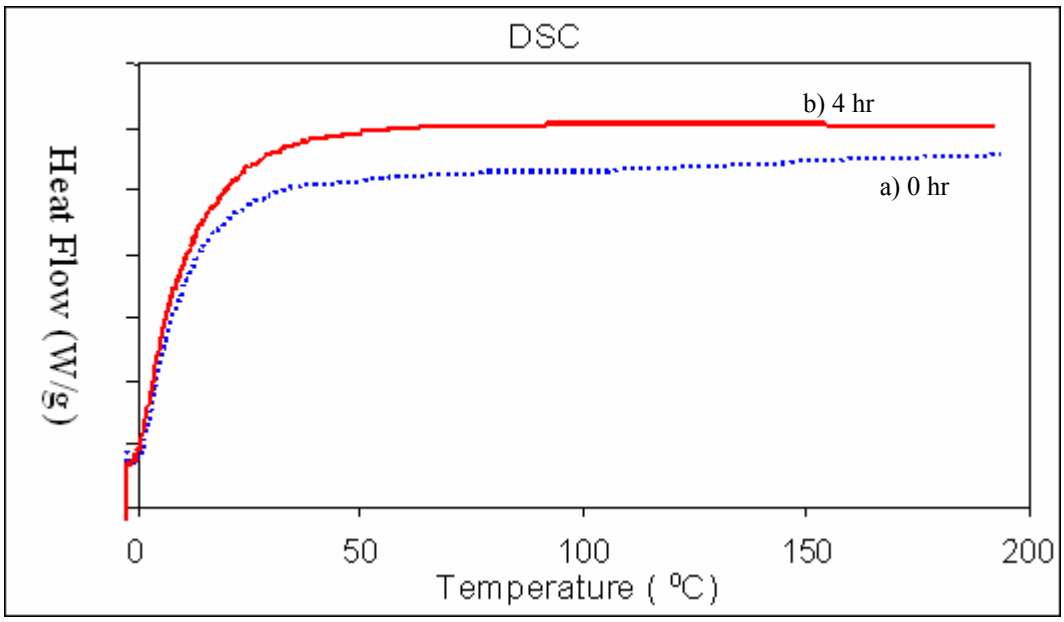

Figure IV-19: DSC thermograms of dextran T500 3c* (21%) at a) 0 hr and b) 4 hr.

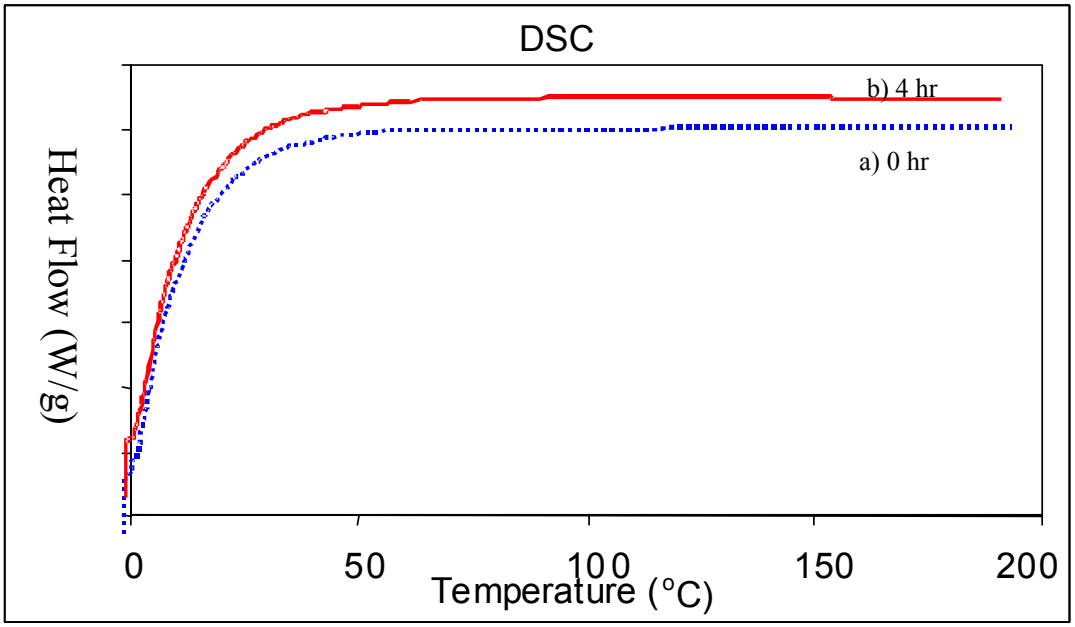

Figure IV-18 and IV-19 showing endotherms at different times do not show any melting peaks, indicating that no crystalline structure is present in concentrated dextran T70 and T500 samples even though the concentrations were as high as 3 times of their overlap concentrations. The same results have also been shown by the X-ray diffraction measurements.

Dextran T70 (66%) and T500 (50%) with different aging times were also subjected to DSC measurements to offer further comparisons. Figure IV-20 and IV-21 show there is no melting endotherm in both samples at different times at these high concentrations which are much higher than their overlap concentrations. The DSC results also meet the X-ray results for all dextran T10, T70 and T500 samples. For dextran T70 and T500, the long chains prevent the formation of an ordered packed structure of molecules when dissolved in water. Molecule chains entangle each other to form an amorphous system which does not crystallize over time due to the weak network formed. The amorphous structure of the entangled system showed no sharp peak in X-ray diffraction and a DSC curve which does not show any melting peaks.

In concentrated starch-water system, the crystallization of amylopectin was found to be a function of time (Keetels et. al., 1996). Starch crystallization melting enthalpy change ΔH increased with time in 65 days storage at 7 ºC. The recrystallization of amylopectin in starch gels results in an increase in stiffness of the gels. Jouppila et al (1998) showed the extent of crystallization of corn starch as a function of storage time for 20 days at different temperatures (50 – 90 ºC). The DSC analysis of crystallization in dextran T10 concentrated solution during storage reflects the crystallites developed over time in the system have different stabilities due to a gradient of water within the sample.

Figure IV-20: DSC thermograms for dextran T70 66% at different aging times: a) 0 hr; b) 2 hr; c) 4 hr.

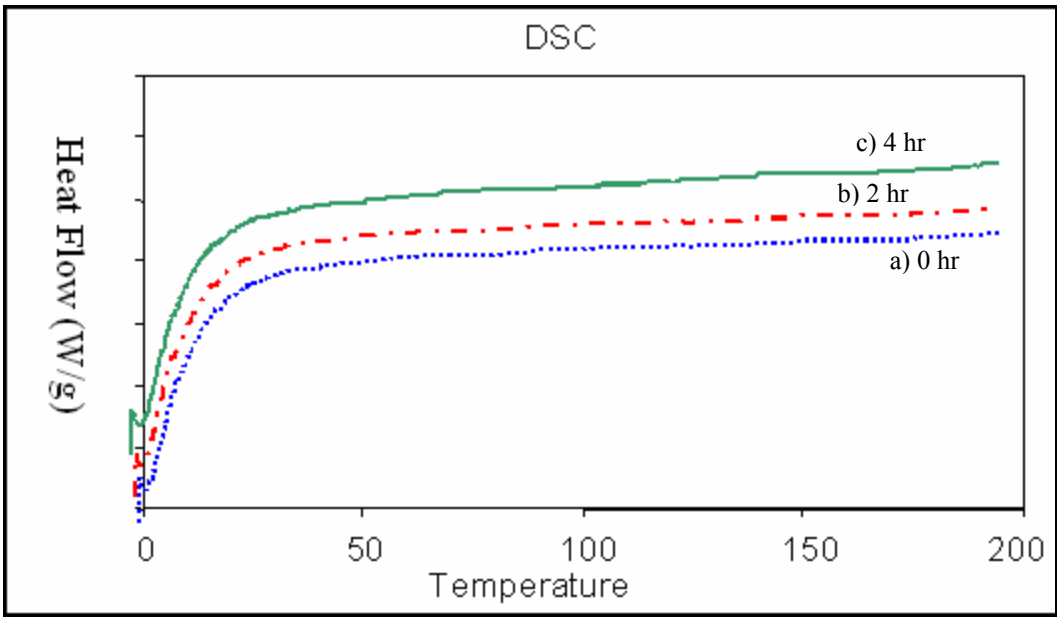

Figure IV-21: DSC thermograms for dextran T500 50% at different aging times: a) 0 hr; b) 2 hr; c) 4 hr.

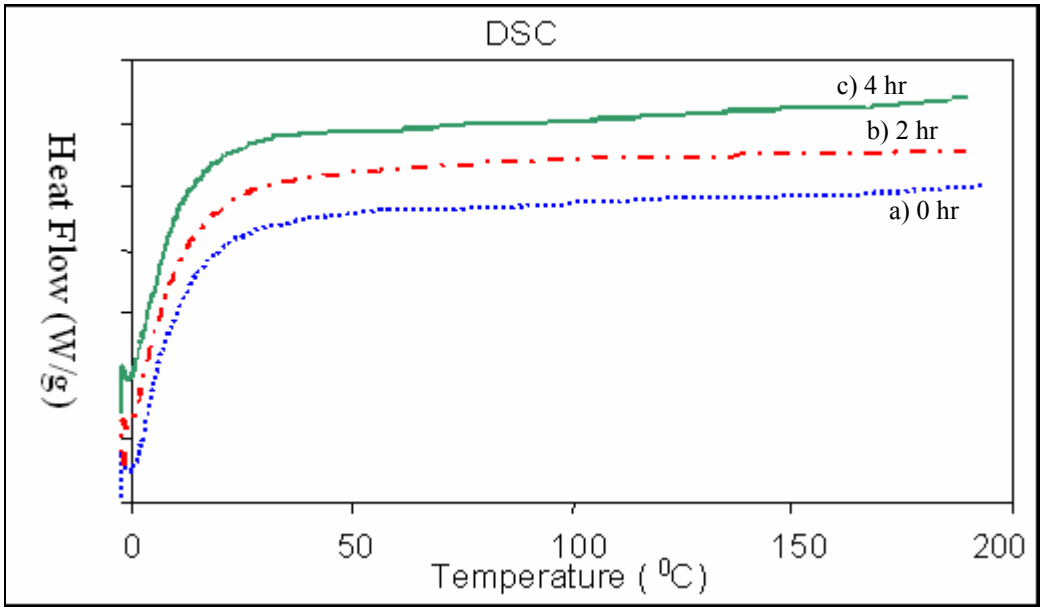

The relative melting endotherm of crystallites in concentrated T10 sample represent the highly cooperative melting of crystallites which have been formed through intermolecular attractions ordering the dextran molecules. As the disordered polysaccharide chains absorb most of the water, water becomes limiting, resulting in insufficient remaining water to facilitate the melting of more stable crystallite. Since the dextran T10 concentrated solution is in a metastable equilibrium state, the material would continuously approach toward the enthalpy of the equilibrium state with aging time, and consequently, the relaxation enthalpy increases. In Figure IV-16, the enthalpy increase proceeded rapidly at the beginning of aging and reached a plateau as aging continued. Montserrat (1992, 1994) stated that was due to decreased free volume and molecular mobility of chain segments.

4. Fourier Transform Infrared Spectroscopy

FTIR was used to understand the origin of the phase transition that happened in different molecular weight dextrans with time. Figure IV-22, IV-23 and IV-24 show the FTIR spectra for dextran T10 66%, T70 42% and T500 21% at different aging times.

Figure IV-22: FTIR spectra of dextran T10 3C* (66%) with different aging times.

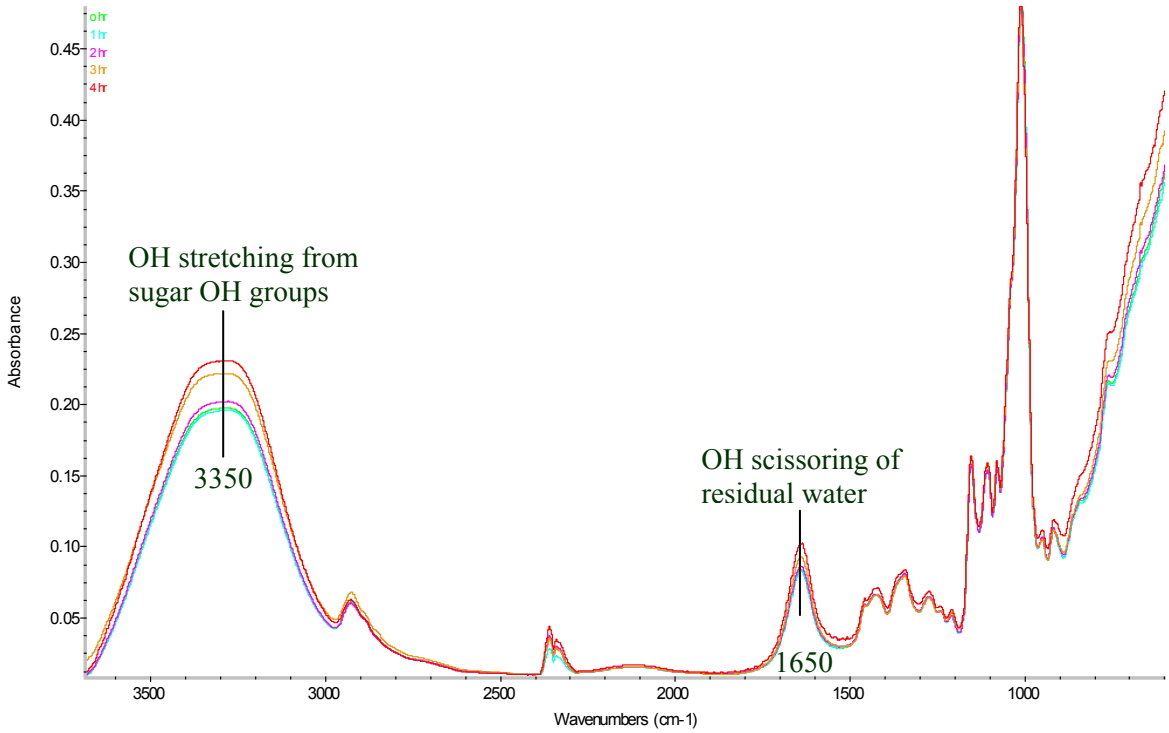

Figure IV-23: FTIR spectra of dextran T70 3C* (42%) with different aging times.

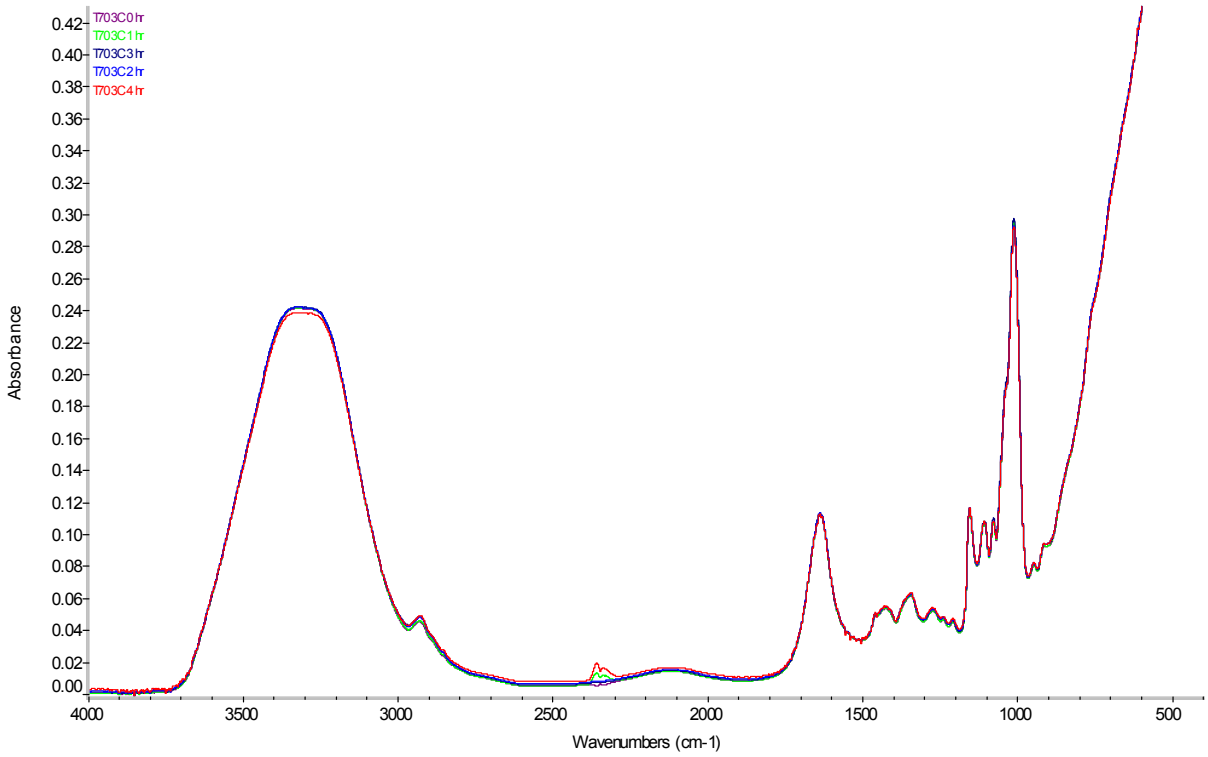

Figure IV-24: FTIR spectra of dextran T500 3C* (21%) with different aging times.

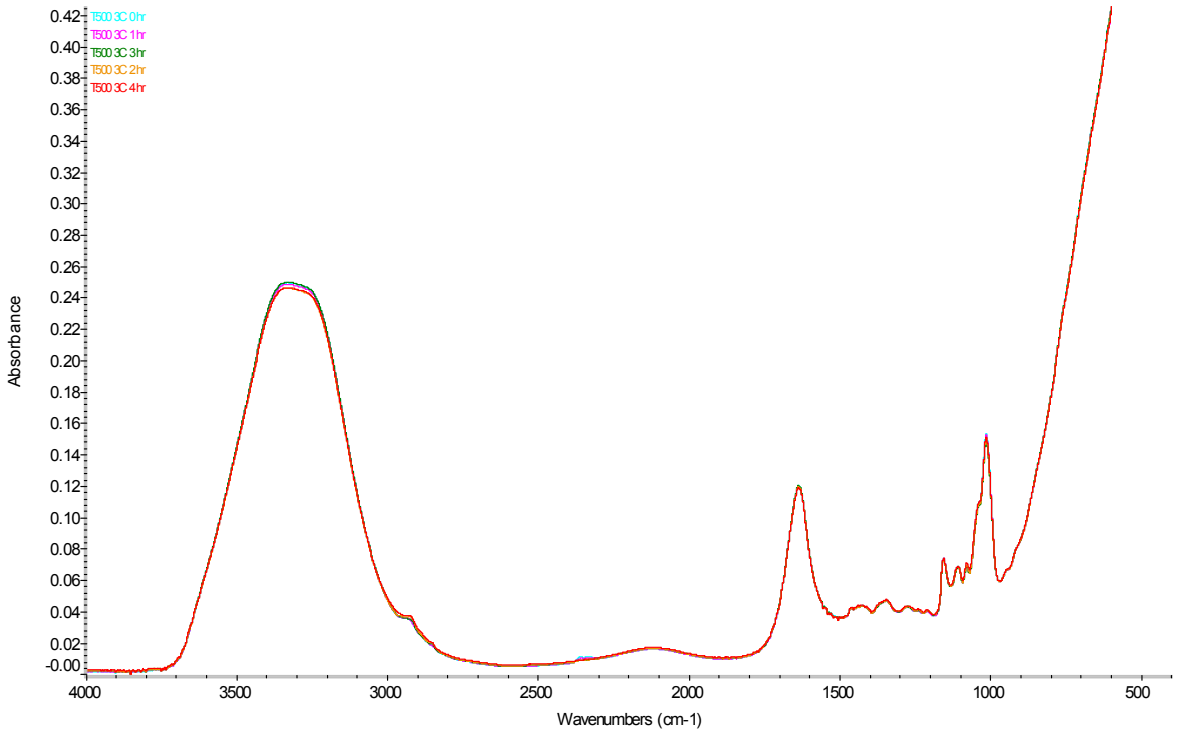

Dextran T10 66% samples showed an increase in the absorbance bands throughout the IR region from 3600 to 3000 cm^{-1}, which is depicted by the OH stretching mode of the carbohydrates. In all cases, the OH stretching band was a broad band, with an absorbance maximum at approximately 3350 cm^{-1}. It is evident that the OH band absorbance had a sudden increase from 2 hr sample to 3 hr sample. The increase in intermolecular OH bonds may lead to the phase transition that was observed through visual measurements, X-ray diffraction and DSC. The intensity of the OH scissoring vibration mode of crystal water (at ~ 1650 cm^{-1}) increased slightly with time which indicated the water molecules more hydrogen bonded to the dextran molecules with time. The peaks within 1500 – 900 cm^{-1} belonged to the fingerprint region of CH deformation vibrations and CO stretching as well as OH bending modes of dextrans. The bands at 1150 cm^{-1} and 980 cm^{-1} have been assigned to the glycosidic linkage (Kačuráková and Mathlouthi, 1996; Wolkers et. al., 1998, 2004).

Dextran T70 42% and T500 21% FTIR spectra showed no obvious change of the IR absorbance during measurement time up to four hours indicating a stable system was formed in both dextran T70 and T500 samples even with 3 times of their overlap concentrations.

T500 50% (Figure IV-25) also did not show obvious change of the IR absorbance during measurement time up to four hours. Both dextran T70 and T500 samples were stable when the concentrations were much higher than their overlap concentrations.

Figure IV-25: FTIR spectra of dextran T500 50% with different aging times.

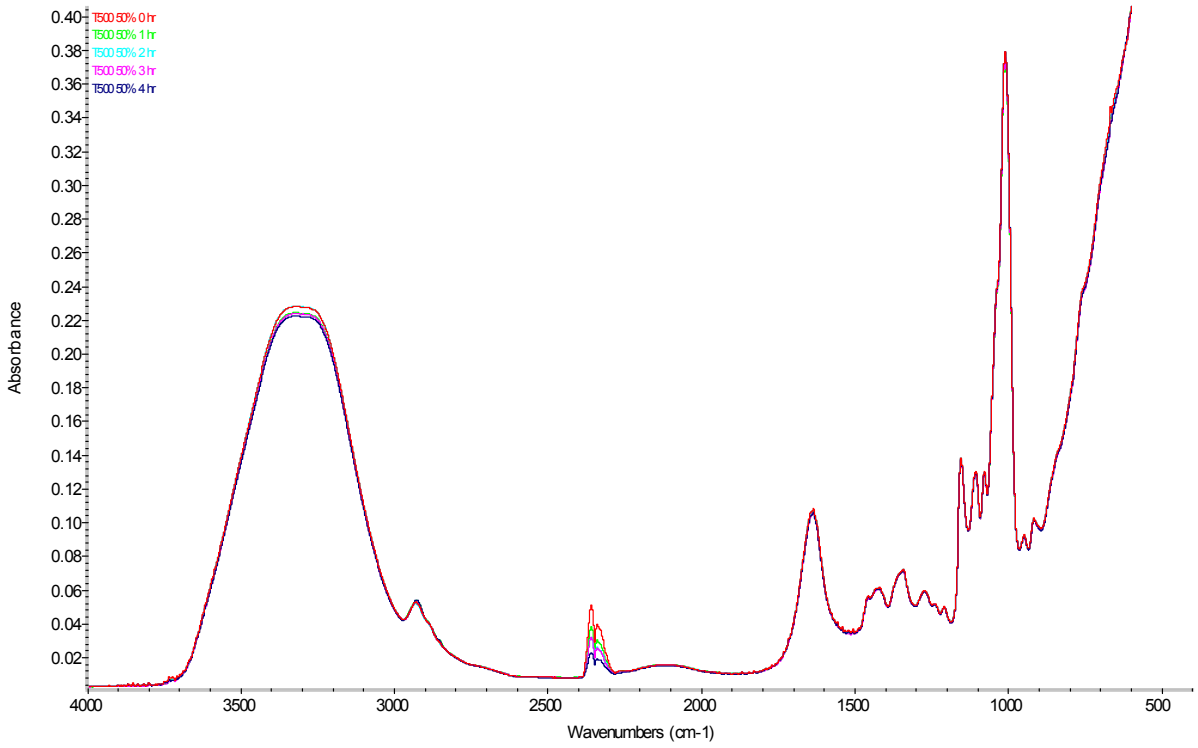

5. Summary

Both WAXS and DSC data showed the sample crysallinity increased fast within the first several hours and then slowed down and finally reached a plateau. The crystallization kinetics of dextran determined by WAXS and DSC at room temperature followed Avrami equation (Jouppila et al., 1998). From both equations when the concentrated dextran sample ages for a finite time the total crystalline content would reach to around 20%. The n value in the Avrami equation from WAXS and DSC were both unity which is agree with Colwell et. al. (1969) who found that the value of n was unity over the temperature range from –1 to 43°C for crystallization of starch gels containing 50% solids. In WAXS results the strong diffraction peak at 18° was due to the presence of water. The dextran crystals could grow from forming the association of the chains through the hydrogen bonds with the presence of water. The FTIR spectra showed clear intermolecular hydrogen bonds formed in the sample. The increase in the intensity of residual water also indicated the sample crystal formed due to the hydrogen bonds between dextran and water molecules.

C. Rheological measurements of dextran in high concentration environment

Dextran samples presented different behavior depending on the molecular weights that were used in this study. Dextran T10 with 3 times of its overlap concentration showed a fast appearance change within several hours while dextran T70 and T500 with 3 times of their overlap concentrations kept unchanging even after 24 hr storage time at room temperature. The sample measurement time was limited to 4 hr because the dextran T10 samples with 3c* crystallized within several hours and after 5 hours the sample could not be analyzed by rheometer due to the hardening of the samples. Thus the dextran T10 with 3 times of its overlap concentration behavior described in the following sections is based on analysis of samples at meta-stable conditions.

1. Small amplitude dynamic oscillatory measurements

a) Strain sweeps

Figure IV-27a shows typical strain sweep plots conducted at room temperature for dextran T10 3c* samples with different aging times from 0 hr to 4 hr. The dextran T10 system presented linear viscoelasticity up to a critical strain value. The critical strain values varied in the range of 1% to 20% decreasing as the aging time increased. The G' changed very small for samples with aging times 0 hr, 1 hr and 2 hr. When time increased to 3 hour a sudden increase in G' was observed and the critical strain value also decreased fast. For 3 and 4 hours samples, the critical strain values were in the lower range of 0.1~1.5%, typical of more solid systems. This result indicated that dextran T10

3c* changed to a brittle structure when time increased that could not withstand high levels of strain. In comparison, Figure IV-27b shows the strain sweeps of dextran T500 50% with different aging times. The critical strain values kept the same (up to 50%) for dextran T50 50% at different aging times which indicated the sample structure did not change with time.

Figure IV-27: Strain sweeps for: a) dextran T10 3c* with different aging times; b) dextran T500 50% with different aging times.

a)

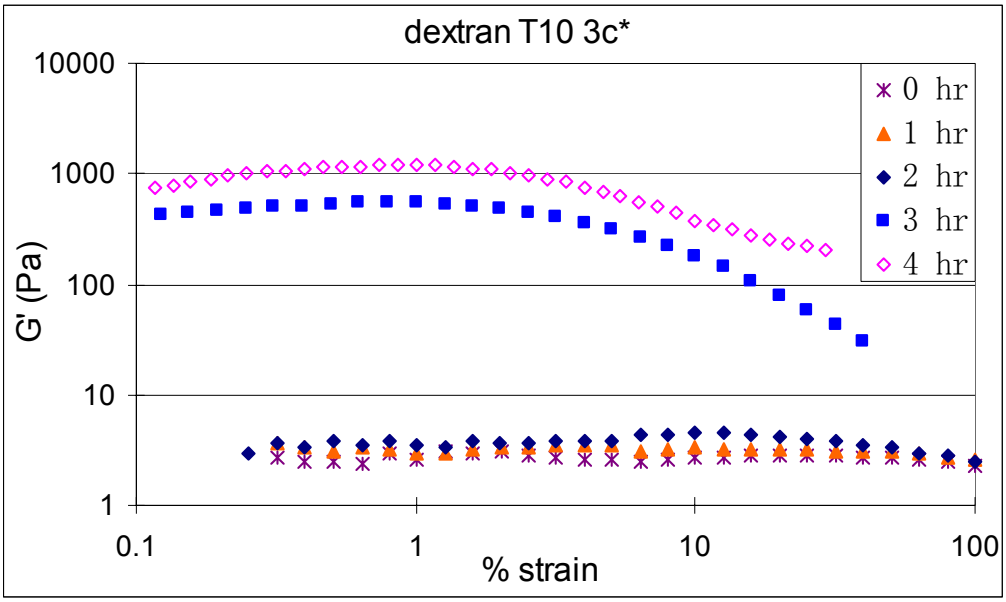

b)

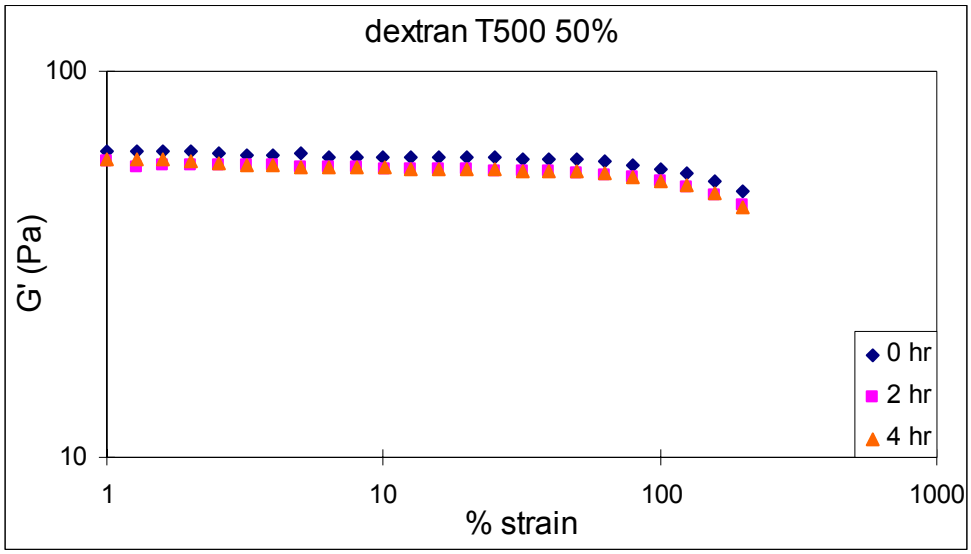

Figure IV-28 shows strain sweeps for dextran T10 3c* at 0, 1, 2, 3 and 4 hr. Figure IV-28a shows that at time 0 to 3 hour, the samples flowed (G”>G’) at % strains ranging from 2% for 3 hours sample to 0.1% for 0 to 2 hours samples. Thus, the structure of the samples became stronger with the time increases due to the sample crystallization. Figure IV-28b shows that 4 hours sample showed flow (G”>G’) at strains 7% with a high modulus (~1000). Thus, at 4 hour, the samples had a higher modulus as time increased and became more difficultly deformable (flowed at higher strains). These are indicators of a dextran structure formed by crystallization.

Figure IV-28: Strain sweeps for dextran T10 3c* at a) 0 to 2 hours, b) 3 hours, and c) 4 hous.

a)

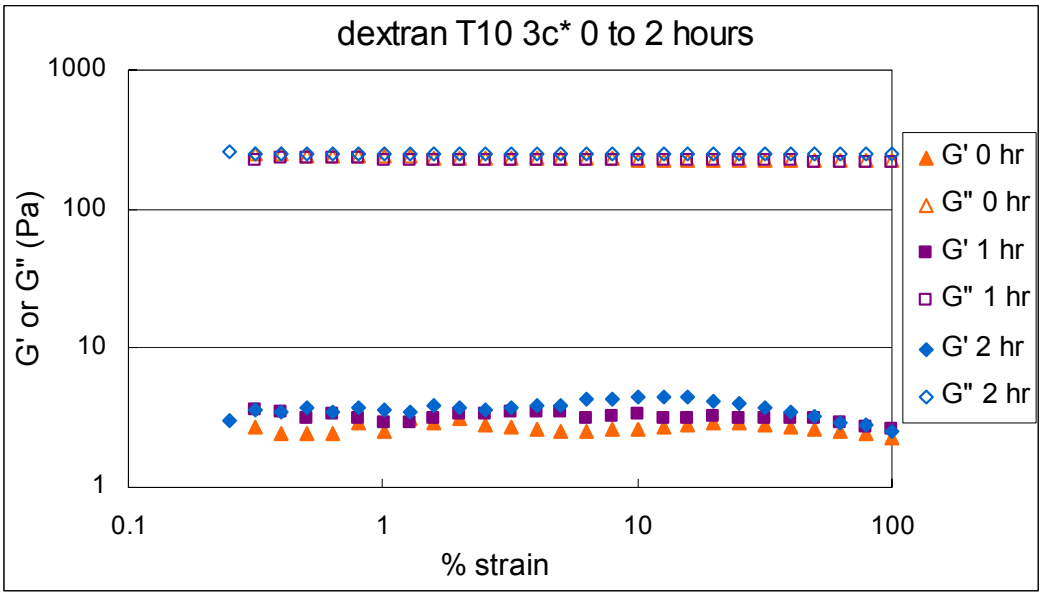

b)

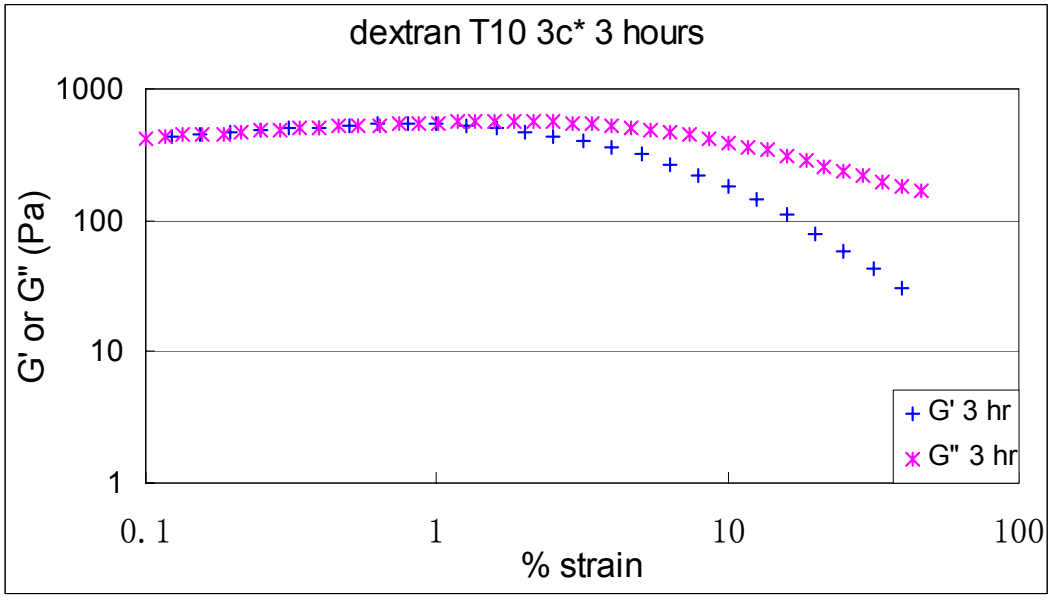

c)

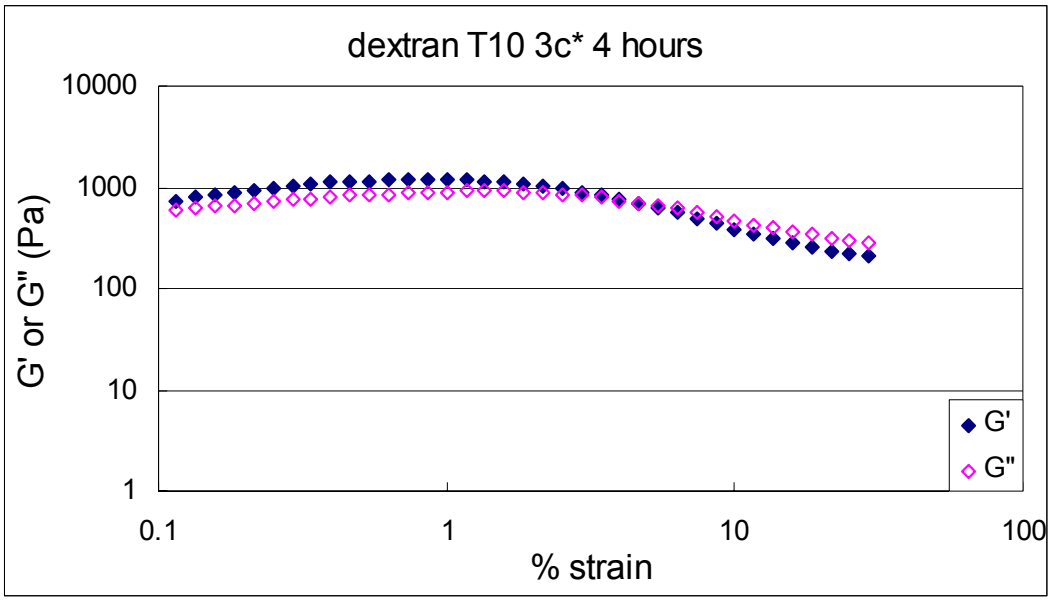
dextran T10 3c* 4 hours
10000
1000
100
10
1
G' or G" (Pa)
0.1
1
10
100
% strain
G'
G"

b) Frequency sweeps

Dextran T10, T70 and T500 with 3 times of their overlap concentrations were subjected to frequency sweep analysis within their linear behavior region. Sample data at 0 hr, 1 hr, 2 hr, 3 hr and 4 hr are shown in Figure IV-29, IV-33 and IV-34.

Figure IV-29: Frequency sweeps for dextran T10 66% at a) 0 ~ 2 hr, b) 3 and 4 hr.

a)

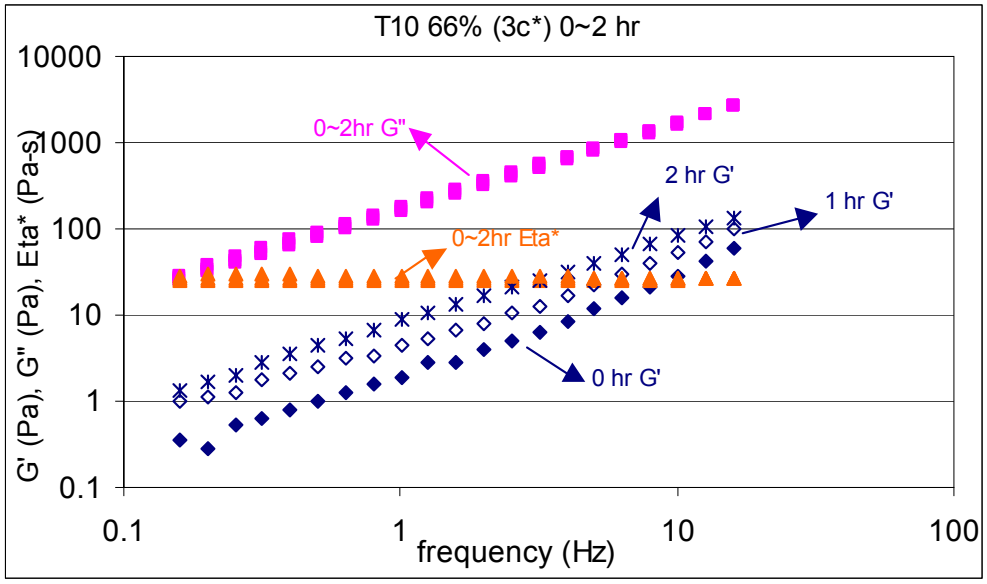

b)

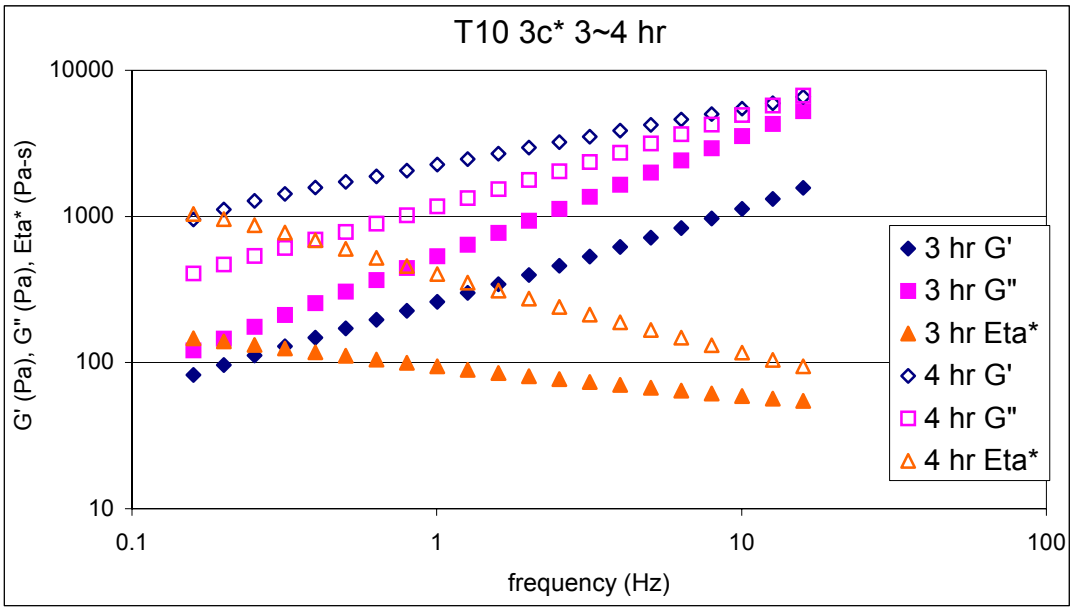

Results shown are an average of at least two sets of data. At time 0 to 3 hours the samples presented characteristics of a non-gelling, liquid-like system: G'<G" over the entire frequency range, and a strong frequency dependence for both G' and G" was observed.

A change in behavior was observed at 4 hr, in which characteristics of a weak gel system were present: the storage modulus was higher than the loss modulus (G' >G") throughout the whole range of frequency, and both moduli were frequency-dependent. A sudden increase of G' was observed from 3 hours. Although the moduli reached a high magnitude (100~10000 Pa) the 3 hour sample still showed a G">G' indicating a "liquid-like" behavior. Then the structure should correspond to one which has no entanglement at all, with particles sliding one on top of the other, resulting in a "liquid-like" behavior. For 4 hours samples, a weak gel behavior was observed: G'>G" throughout the frequency range and the moduli were strongly frequency dependent. The weak gel behavior should

correspond to one with weak entanglements, with particles coming to connect each other in the sample. The weak entanglements could be from the interactions induced at the amorphous – crystalline interface. The interactions act as physical cross-links and add rigidity to the amorphous regions (Jin et. al., 1984; Slade & Levine, 1988, 1991, 1995).

G' and G" at different frequencies were plotted against time. Figure IV-30 shows a time dependent property of G' and G".

Figure IV-30: Time dependent of G' and G". a) G', b) G".

a)

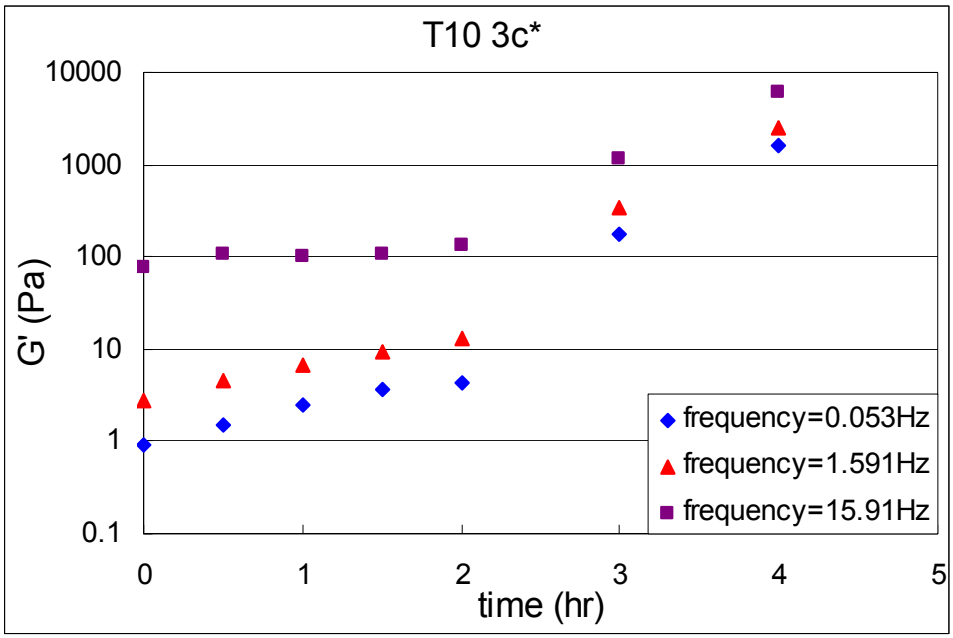

b)

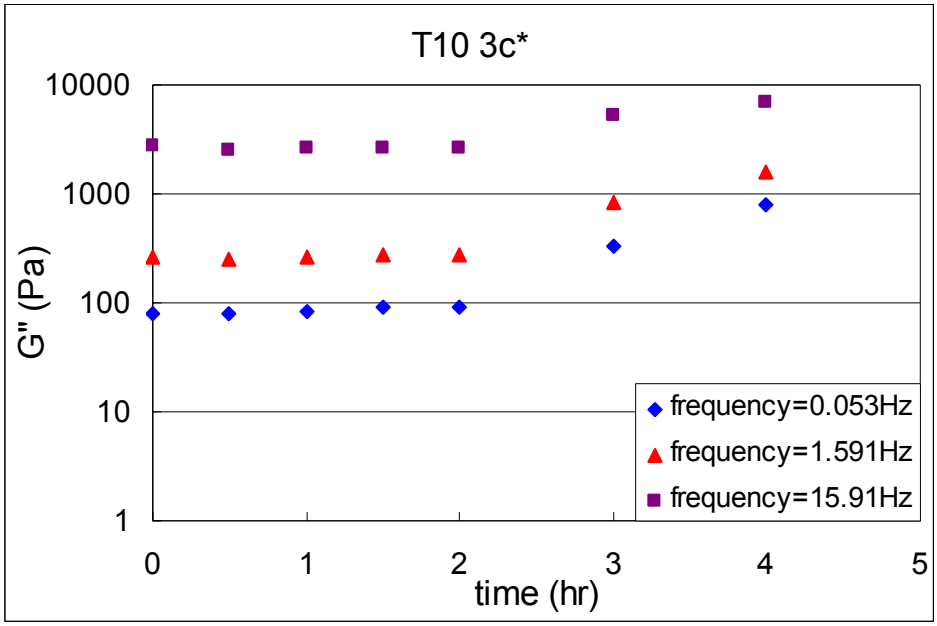

Both G' and G" increased with time. The shape of the G' and G" curves were the same regardless of the frequency indicating the change of G' and G" was not affected by the change of deformation, frequency.

Dynamic viscosity also showed a change with time. Figure IV-31 shows the dynamic viscosity (Eta*) vs. time.

Figure IV-31: Dextran T10 3c* dynamic viscosity vs. time.

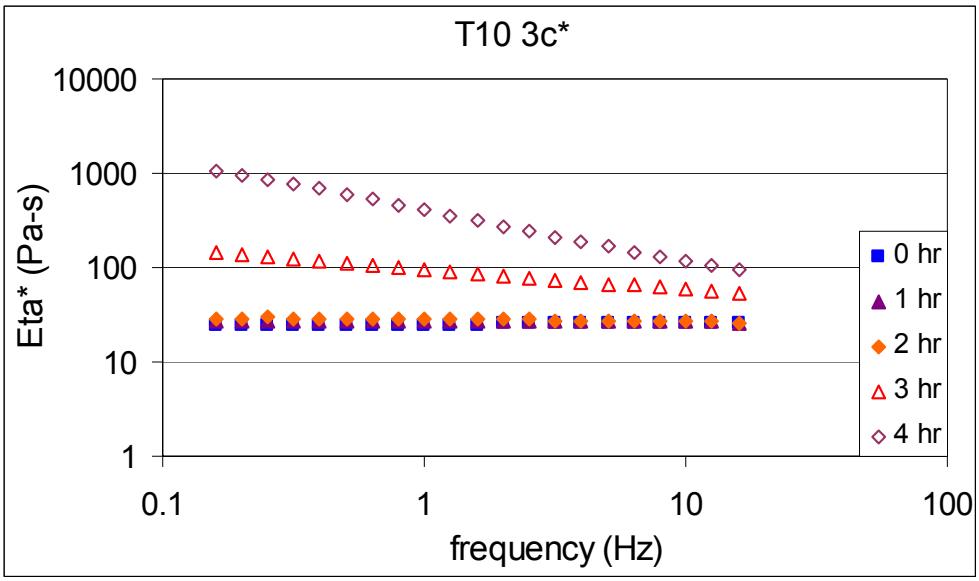

For time 0 up to 2 hr, the sample showed a frequency independent dynamic viscosity. 3 hr and 4 hr sample were strongly frequency dependent and decreased with increased frequency. The slopes of the dynamic viscosity curves were obtained and shown in Table IV-5. The absolute value of the slopes of the dynamic viscosity curves were plotted against time to obtain the time effect on the sample viscosities (Figure IV-32).

Table IV-5: Slopes of dynamic viscosity curves of dextran T10 3c* at different aging times.

Time (hour)	average abs|slope|
0	0.0106
0.5	0.0124
1	0.0151
1.5	0.0246
2	0.0239
3	0.2172
4	0.5402

Figure IV-32: Dextran T10 3c* dynamic viscosity slopes vs. time.

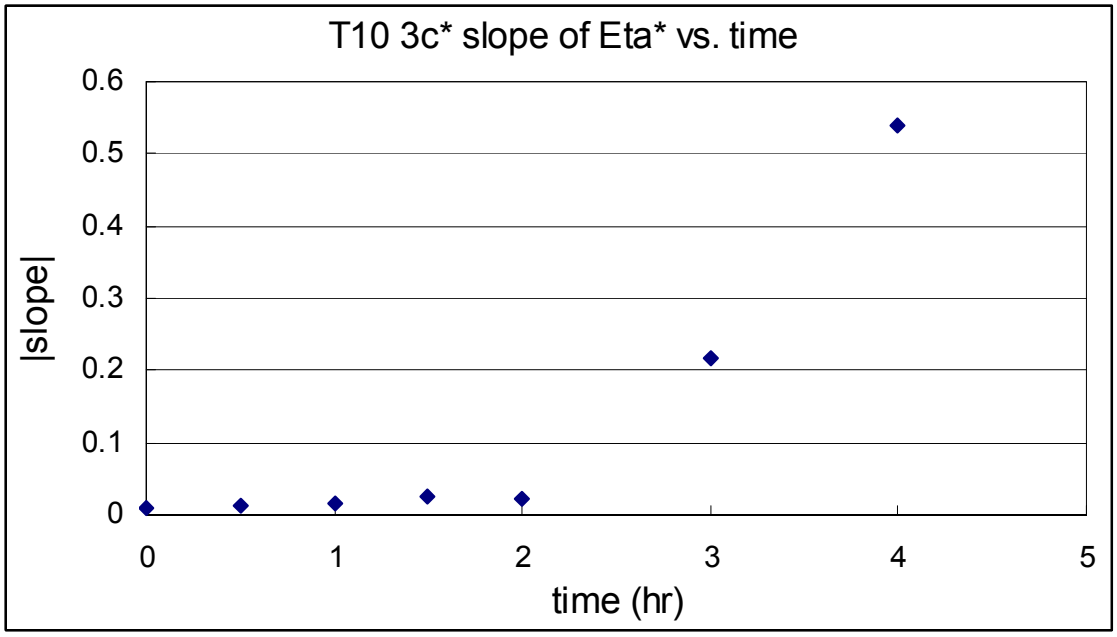

A sudden increase of the slope was observed at 3 hr which meets the FTIR results of an increase in the molecular OH bonds. The crystal formed in concentrated dextran solutions with time changed the sample rheological behavior from liquid like to more solid like.

Dextran T70 3c* and T500 3c* were analyzed by frequency sweep also. With time up to 4 hours, no change in G', G" and Eta* was observed for both dextran T70 and T500 at 3c* concentration. In comparison, dextran T500 50% was also subjected to frequency sweep test. With a concentration much higher than its overlap concentration, dextran T500 50% did not show changes in G', G" and Eta* at different aging times. Figure IV-33, Figure IV-34 and Figure IV-35 show the frequency sweeps for dextran T70 3c*, T500 3c* and T500 50%.

Figure IV-33: Frequency sweep for dextran T70 3c* with different aging times 0 to 4 hours.

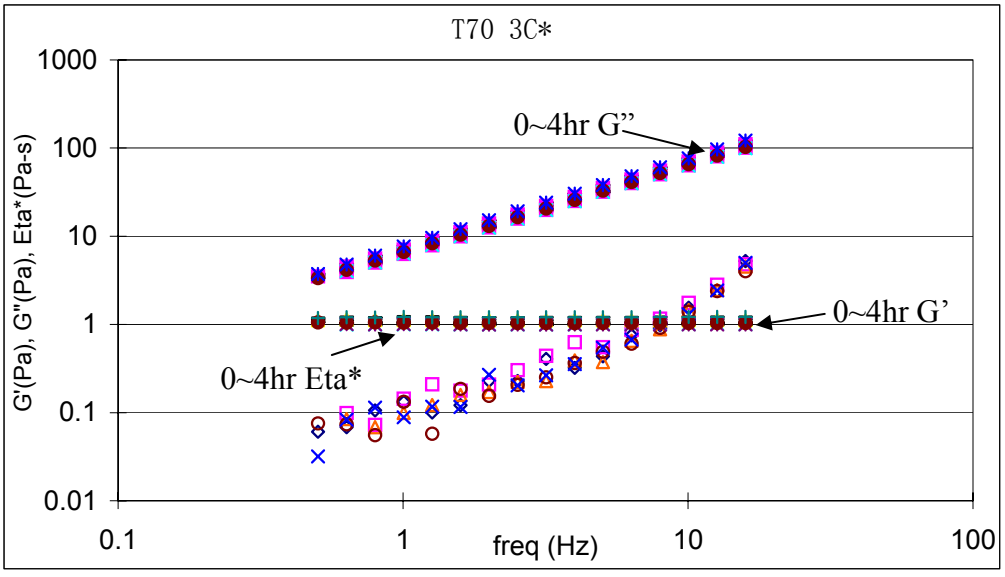

Figure IV-34: Frequency sweep for dextran T500 3c* with different aging times 0 to 4 hours.

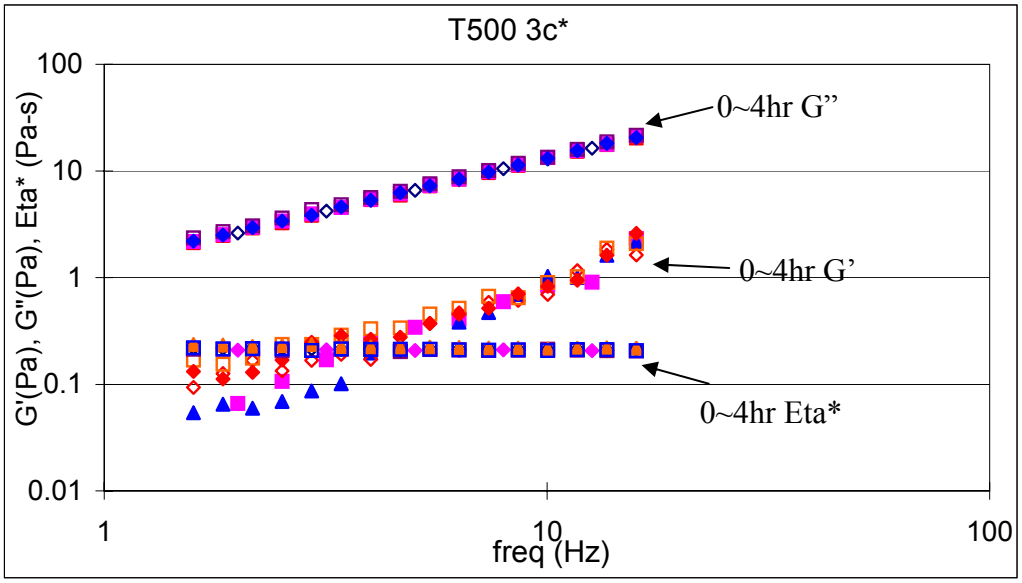

Figure IV-35: Frequency sweep for dextran T500 50% with different aging times.

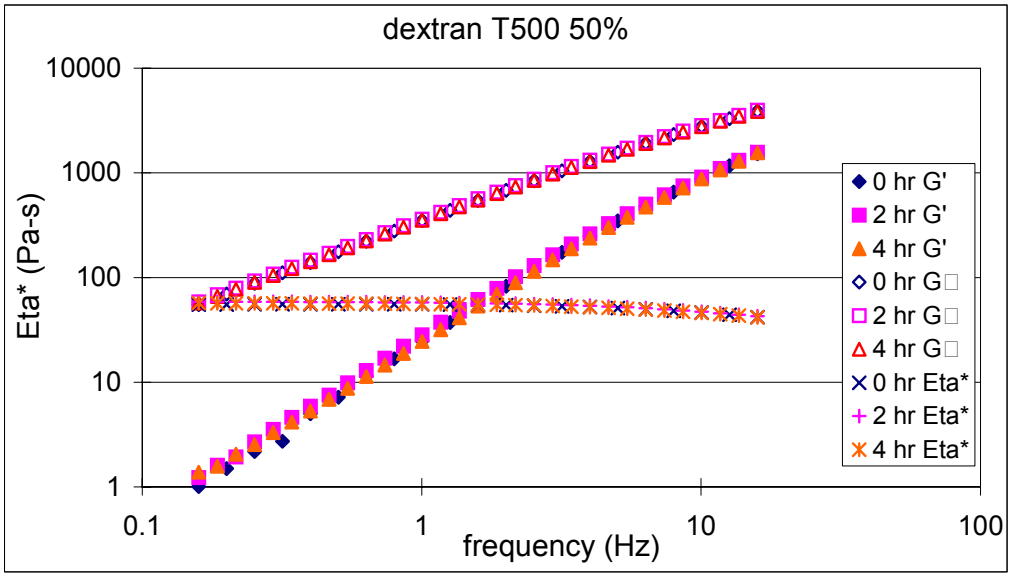

2. Steady shear measurements

The steady shear rheological characterization of the different molecular weight samples with different aging times of 0 hr, 1 hr, 2 hr and 4 hr is shown in Figure IV-36, respectively.

The 0 to 2 hours data presented a shear plateau and viscosities kept constant with increasing shear rate corresponding to a Newtonian behavior. The 3 hours data presented a low shear plateau and viscosity decreased with increasing shear rate, corresponding to a shear-thinning behavior. The 4 hours data presented a typical shear-thinning behavior: viscosity decreased with increasing shear rate. Thus dextran/dextran interactions seem to be significant from 3 hours which meets the FTIR results about the sudden increase of the OH bonds. With a concentration much higher than its c* dextran T10 coils overlapped each other and crystallized. The crystallized portion connected each other through OH bonds with the presence of water. The OH bonds formed among different crystallized portion were weak and can be broken by the deformation force, in the steady sweep it was shear rate. The OH bonds formed among the crystallized portion also took time that is why the shear thinning behavior can be observed from 3 hours.

In comparison, the shear sweeps data of dextran T500 50% with different aging time is shown in Figure IV-37. All dextran T500 50% data showed a low shear plateau and viscosities decreased with increasing shear rate, corresponding to a shear-thinning behavior. This is not difficult to understand, since 50% is too much higher than dextran T500 overlap concentration. At this high concentration, dextran T500 which has long chain branches overlapped and entangled each other. At high deformation force, the

entanglements between the polymer coils were broken so a shear thinning behavior was observed at high shear rates.

Figure IV-36: Dextran T10 3c* with different aging times from 0 hr to 4 hr.

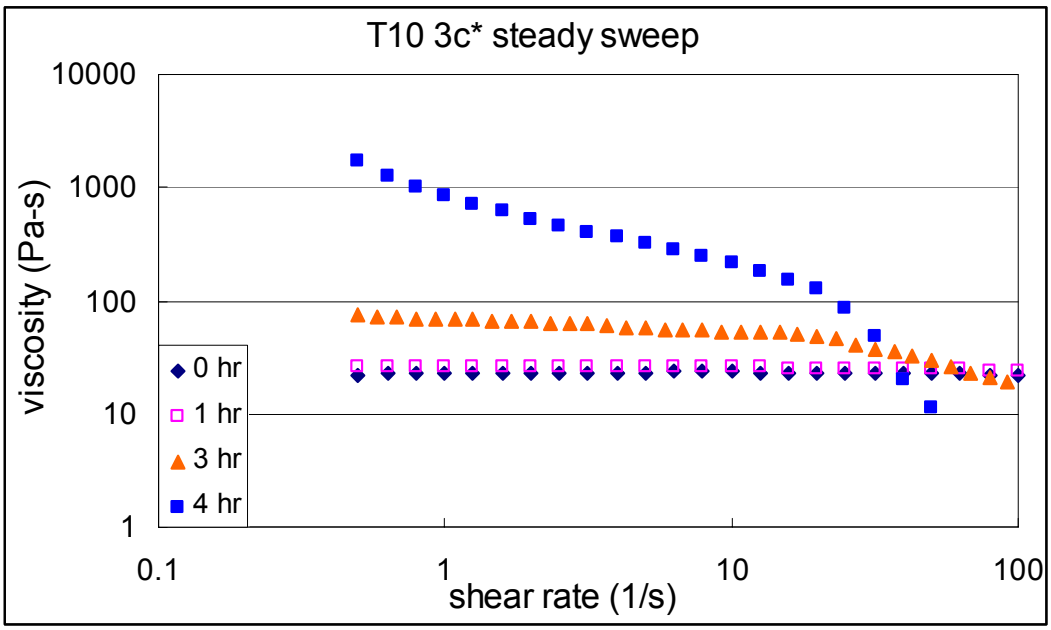

Figure IV-37: Steady shear characterization of dextran T500 50% samples with different aging times.

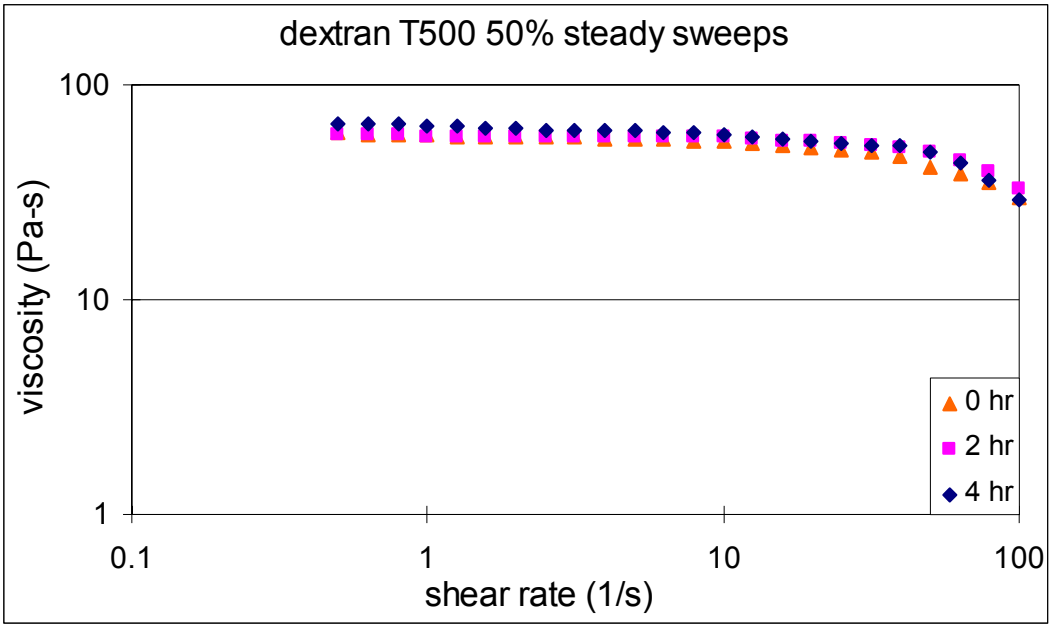

3. Cox-Merz rule

Figure IV-38 presents the Cox-Merz rule applied to the dextran T10 3c* systems at different aging times of a) 0 hr, b) 1 hr, c) 2 hr, d) 3 hr and e) 4 hr. T10 3c* samples followed the Cox-Merz rule up to 2 hours. 3 and 4 hours samples did not follow the Cox-Merz rule and showed greater divergence at high shear with $\eta^* > \eta$. Soltero et al. (1995) indicated that η* is usually larger than η since structure is usually disturbed to a lesser extent by the small amplitude dynamic test tan by steady shear tests. The divergence of linear viscosity and complex viscosity in 3 and 4 hours samples would suggest dextran T10 3c* system existed as a non-entangled system up to 2 hours. From 3 hours due to the crystallization of the system dextran T10 3c* sample demonstrated an entanglement behavior and the system behaved like a weak gel. In comparison, dextran T500 50% systems at different aging times are shown in Figure IV-39. All of the samples followed the Cox-Merz rule but a small divergence at high shear indicating T500 50% had weak chain entanglement and there was no structure change or additional entanglement developed with time in the system.

Figure IV-38: Cox-Merz rule applied to dextran T10 3c* samples with different aging times of a) 0 hr, b) 1 hr, c) 2 hr, d) 3 hr and e) 4 hr.

a)

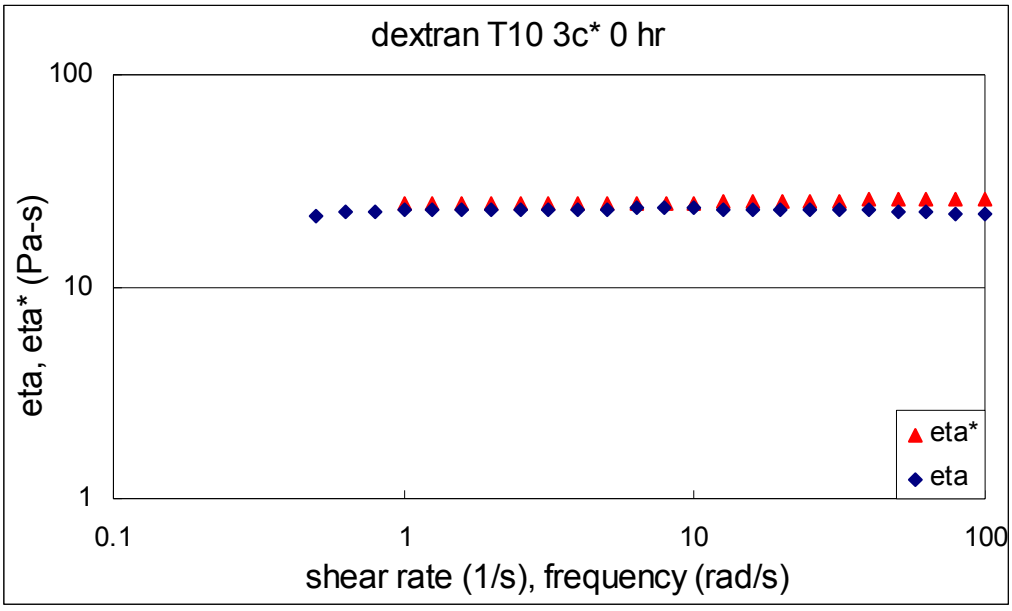

b)

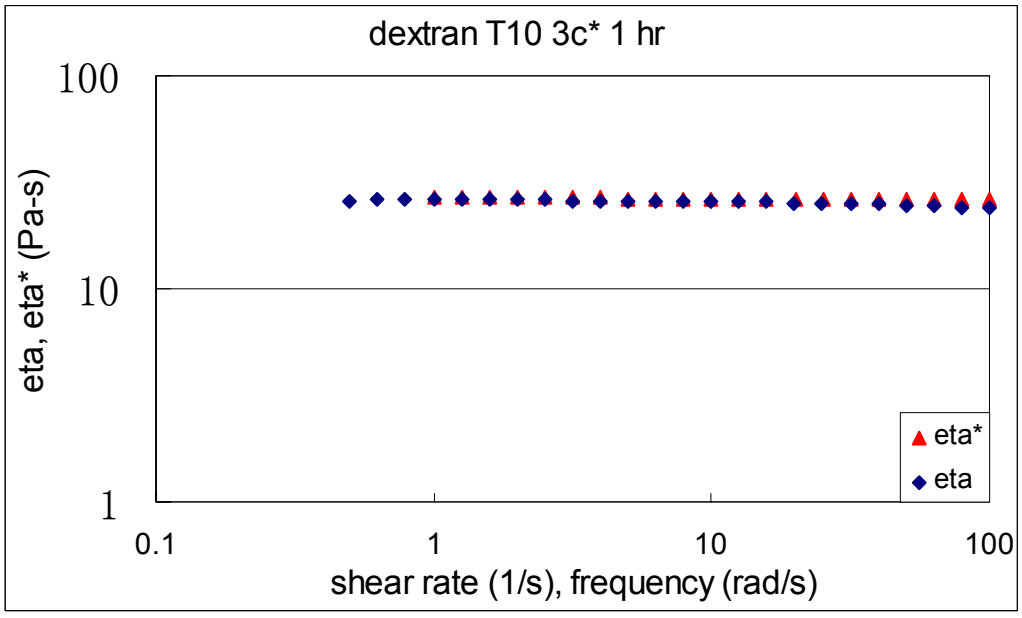

c)

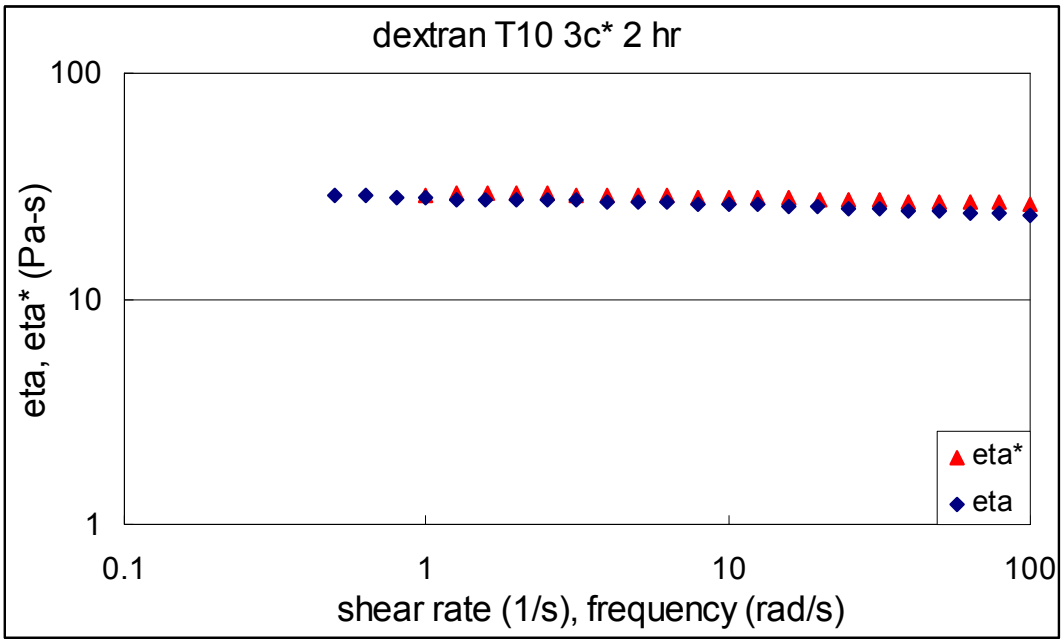
dextran T10 3c* 2 hr
100
10
1
eta, eta* (Pa-s)
0.1
1
10
100
shear rate (1/s), frequency (rad/s)
eta*
eta

d)

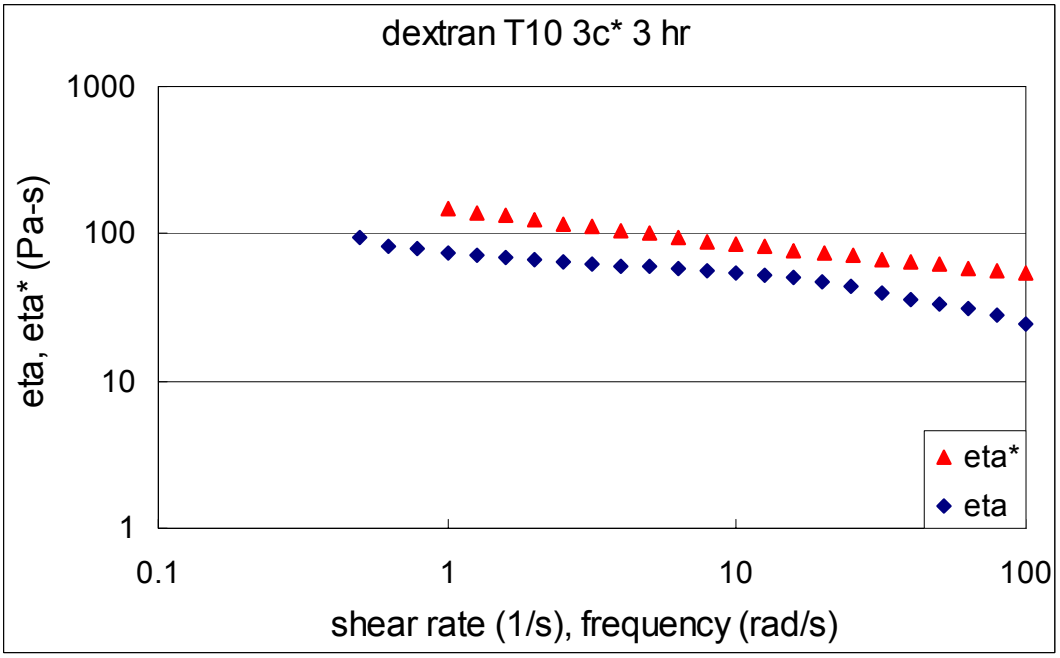
dextran T10 3c* 3 hr
1000
100
10
1
eta, eta* (Pa-s)
0.1
1
10
100
shear rate (1/s), frequency (rad/s)
eta*
eta

e)

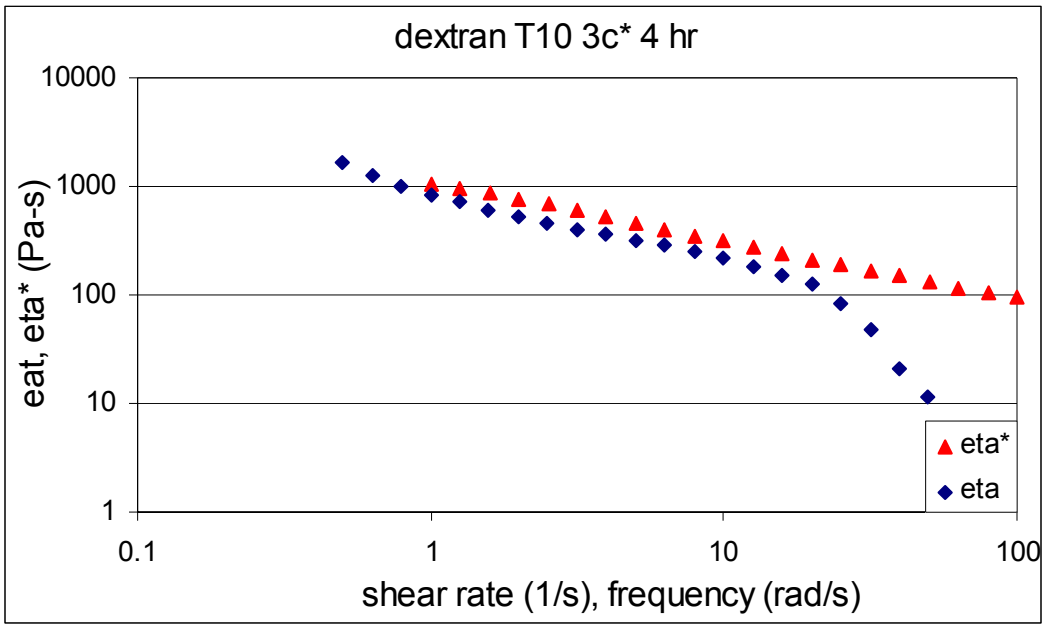

Figure IV-39: Cox-Merz rule applied to dextran T500 50% samples with different aging times of a) 0 hr, b) 2 hr and c) 4 hr.

a)

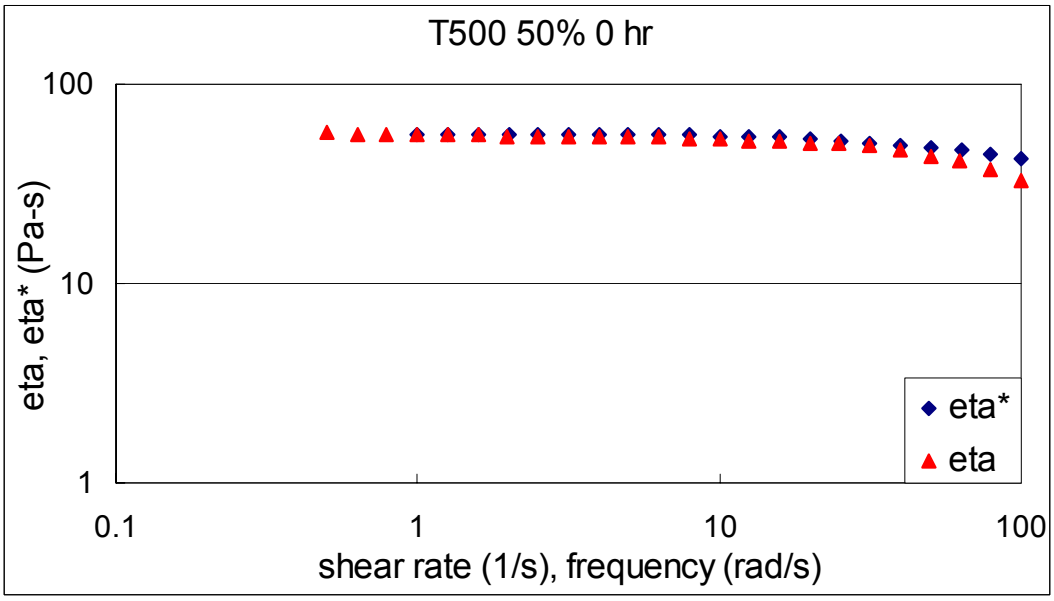

b)

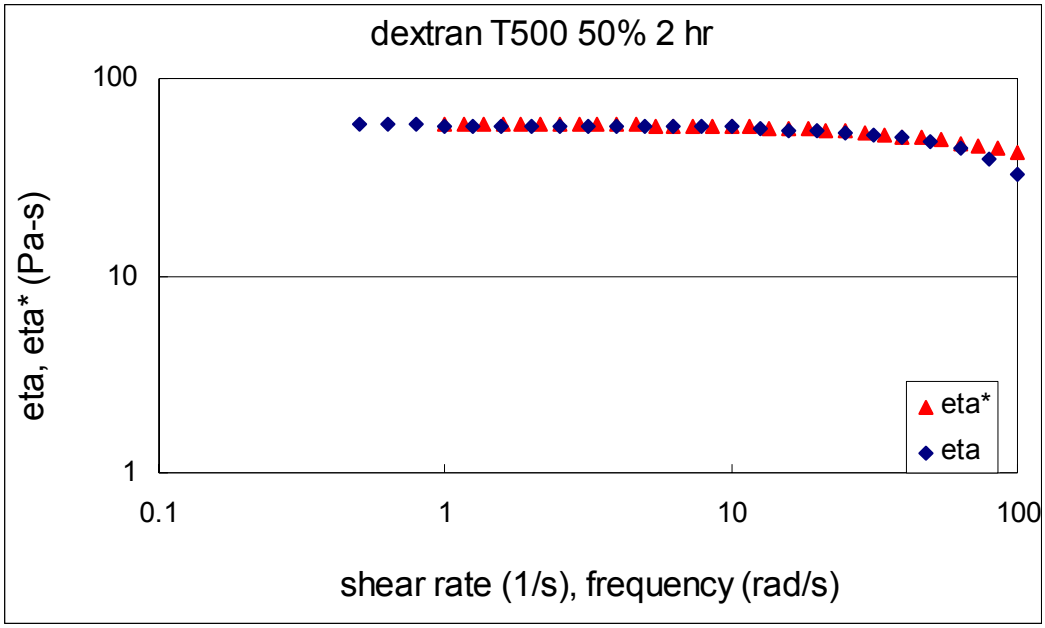
dextran T500 50% 2 hr
100
10
1
eta, eta* (Pa-s)
0.1
1
10
100
shear rate (1/s), frequency (rad/s)
eta*
eta

c)

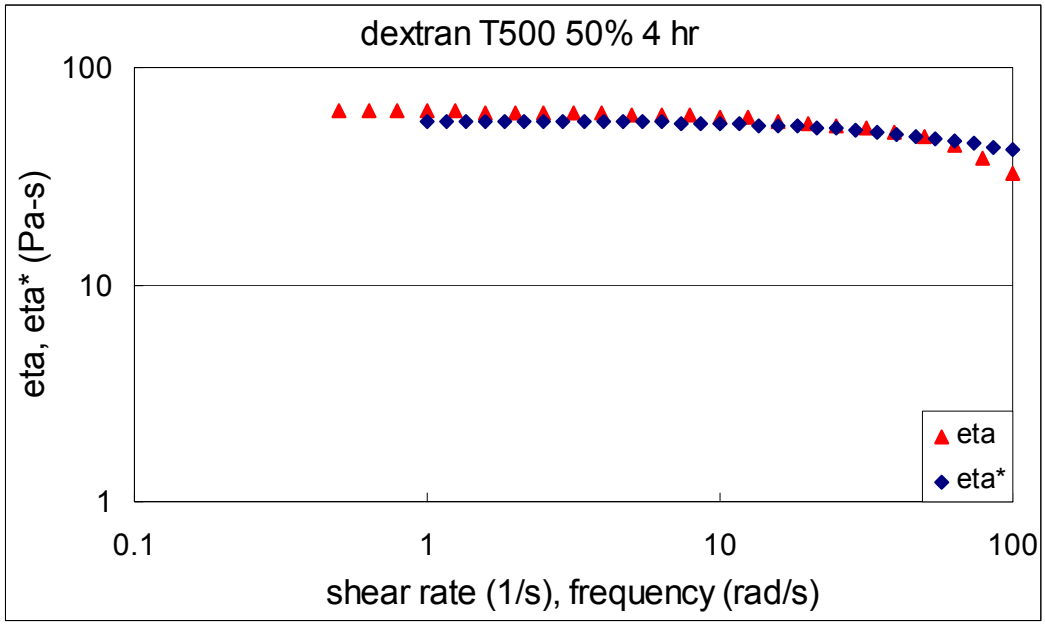
dextran T500 50% 4 hr
100
10
1
eta, eta* (Pa-s)
0.1
1
10
100
shear rate (1/s), frequency (rad/s)
eta
eta*

V. Conclusion

The study of dextran's physicochemical behavior and its interactions in concentrated conditions were based on polymer science principles. From the dilute and moderate concentration environments the dextran molecular conformation and overlap concentration were determined. The molecular interactions were studied in concentrated environment.

A. Dilute and moderate concentration environments

The eight different molecular weight dextrans investigated demonstrated random coil type of behavior in solution from the evidence drawn from η_{sp}/c vs c, ln (η_r/c) vs. c techniques and Mark-Howink equation. The molecular weight between 5,000 and 70,000 fit into the random coil range while molecular weight lower than 5,000 assumes more expanded conformation in solution and molecular weight higher than 70,000 has long chain branches. The overlap concentrations for dextrans with molecular weight fit into the random coil conformation and with long chain branches were determined through zero shear viscosity vs. concentration. The overlap concentration decreased with increase of molecular weight. The overlap concentration divided the concentration to two distinct regions. In the dilute region below the critical concentration, the viscosity-concentration plot showed a slope of small value and above overlap concentration coil overlap was evident and the dependence of viscosity on concentration was significantly more pronounced. The carbohydrate chains of the polysaccharides are generally less flexible and therefore adopt considerably more expanded coil geometry than synthetic polymers with random coil (Tirtaatmadja et al., 2001). However, the results obtained here showed

that dextran has an exceptionally large overlap concentration compared to the other polysaccharides and hence considerable lower [η]. This exceptional behavior is probably due to the high percentage α-1,6 glocosidic linkage which gives dextran a very flexible backbone. In the high molecular weight case, the branched nature of the dextran molecules with a number of very long side-chain in these branches causes a more compact molecular configuration and a reduction in the molecular volume in solution. The consequence is a reduction in [η] and an increase in overlap concentration for dextrans. The steady shear viscosities of dextran solutions increased with increase concentration and showed a Newtonian behavior. The dependence of intrinsic viscosity on molecular weight indicates that the dextran molecules are non-linear and possibly highly branched. All these results point out that the dextran molecules are less stiff than most carbohydrates and are highly branched when molecular weight increases, so that the molecules are in a highly compact configuration in aqueous solution.

B. High concentration environments

Dextran T10, T70 and T500 systems were analyzed at high concentration environments (≥ 3c* w/w), at which the crystalline properties of the materials were studied in a time frame.

Although dextrans are known to be well soluble in water, precipitation was observed in concentrated aqueous solutions of low molecular weight dextran (dextran T10), whereas for solutions of dextran with higher molecular weights (dextran T70 and T500) no precipitation was observed in the time-frame studies. The kinetic of the precipitation process were studied by spectroscopic, thermotropic and rheologic methods.

The wide angle X-ray diffraction showed that the cyrstallinity of dextran T10 3c* system increased with time and reached steady state after 1 day. The development of sample crystallinity can be fitted to the Avrami equation. The same crystallinity behavior can be also obtained by thermotropic methods. The DSC thermograms of dextran T10 3c* systems showed clear melting peaks from 1 hour samples. The heat of fusion which represents the sample crystallinity increased with aging time and reached a steady state after 1 day. The sample crystallinity can be also fitted into Avrami equation.

The rheological response of the samples to shear and dynamic flows was strongly related to phase behavior and structure of the systems. Dextran T10 3c* showed a Newtonian behavior with aging time up to 2 hours. From 3 hours a slight shear thinning existed at high shear rates indicating the chain entanglements started forming in the system. Such change in rheological properties was confirmed through dynamic mechanical analysis that resulted in plots of modulus vs. concentration. From the dynamic oscillatory analysis, up to 2 hours the dextran T10 3c* systems behaved like a non-gelling liquid like system. 3 hours sample started showing weak entanglement behavior. From 4 hours the systems showed a weak gel behavior. The complex viscosity also followed the same trend as the apparent viscosity from the steady measurements.

The empirical Cox-Merz rule, which correlates steady shear and complex viscosities, was not followed by the dextran T10 3c* systems with aging time more than 3 hours. The Cox-Merz rule has been found to be not applicable to biopolymer dispersions with an aggregated structure. The divergence of linear shear and complex viscosity in dextran T10 3c* systems should due to the crystalline structure that developed with time.

FTIR spectroscopy was used to investigate the origin of the dextran precipitation process from aqueous solutions. Intermolecular hydrogen bonds increased with aging time in dextran T10 3c* systems. From 3 hours a sudden increase in the OH stretching intensity which matches the rheological results indicating hydrogen bonds form physical cross-links that contribute to the gel formation. From the intensity ratio that reflects the water-sugar interactions a constant ratio was obtained for dextran T500 50% systems showing there was no interaction or modification in conformation occurred with time. While for dextran T10 3c* system an increase in the intensity ratio was observed from 3 hours indicating the molecular interaction increased and led to the change in the system conformation.

Combined all the analysis results the polymer crystallite formation in low molecular weight dextran is due to the organization of the network chain segments into crystallites. While in amorphous regions chain segments are in disorderly arrangement. The large polymer/water ratio in concentrated dextran T10 solutions results in association of the chains through hydrogen bonding which ultimately leads to crystallization. Crystallization is then initiated by nucleation and subsequent growth of the crystal nuclei by the incorporation of macromolecular chains. In concentrated solution, the dextran chains are hydrated to a lesser extent. The low degree of hydration facilitates association of the chains and thereby crystallization, whereas for solutions with lower dextran concentrations, the dextran chains are surrounded by sufficient water molecules to prevent association.

Dextran molecules have increasing branching with increase molecular weight. Native dextran has around 5% branching while dextran T10 has only 3% branching since

degree of branching is found to decrease on partial acid hydrolysis (de Belder, 2003). Obviously, chains with a low degree of branching crystallize easily than highly branched polymers. This also explains the precipitation of high molecular weight dextran was not observed.

VI. Recommendations for future work

Future research can build on this present research as a result of the improved understanding of the dextran properties. Future research could include studying the phase behavior of dextran under different PH, temperatures and ionic strengths. This additional information would lead to the development of biopolymers with improved functional properties and a wider range of application in the food industry. A different solvent system, such as glycerol, can be investigated to understand whether the observed phase behavior was dictated by water affinity or by polymer-polymer incompatibility. Addition of another polymer can also be an interesting follow up. The mixed systems would explain further the characteristic of dextran interacting with other ingredients under a real food system.

VII. Appendices

A. Molecular weight of dextrans

Dextran	M_w (g/mol)
T1	1047
T5	5200
T10	10800
T20	21400
T40	43000
T70	67200
T500	482000
T2000	2000000

(Manufacturer information)

B. Intrinsic viscosity of dextrans

	concentration (g/dl)	0.019	0.040	0.075	0.100	0.150	0.250
specific viscosity/[c]	T1	0.065119	0.072742	0.067856	0.074885	0.074096	0.070861
	T5	0.074225	0.076749	0.08859	0.087602	0.087565	0.086515
	T10	0.122461	0.137575	0.128297	0.110148	0.104885	0.095629
	T20	0.165041	0.163161	0.162662	0.1611	0.182205	0.189456
	T40	0.253235	0.247561	0.219797	0.20854	0.188301	0.178046
	T70	0.254691	0.319599	0.287984	0.295909	0.264565	0.247378
	T500	0.467129	0.503224	0.487686	0.513157	0.501886	0.51087
	T2000	0.496972	0.588059	0.561769	0.578269	0.616146	0.662632

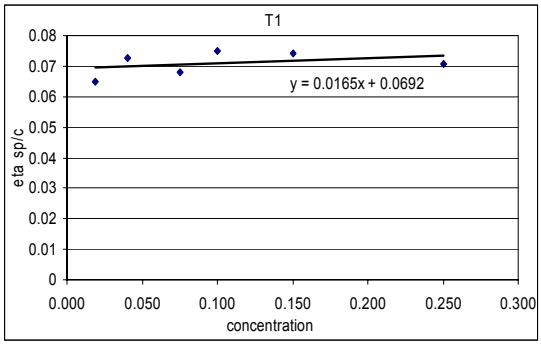

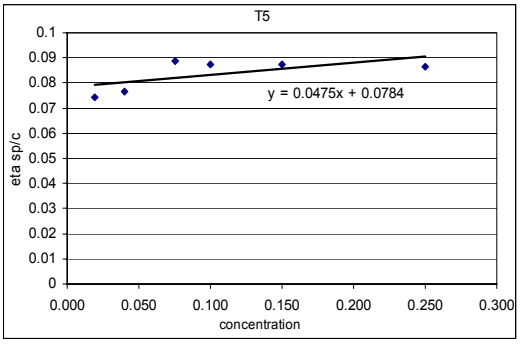

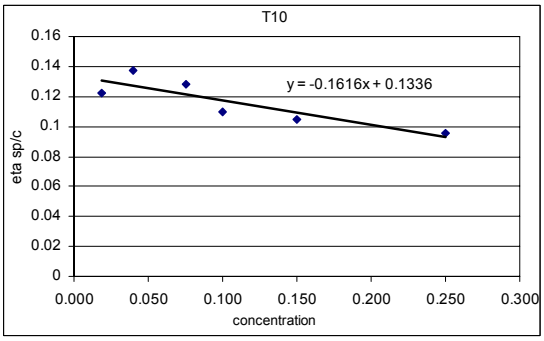

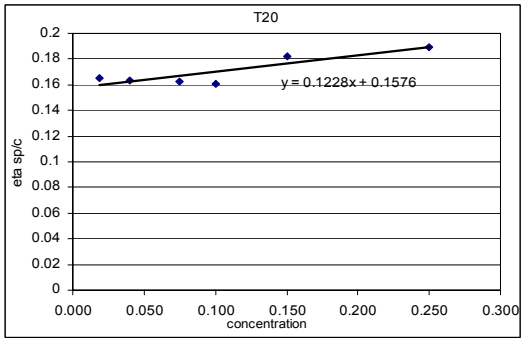

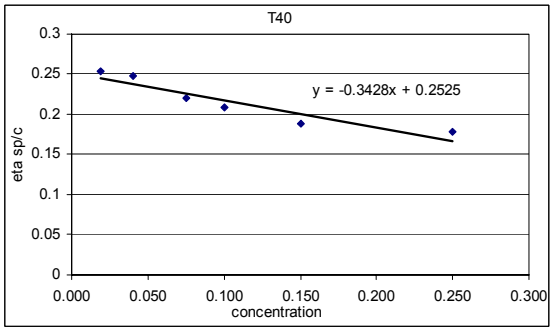

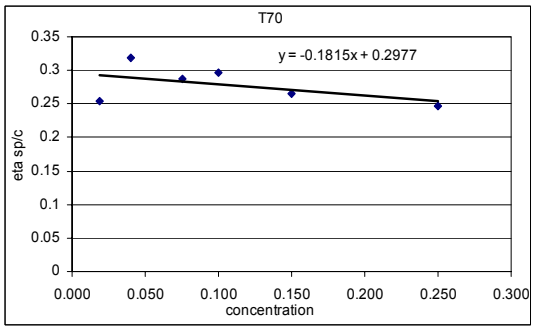

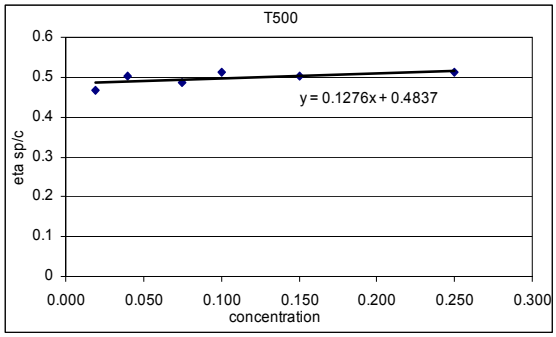
T500
eta sp/c
0.6
0.5
0.4
0.3
0.2
0.1
0
y = 0.1276x + 0.4837
0.000
0.050
0.100
0.150
0.200
0.250
0.300
concentration

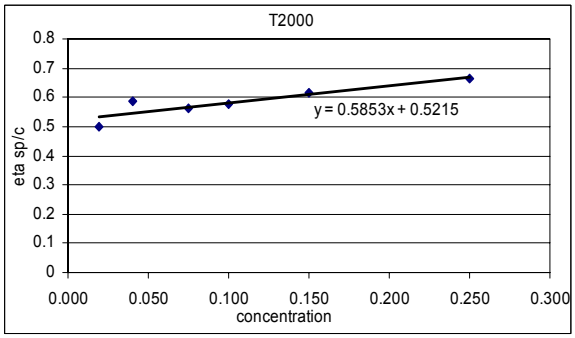
T2000
eta sp/c
0.8
0.7
0.6
0.5
0.4
0.3
0.2
0.1
0
y = 0.5853x + 0.5215
0.000
0.050
0.100
0.150
0.200
0.250
0.300
concentration

C. Zero shear viscosity of dextrans

T10

concentration (wt%)	viscosity (Pa-s)
0.99%	0.0012
4.76%	0.0013
9.09%	0.0021
13.04%	0.0029
16.67%	0.0039
23.08%	0.0069
25.93%	0.0085
28.57%	0.0133
31.03%	0.0167

T40

concentration (wt%)	viscosity (Pa-s)
4.76%	0.0018
9.09%	0.004
13.04%	0.0057
16.67%	0.0115
20.00%	0.0181
23.08%	0.0271
25.93%	0.0381

T70

concentration (wt%)	viscosity (Pa-s)
4.76%	0.0023
9.09%	0.0055
13.04%	0.0084
16.67%	0.0127
20.00%	0.0283
23.08%	0.0439
25.93%	0.0532
28.57%	0.0963
31.03%	0.1339

T500

concentration (wt%)	viscosity (Pa-s)
0.99%	0.0014
2.91%	0.0034
4.76%	0.0068
7.41%	0.0135
9.09%	0.0205
10.71%	0.0302
13.04%	0.047
16.67%	0.0978

D. Percent crystalinity by Wide Angle X-ray Scattering

time (min)	P1	P2	P3	P4	P5	P6	P7	Total Area	% crysalinity
5760	326	138	703	1854	345	438	802	22236	17.1596751
1440	249	78	586	1555	325	393	680	20059	16.1588297
300	161	65	399	1199	244	267	485	19282	12.7590263
275	184	57	421	1110	220	278	498	19378	12.4988711
250	187	56	382	1094	210	474	261	20100	11.7026885
225	139	53	370	981	220	242	414	19561	11.0054595
200	116	75	303	146	876	168	357	19822	9.33540685
175	95	64	266	132	672	193	365	19754	8.29580799
150	129	36	213	139	549	179	266	19904	7.05580201
125	91	34	90	67	350	69	260	20358	4.50771612
100	93	44	144	144				20307	2.04997106
75	41	59	68					20385	0.81739892
50	33	39						20315	0.35316623

E. Percent crystalinity by Differencial Scanning Calorimetry

time	#1 peak area (J/g)	#2 peak area (J/g)	average peak area
1	4.729	6.409	5.569
2	8.492	8.79	8.641
3	10.67	10.42	10.545
4	14.02	11.1	12.56
24	13.57		13.57
72	13.98		13.98

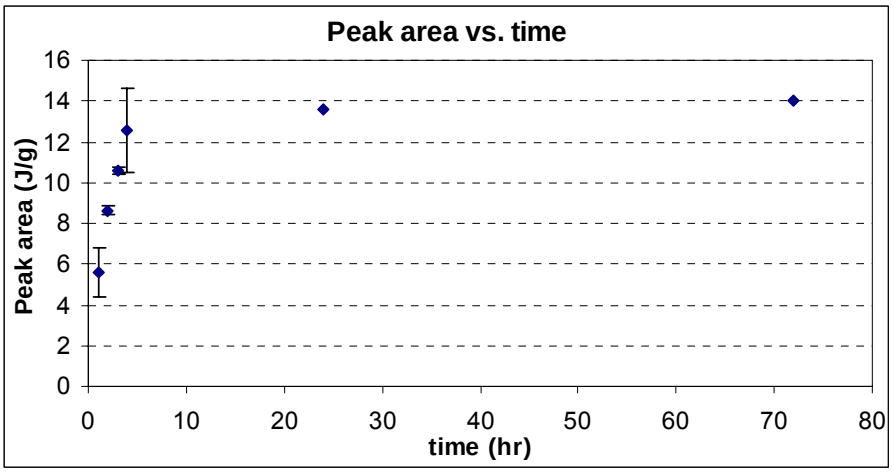

F. Example of standard deviation

1. Steady shear

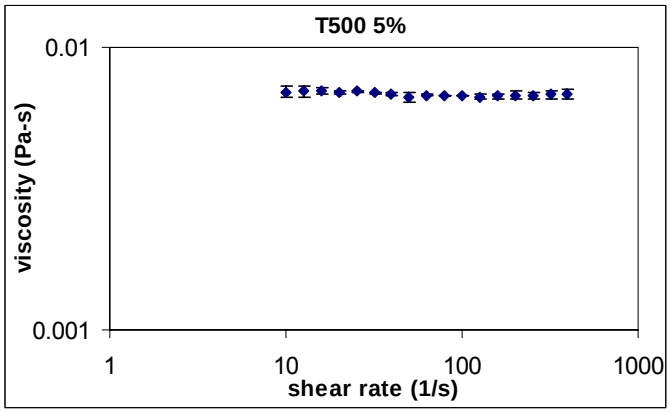

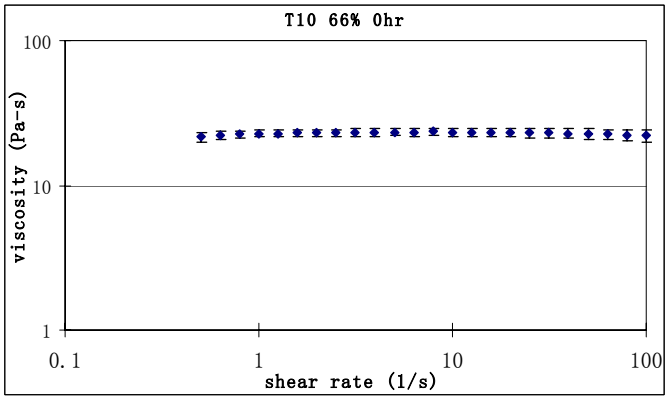

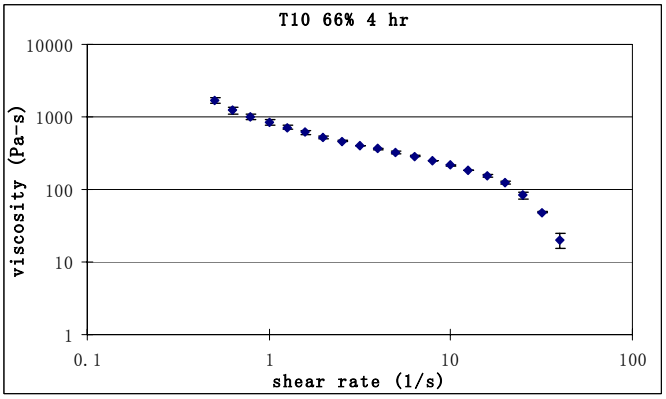

2. Small amplitude dynamic analysis

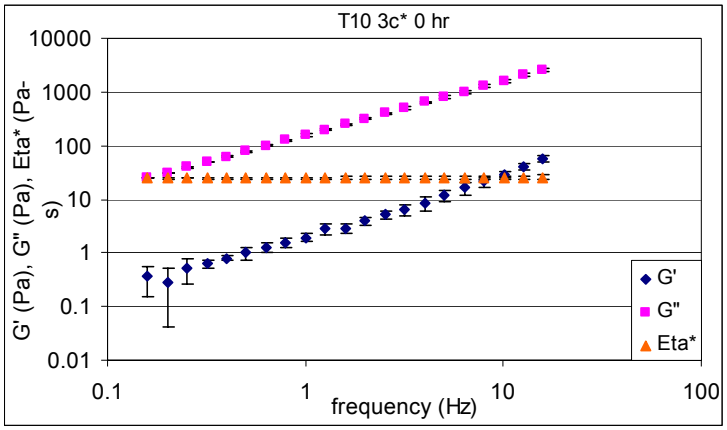

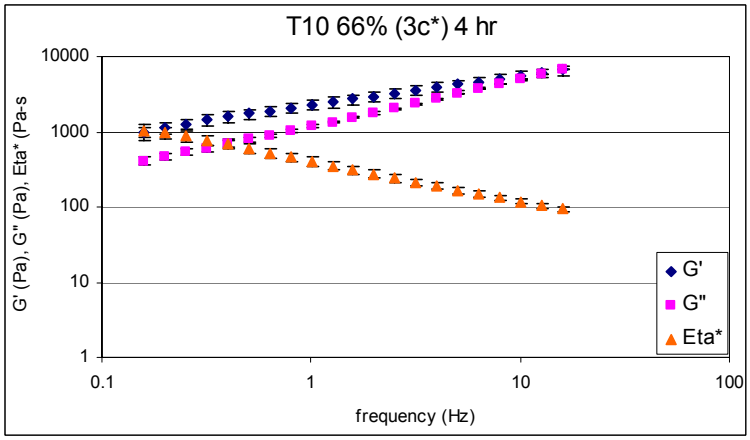

G. Raw data in CD

- Intrinsic viscosity calculation
- Wide Angle X-ray Scattering calculation
- DSC
- FTIR analysis
- Steady shear calculation
- Small amplitude dynamic analysis

VIII. Reference

Acierno, S., and Grizzuti, N. 2003. Measurements of the rheological behavior of a crystallizing polymer by an "inverse quenching" technique. *J. Rheol.* 563- 576.
Allegra, G., Corradini, P., Elias, H.G., Geil, P.H., Keith, H.D., and Wunderlich, B. 1989. Definitions of terms relating to crystalline polymers. *Pure Appl. Chem.* 61: 769- 785.
Avaltroni, F., Bouquerand, P.E., and Normand, V. 2004. Maltodextrin molecular weight distribution influence on the glass transition temperature and viscosity in aqueous solutions. *Carbohydr. Polym.* 58: 323- 334.
Basedow, A.M. and Ebert, K.H. 1979. Production, characterization, and solution properties of dextran fractions of narrow molecular distributions. *J. Polym. Sci. Pol. Sym.* 66:101- 115.
de Belder, A.N. 2003. Dextran. AA ed. Amersham Biosciences AB, Sweden. pp. 9- 28.
Bistany, K.L. and Kokini, J.L. 1983. Comparison of steady shear rheological properties and small amplitude dynamic viscoelastic properties of fluid food materials. *J. Texture Studies.* 14: 113-124.
Brugnerotto, J., Desbrieres, J., Roberts, G., and Rinaudo, M. 2001. Characterization of chitosan by steric exclusion chromatography. *Polymer.* 42:9921- 9927.
Castro, J.V., Ward, R.M., Gilbert, R.G., and Fitzgerald, M.A. 2005. Measurement of the molecular weight distribution of debranched starch. *Biomacromolecules.* 6: 2260- 2270.
Chanzy, H., Guizard, C., and Sarko, A. 1980. Single crystals of dextran: 1. low temperature polymorph. *Int. J. Biol. Macromol.* 2: 149- 153.
Chen, R.H., and Tsaih, M.L. 1997. Effect of molecular weight and urea on the conformation of chitosan molecules in dilute solutions. *Int. J. Biol. Macromol.* 20:233- 240.
Chen, R.H., and Tsaih, M.L. 1998. Effect of temperature on the intrinsic viscosity and conformation of chitosans in dilute HCl solution. *Int. J. Biol. Macromol.* 23:135- 141.
Chen, R.H., and Tsaih, M.L. 1999. Urea-induced conformational changes of chitosan molecules and the shift of break point of Mark-Houwink equation by increasing urea concentration. *J. Appl. Polym. Sci.* 75: 452- 457.
Cheng, Y., Prud'homme, R.K., Chik, J. and Rau, Donald. 2002. *Macromolecules.* 35: 10155- 10161.
Chinachoti, P. and Steinberg, M.P. 1986. Crystallinity of sucrose by X-ray diffraction as influenced by absorption versus desorption, waxy-maize starch content, and water activity. *J. Food Sci.* 51(2): 456- 459, 463.
Chung, H.J., Chang, H.I., and Lim, S.T. 2004. Physical aging of glassy normal and waxy rice starches: effect of crystallinity on glass transition and enthalpy relaxation. *Carbohydr. Polym.* 58: 101- 107.
Colwell, K.H., Axford, D.W.E., Chamberlain, N., and Elton, G.A.H. 1969. Effect of storage temperature on the ageing of concentrated wheat starch gels. *J. Sci. Food Agriculture.* 20: 550- 555.
Covacevich, M.T. and Richards, G.N. 1977. Frequency and distribution of branching in a dextran: an enzymic method. *Carb. Res.* 54: 311- 315.

Dimler, R.J., Wolff, I.A., Sloan, J.W. and Rist, C.E. 1951. Interpretation of periodate oxidation data on degraded dextran. *J. Am. Chem. Soc.* 77: 6568- 6573.
Ewald, R.A. and Crosby, W.H. 1963. Reported experiences with dextran in communist countries. *Transfusion.* 8: 376.
Ferry, J.D. 1980. *Viscoelastic Properties of Polymers.* 3rd ed. John Wiley & Sons, Inc. N.Y.
Fessas, D., and Schiraldi, A. 2000. Starch gelatinization kinetics in bread dough DSC investigation on "simulated" baking process. *J. Therm. Anal. Calorim.* 61: 411- 423.
Fournier, C., Leonard, M., and Dellacherie, E. 1998. EPR spectroscopy analysis of hydrophobically modified dextran-coated polystyrene. *J. Colloid Interface Sci.* 198: 27- 33.
FTIR Seminar. Jasco In. http://www.jascofrance.fr/pdf/ftir.pdf
Gekko, K. 1981. Solution properties of dextran and its ionic derivatives. *American Chemical Society Symposium Series.* 150: 415- 438.
Glicksman, M. 1982. Functional properties of hydrocolloids. Food Hydrocolloids, M. Glicksman (Ed.), 47- 99.
Goossens, J.G.P. and Lemstra, P.J. 2006. The use of synchrotron radiation to improve polymer systems. SRMS-5 Conference, Chicago July 30- August 2, 2006.
Granath, K.A. 1958. Solution properties of branched dextrans. *J. Colloid Sci.* 13: 308- 328.
Guizard, C., and Chanzy, H. 1984. Molecular and crystal structure of dextrans: a combined electron and x-ray diffraction study. 1. the anhydrous high-temperature polymorph. *Macromolecules*. 17: 100- 107.
Harrick, N.J. 1967. Internal reflection spectroscopy. New York: John Wiley & Sons, Inc.
Hirata, Y., Sano, Y., Aoki, M., Shohji, H., Katoh, S., Abe, J., Hitsukuri, S., and Yamamoto, H. 2003 Small-angle X-ray scattering studies of moderately concentrated dextran solution. *Carbohydr. Polym.* 53: 331- 335.
Hokputsa, S., Hu, C., Paulsen, B.S., and Harding, S.E. 2003. A physico-chemical comparative study on extracellular carbohydrate polymers from five desert algae. *Carbohydr. Polym.* 54: 27- 32.
Horiuchi, K. 2004. DSC studies on structural phase transitions and molecular motions in some A_2MCl_4 compouds. *Phys. Stat. Sol. (a)* 201(4): 723- 726.
Icoz, D.Z., Moraru, C.I., and Kokini, J.L. 2005. Polymer-polymer interactions in dextran systems using thermal analysis. *Carbohydr. Polym.* 62: 120- 129.
Icoz, D.Z. and Kokini, J.L. 2006. Probing the boundaries of miscibility in model carbohydrates consisting of chemically derivatized dextrans using DSC and FTIR spectroscopy. *Carbohydr. Polym.* In Press.
Iijima, M., Hatakeyama, T., Nakamura, K., and Hatakeyama, H. 2002. Effect of annealing on calcium pectin gel formation by thermomechanical analysis. *J. Therm. Anal. Calorim.*70: 815- 824.
Ioan, C.E., Aberle, T., and Burchard, W. 2000. Structure properties of dextran. 2. Dilute solution. *Macromolecules.* 33: 5730- 5739.
Jacobs, H. and Delcour, J.A. 1998. Hydrothermal modifications of granular starcdh, with retention of the granular structure: a review. *J. Ag. Food Chem.* 46: 2895- 2905.

Jeans, A. and Seymour, F.R. 1979. The α-D-glucopyranosidic linkages of dextrans: comparison of percentages from structural analysis by periodate oxidation and by methylation. *Carb. Res.* 74: 31- 40.
Jeanes, A., Schieltz, N.C., Wilham, C.A. 1948. Molecular association in dextran and in branched amylaceous carbohydrates. *J. Biol. Chem.* 176: 617- 627.
Jin, X., Ellis, T.S., and Karasz, F.E. 1984. The effect of crystallinity and crossliking on the depression of the glass transition temperature in nylon 6 by water. *J. Polym. Phys. Ed.* 22 : 1701- 1717.
Jouppila, K., Kansikas, J. and Roos, Y.H. 1998. Factors affecting crystallization and crystallization kinetics in amorphous corn starch. *Carbohydr. Polym.* 36: 143- 149.
Kačuráková, M. and Mathlouthi, M. 1996. FTIR and laser-Raman spectra of oligosaccharides in water: characterization of the glycosidic bond. *Carbohydr. Res.* 284: 145- 157.
Keetels, C.J.A.M., Vliet, T.V., and Walstra, P. 1996. Gelation and retrogradation of concentrated starch systems: 1. Gelation. *Food Hydrocolloids.* 10: 343- 353.
Kenley, R.A., Lee, M.O., Mahoney, T.R., II, and Sanders, L.M. 1987. Poly(lactide-co-glycolide) decomposition kinetics in vivo and in vitro. *Macromol.* 20:2398- 2403.
Klug, H.P. and Alexander, L.E. 1974. *X-ray Diffraction Proccedures.* 2nd ed. Wiley & Sons, N.Y. pp. 733- 736.
Kolhed, M., Lendl, B., and Karlberg, B. 2003. On-line infrared detection in aqueous micro-volume systems. *Analyst.* 128:2- 6.
Lai, L.S., and Chao, S.J. 2000. A DSC study on the gel-sol transition of a starch and hsian-tsao leaf gum mixed system. *J. Agric. Food Chem.* 48: 3268- 3274.
Larm, O., Lindberg. B. and Svensson, S. 1971. Studies on the length of the side chains of the dextran elaborated by Leuconostoc mesenteroides NRRL B-512. *Carb. Res.* 20: 39- 48.
Laumonier, T., Mohacsi, P.J., Matozan, K.M., Banz, Y., Haeberli, A., Korchagina, E.Y., Bovin, N.V., Vanhove, B. and Rieben, R. 2004. Endothelial cell protection by dextran sulfate: a novel strategy to prevent acute vascular rejection in xenotransplatation. *Am. J. Transplant.* 4: 181- 187.
Lawford, G.R., Kligerman, A., Williams, T. and Lawford, H.G. 1979. Dextran biosynthesis and dextransucrase production by continuous culture of Leuconostoc mesenteroides. *Biotechnol. Bioeng.* 21: 1121- 1131.
Lindberg, B. and Svensson, S. 1968. Structural studies on dextran from Leuconostoc mesenteroides NRRL B-512. *Acta Chem. Scand.* 22, 1907.
Loret, C., Meunier, V., Frith, W.J., and Fryer, P.J. 2004. Rheological characterization of the gelation behavior of maltodextrin aqueous solutions. *Carbohydr. Polym.* 57(2): 153- 163.
Montserrat, S. 1992. Vitrification and further structural relaxation in the isothermal curing of an epoxy resin. *J. Appl. Polym. Sci.* 44: 545- 554.
Montserrat, S. 1994. Physical aging studies in epoxy resins. I. Kinetics of the enthalpy relaxation process in a fully cured epoxy resin. *J. Polym. Sci.: part B: Polym. Phy.* 32 : 509- 522.
McCurdy, R.D., Goff, H.D., Stanley, D.W., and Stone, A.P. 1994. Rheology properties of dextran related to food application. Food *Hydrocolloids.* 8(6): 609- 623.

Morris, E.R., and Ross-Murphy, S.B. 1980. Chain flexibility of polysaccharides and glycoproteins from viscosity measurements. *Techniques in Carbohydrate Metabolism.* 310(B): 1- 46.
Naessens, M., Cerdobbel, A., Soetaert, W., and Vandamme, E.J. 2005. Leuconostoc dextransucrase and dextran: production, properties and applications. *J. Chem. Technol. Biotechnol.* 80:845- 860.
Nagy, D.J. 1996. Characterization of nonionic and cationic amine-functional polymers by aqueous SEC-MALLS. *J. Appl. Polym. Sci.* 59:1479- 1488.
Nadel, H., Randles, C.I. and Stahly, G.L. 1953. The influence of environmental factors on the molecular size of dextran. *Appl. Microbiol.* 1: 217- 224.
Nordmeier, E. 1993. Static and dynamic light-scattering solution behavior of pullulan and dextran in comparison. *J. Phys. Chem.* 97(21): 5770- 5785.
Olsen, A.P., Flagan, R.C., and Kornfield, J.A. 2005. Deliquescence, diffusion, and crystal nucleation in levitated polyethylene oxide. The 2005 Annual Meeting. Cincinnati, OH.
Padmanabhan, P.A., Kim, D-S. Pak, D. and Sim, S.J. 2003. Rheology and gelation of water-insoluble dextran from *Leuconostoc mesenteroides* NNRL B-523. *Carbohydr. Polym.* 53: 459- 468.
Picout, D.R., Ross-Murphy, S.B., Jumel, K., and Harding, S.E. 2002. Pressure cell assisted solution characterization of polysaccharides. 2. Locust bean gum and tara gum. *Biomacromolecules*. 3: 761- 767.
Picton, L., Mocanu, G., Mihai, D., Carpov, A., and Muller, G. 1995. Chemically modified exopolysaccharide pullulans: physico-chemical characteristics of ionic derivatives. *Carb. Polym*. 28:131- 136.
Rankin, J.C. and Jeanes, A. 1954. Evaluation of the periodate oxidation method for structural analysis of dextrans. *J. Am. Chem. Soc*. 78: 4435.
Richter, A.W. and Hedin, H. 1982. Dextran hypersensitivity. *Immunol. Today*. 3:132- 138.
Roessner, D., and Kulicke, W.M. 1994. On-line coupling of flow field-flow fraction and multi-angle laser light scattering. *J. Chromatogr. A.* 687:249- 258.
Roos, Y.H. 1995. *Phase Transition in Foods.* Academic Press, Inc. San Diego, CA. pp. 49- 107.
Rouzes, C., Gref, R., Leonard, M., Delgado, A.D., and Dellacherie, E. 2000. Surface modification of poly(lactic acid) nanospheres using hydrophobcally modified dextrans as stabilizers in an o/w emulsion/evaporation technique. *J. Biomed. Mater. Res.* 50: 557- 565.
Senti, F.R., Hellman, N.N., Ludwig, N.H., Babcock, G.E., Tobin, R., Glass, C.A., and Lamberts, B.L. 1955. Viscosity, sedimentation,and light-scattering properties of fraction of an acid-hydrolyzed dextran. *J. Polym. Sci.* 17: 527- 546.
Scott, T.A., Hellman, N.N., Senti, F.R. 1957. Characterization of dextrans by the optical rotation of their cuprammonium complexes. *J. Am. Chem. Soc.* 79: 1178.
Shoemaker, W.C. 1976. Comparison of the relative effectiveness of whole blood transfusions and various types of fluid therapy in resuscitation. *Crit. Care Med.* 4: 71- 78.
Singel, K.I. 2002. Determination of structural peculiarities of dextran, pullulan and γ-irradiated pullulan by Fourier-transform IR spectroscopy. *Carbohydr. Res.* 337: 1445- 1451.

Slade, L., and Levine, H. 1991. Beyond water activity: recent advances based on an alternative approach to the assessment of food quality and safety. *Crit. Rev. Food Sci. Nutr.* 30: 115- 360.
Slade, L., and Levine, H. 1995. Glass transitions and water-food structure interactions. *Adv. Food Nutr. Res.* 38: 103- 269.
Slade, L., and Levine, H. 1998. Non-equilibrium melting of natve granular gelatinization of A-type cereal starches. *Carbohydr. Polym.* 8: 183- 208.
Snabre, P., Grossmann, G.H., and Mills, P. 1985. Effects of dextran polydispersity on red blood cell aggregation. *Colloid. Polym. Sci.* 263:478- 483.
Smit, J.A.M., van Dijk, J.A.P.P., Mennen, M.G., and Daoud, M. 1992. Polymer size exponents of branched dextrans. *Macromol.* 25:3585- 3590.
van Soest J.J.G, Vliegenthart, J.F.G. 1997. Crystallinity in starch plastics: consequences for material properties. *Tib. Tech*. 15: 208- 213.
Soltero, J.F.A. Robles-Vásquez, O. and Puig, J.E. 1995. Note: Thixotropic-antithixotropic behavior of surfactant-based lamellar liquid crystals under shear flows. *J. Rheol.* 39(1): 235- 240.
Sperline, R.P., Song, Y., and Freiser, H. 1992. Fourier transform infrared attenuated total reflection spectroscopy linear dichroism study of sodium dodecyl sulfate adsorption at the Al_2O_3-coated optics. *Langmuir.* 8:2183- 2191.
Sperling, L.H. 1992. *Introduction to Physical Polymer Science.* 2nd ed. John Wiely & Sons, Inc. N.Y. pp. 65- 77, 104- 107, 173- 175, 198- 268, 320- 323.
Sperling, L.H. 2001. *Introduction to Physical Polymer Science.* 3rd ed. John Wiely & Sons, Inc. N.Y. pp.
Stacey, M. and Swift, G. 1948. Structure of the dextran synthesized from sucrose by a new strain of betacoccus arabinosaceous. *J. Chem. Soc.* 1948: 1555- 1959.
Stenekes, R.J.H., Talsma, H. and Hennink, W.E. 2001. Formation of dextran hydrogels by crystallization. *Biomaterials.* 22: 1891- 1898.
Tadokoro, H. 1979. *Structure of Crystalline Polymers.* John Wiley & Sons. N.Y. pp. 179- 311.
Tirtaatmadja, V., Dunstan, D.E. and Boger, D.V. 2001. Short communication: Rheology of dextran solutions. *J. Non-Newtonian Fluid Mech.* 97: 295- 301.
Toda, A., Arita, T., and Hikosaka, M. 2001. Three-dimensional morphology of PVDF single crystals forming banded spherulites. *Polymer* 42: 2223- 2233.
Tsuchiya, H.M., Koepsell, H.J., Corman, J., Bryant, G., Bogard, M.O., Feger, V.H. and Jackson, R.W. 1952. The effect of certain cultural factors on production of dextransucrase by leuconostoc mesenteroides. *J. Bacteriol.* 64: 521- 526.
Van Cleve, J.W., Schaefer, W.C. and Rist, C.E. 1956. The structure of NRRL B-512 dextran. Mehtylation studies. *J. Am. Chem. Soc.* 78: 4435- 4438.
Vianna-Soares, C.D., Kim, C.J., and Borenstein, M.R. 2002. Use of hydrophilic hydroxypropyl methacrylate/ethylene glycol methacrylate packing material in size-exclusion chromatography. *J. AOAC Int.* 85: 1308- 1315.
Vieira, N.A.B., Moscardini, M.S. Tiera, V.A.O., and Tiera, M.J. 2003. Aggregation behavior of hydrophobically modified dextran in aqueous solution: a fluorescence probe study. *Carbohydr. Polym.* 53: 137- 143.
Wales, M., Marshall, P.A., and Weissberg, S.G. 1953. Intrinsic viscosity-molecular weight relationships for dextran. *J. Polym. Sci.,* 10: 229- 240.

Wang, W., Bo, S.Q., Li, S.Q., and Qin, W. 1991. Determinnation of the Mark-Houwink equation for chitosans with different degrees of deacetylation. *Int. J. Biol. Macromol.* 13: 281- 285.
Wittgren, B., and Wahlund, K.G. 1997. Fast molecular mass and size characterization of polysaccharides using asymmetrical flow field-flow fractionation-multiangle light scattering. *J. Chrom. A.* 760:205- 218.
Wolff, D., Czapla, S., Heyer, A.G., Radosta, S., Mischnick, P., and Springer, J. 2000. Globular shape of high molar mass inulin revealed by static light scattering and viscometry. *Polymer*. 41: 8009- 8016.
Wolkers, W.F., Oliver, A.E., Tablin, F., and Crowe, J.H. 2004. A Fourier-transform infrared spectroscopy study of sugar glasses. *Carbohydr. Res.* 339(6): 1077- 1085.
Wu, T., Zivanovic, S., Baxter, S.R., and Weiss, J. 2005. Molecular weight and conformation analysis of chitosan molecules treated by high intensity ultrasound. IFT Annual Meeting, New Orleans, Louisiana.
Wu, C. 1993. Laser light-scattering characterization of the molecular weight distribution of dextran. *Macromolecules.* 26: 3821- 3825.
Zhang, H.B., Voglis, B.S., Kim, C.H. and Slutsky, A.S. 2003. Effects of albumin and ringer's lactate on production of lung cytokines and hydrogen peroxide after resuscitated hemorrhage and endotoxmia in rats. *Crit. Care Med.* 31: 1515- 1522.
Zobel, H.F. 1988. Starch crystal transformations and their industrial importance. *Starch/Stärke.* 40: 1- 7.

IX. Curriculum Vita

Yunhong Rong

Education

June 2002 South China University of Technology: Bachelor of Engineering in Biologic Pharmaceuticals and Bachelor of Arts in English.

May 2008 Rutgers University: Master of Science in Food Science

Position Held:

Feb. 2006 – present Chemist, Firmenich Inc., Plainsboro, NJ

Oct. 2005 – Nov. 2005 Laboratory Technician, Robertet Flavors Inc., Piscataway, NJ

Sept. 2004 – August 2005 Graduate Assistant, Food Science Department, Rutgers University, New Brunswick, NJ

Sept. 2003 – August 2004 Teaching Assistant, Food Science Department, Rutgers University, New Brunswick, NJ

Sept. 2002 – August 2003 Excellence Fellow, Food Science Department, Rutgers University, New Brunswick, NJ